AN INVESTIGATION OF NON-EQUILIBRIUM EFFECTS IN AN ARGON FREE-JET PLASMA

Thesis by

Philip E. Cassady

In Partial Fulfillment of the Requirements

For the Degree of

Doctor of Philosophy

California Institute of Technology

Pasadena, California

1970

(Submitted February 10, 1970)

ACKNOWLEDGEMENTS

I would like to express my appreciation to Professor Lester Lees for his interest in this work and his guidance of this research program and to Professor Miklos Sajben for the many hours of stimulating discussion that he contributed.

I would also like to thank Mrs. Truus Van Harreveld, Mrs. Betty Wood and Mr. Gerrit Van Halewyn for their careful graphical work; the staff of the Galcit Hypersonic Wind Tunnel, especially Mr. Paul Baloga and Mr. Henry Mazurowski and the staff of the Aeronautics Machine Shop under the direction of Mr. George Carlson for their assistance in the experimental program.

I wish to acknowledge with appreciation the National Science Foundation, the California Institute of Technology, and the Ford Foundation all of whom provided financial support for myself and my family throughout this endeavor. Acknowledgement is also due to the U. S. Army Research Office and the Advanced Projects Agency who supported the experimental program under Contract No. Da-31-124-ARO(D)-33.

I wish to also express my appreciation to my wife, Katherine, who typed this thesis.

This work is dedicated to the memory of my mother, Mrs. Vivian C. Cassady,who truly loved and unselfishly guided her son, and to my own sons, Sean Erik and Edward Julian,for whom I hope that I can do the same.

ABSTRACT

The non-equilibrium effects present in the formation of a strong normal shock wave in a low density, slightly ionized argon flow field, particularly as evidenced by the appearance of a dark region upstream of the shock wave, have been analyzed both theoretically and experimentally. A model for the flow through the shock wave was formulated which incorporates a quantum mechanical theory to explain the existence of the dark region, and the problem was solved numerically to yield flow field property distributions. A precursor region of high electron temperature was found to exist upstream of the main body of the heavy-particle shock wave.

An experimental investigation of the phenomenon was carried out in an arc heated free jet flow field. A test facility was constructed in which the goal has been to attain operation at low enough enthalpies to allow precise and extensive diagnostic testing while still high enough to exhibit the interesting non-equilibrium effects. Extensive study was carried out on the effect of electrode design and gas flow phenomena on the stability of the arc discharge. The completed unit was instrumented fully for measurement of the operating parameters and a computer program was developed to monitor its operation as a supply of slightly ionized argon for free-jet experiments.

The non-equilibrium aspects of the free-jet were analyzed both theoretically and experimentally. A theoretical model was developed and numerically solved for the free-jet expansion of slightly ionized argon. Pitot pressure measurements were completed and compared favorably with predictions calculated from this theoretical model.

Electron temperature and ion density profiles were measured both along the axis of the empty free-jet and through the normal shock wave in front of a cooled blunt body using a new type of cooled Langmuir probe, the operation of which was theoretically analyzed. The existence of a region of electron temperature in front of a strong normal shock wave coincident with the observed dark region was experimentally verified.

TABLE OF CONTENTS

LIST OF FIGURES

Tables

LIST OF SYMBOLS

A	Area
a	Recombination coefficient (Equation III-13)
B	Electron mass flow constant (Equation III-18)
b	Function given in Equation (II-26)
C	Correction factor (Equation III-3)
D	Orifice diameter
d	Diameter
e	Electronic charge (positive number)
H	Inelastic collisional energy transfer term (Equation III-19)
h	Enthalpy
I	Current
I	Ionization energy
j	Current density
K	Coefficient of thermal conductivity
Kn	Knudsen number
k	Boltzmann's constant
L	length
L	Mean free path (with subscript)
M	Mach number
m	Mass
N	Slope of electron temperature profile (Equation II-23)

n	Number density
P	Pressure
Q	Collisional cross-section
R	Polar radius
Re	Reynolds number
r	Cylindrical radius
S	Thermal non-equilibrium parameter (Equation II-1)
s	Collisional impact parameter
T	Temperature
t	Characteristic time
u	Average velocity
V	Potential
v	Ion acoustic speed
W	Dimensionless potential difference (Equation C-18)
X	Dimensionless potential difference (Equation C-20)
x	Axial coordinate
y	Dimensionless coordinate (Equation II-12)
Z	Elastic collisional energy transfer term (Equation B-22)
α	Ionization fraction
γ	Specific heat ratio
ϵ_o	Vacuum permittivity

θ	Polar angle
Λ	Debye length/critical impact parameter (Equation B-6)
μ	Coefficient of viscosity
ν	Collision frequency
ρ	Mass density

Superscripts

*	Sonic conditions
o	Time derivative
~	Dimensionless variable

Subscripts

a	Ambient conditions in vacuum chamber
D	Debye length (with L)
d	Directed ion flux
e	Electron
f	Field particle
f	Floating potential
H	Heavy particles: Ions and neutrals
i	Ions
n	Neutral particles
p	Probe surface conditions
s	Shock conditions

t	Stagnation conditions
1	Upstream of shock
2	Downstream of shock
∞	Conditions at infinity
o	Reference conditions

I. Introduction

The purpose of this research is to investigate non-equilibrium effects in an argon plasma. These effects are presently receiving considerable attention since it is through these non-equilibrium processes that the physical laws governing inter-particle behavior in plasmas are best revealed. The historical trend has been first to study equilibrium situations which can be described by phenomenological, macroscopic laws. Non-equilibrium situations on the other hand require the examination of microscopic laws which demand a much deeper understanding of the physics of the problem. In order to proceed further on the development of such practical projects as magneto-hydrodynamic power generation and controlled chemical processes carried out in the plasma state, it has been necessary to develop this understanding and many researches into transport properties and collisional effects in plasmas have recently been carried out. The present work is an attempt to examine a specific non-equilibrium situation with the goal being to gain some insight into the physical processes by which non-equilibrium phenomena are governed.

The arc-heated free jet flow field offers an environment in which non-equilibrium effects are present and are the cause of observable physical phenomena, one of which is the striking dark

region that precedes a luminous shock wave in the flow field. This dark region has been observed experimentally by many researchers (Clayden (1961), Grewal and Talbot (1963), Witte (1969)) and it was first suggested by Grewal and Talbot that a region of high electron temperature in front of the shock wave might be its cause. At the present time there exists very little experimental data by means of which the existence of this high electron temperature precursor might be verified; however, additional theoretical work has been done, the results of which can be used to gain further insight into the physical processes causing the phenomenon (e. g. Jaffrin (1965)). The present research concerns itself with the formulation of a physical model for the hot electron precursor and with the performance of an experimental program by means of which this precursor could be measured.

A theoretical treatment through which a physical model for the hot electron precursor of a normal shock wave in a slightly ionized gas was developed is presented in Section II. The necessary collision processes and associated transport properties are considered in Appendix B. The quenching of radiation in the dark region is related to this hot electron precursor through a quantum-mechanical model of the recombination process.

An arc-heated free jet test facility was developed with which the hot electron precursor could be measured experimentally in an argon plasma. The free jet flow field has been under investigation

as an experiment in low density gasdynamics for quite some time. A survey of previous work and an outline of the applicable theory is to be found in Section III. A theoretical description of the axial electron temperature profile in a slightly ionized argon plasma free jet is developed there. The pertinent results of investigations of arc heaters that have been developed to supply high enthalpy working gases together with original design innovations are presented in Appendix A. The design, instrumentation and preliminary tests on the facility are described in Section IV-A and in Appendices A and E. In order to verify that the experimentally produced flow field was indeed described by the free jet theory, a pitot pressure survey was carried out. The instrumentation used and the results obtained are presented in Section IV-B.

In conventional hypersonic wind tunnels the total pressure, total temperature, and pitot pressure are measured and, under the assumption of isentropic flow, test section properties are deduced. However in a flowing plasma, ionization-recombination and irreversible processes such as heat transfer in the throat region invalidate the isentropic flow assumption, making the measurement of flow properties in the test section mandatory. Many test section properties may be deduced from the free jet model; however, for the non-equilibrium flow of a partially ionized monatomic gas one must also measure the ion or electron density as well as the electron temperature in order to obtain a full picture of the situation existing in the flow field.

These measurements were carried out with a special cooled Langmuir probe which is described in Appendix F. The theory necessary to obtain the electron temperature and ion density from the experimental probe characteristic is developed in Appendix C.

A cooled blunt body was used to produce the desired normal shock wave and precursor in the flow field. To provide a null experiment with which to compare precursor measurements, the axial electron temperature profile was measured in the empty free jet and compared with the profile predicted by the theory of Section III-C. The ion density profile was measured in the empty free jet to further test the validity of the free jet model for the experimental flow field, particularly to verify the frozen flow assumption. These tests are described in Section V-B.

The cooled blunt body was placed in the flow field and electron temperature measurements were made through the dark region. In order to be certain that any measured hot electron precursor did actually precede the normal shock wave, a study of the ion density profile in this region was also undertaken. The results of these investigations are presented in Section V-C.

The various results are summarized in Section VI together with several conclusions drawn from the experience gained in this research. Some new questions whose importance has been revealed through this research are briefly described and suggestions for further research are advanced.

The history of background researches and previous work pertaining to each part of this investigation is included at the beginning of each section in order to show the importance of the present work to the reader and to present the results in their proper perspective.

II. Normal Shock Wave in a Slightly Ionized Gas

A. The High Electron Temperature Precursor

A shock wave existing in a plasma exhibits many phenomena not present in an ordinary shock wave. The conditions existing inside a shock wave provide an environment in which the differences between the behavior of the heavy particle species and the electron species are manifested in a clear physical manner. One of these manifestations is the existence of a region of elevated electron temperature that precedes the body of the plasma shock wave. In this Section the physical foundations upon which this phenomenon depends will be developed. A theoretical treatment will be presented by means of which a quantitative measure of this effect can be predicted.

The simplest situation in which this phenomenon may be examined is the case of a shock wave in a fully ionized plasma. The question of chemistry rate processes is avoided and the transport properties, which determine both the shock wave and the hot electron precursor, are those for a reasonably well understood binary mixture. The work of Jukes (1957) is a clear analysis of the problem. He analyzed a Navier-Stokes model of the shock

wave and found that a hot electron precursor was predictable. He ignored charge separation and electric field effects, but retained ion viscosity and electron thermal conductivity as the real gas effects causing the phenomena. Valid arguments are presented to justify these assumptions. Li and Mathieu (1961), on the other hand, neglected viscosity and thermal conductivity in their analysis of the same problem. They retained electric field effects and charge separation and relied upon momentum transfer between ions and electrons to provide the dissipative mechanism of the shock. Jaffrin and Probstein (1964) considered both collisional transport effects and electric field effects in their treatment. They also consider the Navier-Stokes model for each species coupled with the Poisson equation to describe electric field effects. Their work is the most comprehensive treatment of the problem available at present. Their results clearly exhibit the existence of a hot electron precursor in a high Mach number situation.

In the case of a shock wave existing in a partially ionized gas the problem becomes much more complicated. With the presence of a third species, the neutral particles, the possibility of chemical reactions arises. The transport property calculations are also considerably more complicated since the mixture is no

longer binary and many of the necessary cross sections are not very well predicted theoretically. Empirically gained values must be utilized when they are available. The most comprehensive treatment of this problem has been carried out by Jaffrin (1965). He used the Navier-Stokes equations for the three-fluid species and Poisson's equation for electric field effects. The ionization fraction was assumed frozen. He integrated the governing equations numerically in the phase plane and found the existence of a hot electron precursor. His analysis was only carried out for S = 1, the equilibrium case.

$$S = T_{eo}/T_{Ho} \qquad \text{(II-1)}$$

where the reference quantities are taken in the undisturbed free stream ahead of the shock.

The non-equilibrium case, $S \neq 1$, was analyzed by Grewal and Talbot (1963) for a flow that is chemically frozen and very slightly ionized. The heavy particle shock was assumed to be unaffected by the presence of charged particles, so that the shock profile is given by the Mott-Smith model. This assumption uncouples the problem and leads to considerable simplification. The work of

Jaffrin (1965) later justified its validity. In the numerical analysis, the shock wave was replaced by a discontinuous jump in heavy particle flow properties. These two assumptions are the underlying breakthroughs in this treatment. The work of Grewal and Talbot is an example of inspired analysis. Many of the assumptions upon which it was based were not able to be proven until much later and yet they were valid. These assumptions will be considered below at the point where they are necessary in the analysis. Grewal and Talbot found a hot electron precursor also.

Kamimoto et al. (1967) extended the approach of Grewal and Talbot to a larger range of the non-equilibrium parameter S. They examined the choice of transport properties more closely, using the calculations presented by Jaffrin. They also analyzed the ion density profile across the shock wave. They attempted to verify their calculations experimentally in the flow issuing from a conical nozzle onto a shock holder. The flow field produced in their facility was nearly uniform ahead of the normal shock wave, as contrasted with the spherical source flow produced in the free-jet facility used here. The free jet flow field is considered in Section III of this report. For their situation the theory predicted virtually no deviation from a constant electron temperature through the whole process.

Within experimental scatter this prediction was found to be true.

In two papers Murty (1968, 1969) extended the Grewal and Talbot analysis to include a very simplified treatment of radiative heat transfer and variable ionization fraction. In both of these papers he has linearized the equations describing flow phenomena that are essentially non-linear in origin, and therefore his treatment can only be considered as a formulation of the problem.

The most recent consideration of the problem is the work of Kirchoff (1969). He modifies the Grewal and Talbot analysis in two important ways. He allows recombination along with its associated energy addition to the electron gas (see Section III-C). He uses experimental data for the heavy particle property profiles through the shock wave, thus dispensing with the thin shock assumption. These assumptions apply well to his situation and he finds that predictions compare well with his experiments which were also carried out in the nearly uniform flow field produced by a contoured nozzle.

As shown in Section III-C the flow may be considered frozen in the present case. It may be thought that the Grewal and Talbot analysis should be applicable. Before application of their results all of their assumptions were rigorously checked in the light of

Jaffrin's later full analysis of the problem. The results are presented below. In particular it was found that these two existing analyses utilized different expressions for the transport properties.

Neglecting electron-neutral collisions, Jaffrin calculated the charged particle cross sections assuming binary collisions and a Debye length cutoff criterion. He calculated K_e using the Fay mixture rule arriving at the value:

$$K_e/k = 0.77 \cdot 10^{13} T_e^{5/2}/\ln\Lambda \qquad (\text{m sec})^{-1}$$

This value was also used in the analysis of Kamimoto et al.

Grewal and Talbot used the Spitzer-Haerm value for K_e in their calculations. This value, as quoted by them is:

$$K_e/k = 3.22 \cdot 10^{13} T_e^{5/2}/\ln\Lambda \qquad (\text{m sec})^{-1}$$

Under the same assumption of negligible electron-neutral influence, Equation (B-21) reduces to

$$K_e/k = 1.35 \cdot 10^{13} T_e^{5/2}/\ln\Lambda \qquad (\text{m sec})^{-1}$$

The problem is that in interpreting Spitzer and Haerm's results, Grewal and Talbot have used the wrong form of K_e. Spitzer and Haerm (1953) postulate phenomenological equations between current flux and heat flux, and electric field and temperature gradient in their equations (25) and (26). The equations are written in the correct form as considered in the theory of irreversible thermodynamics. The flux quantity represented by the current is driven by the linear sum of the force quantities represented by the electric field and the temperature gradient. This equation is easily recognized as a form of the generalized Ohm's law. A similar relation is given for the flux quantity represented by the heat flux. The coefficients of the proportionality are the respective transport coefficients. It is necessary to note that here in the absence of any electric field there will remain a current flux driven by the temperature gradient. In the case that there is no current flux, as we have here, an electrostatic field will be set up to oppose this effect. This is indeed the result found from the consideration of the electron momentum equation. The temperature gradient causes an electric field to be formed inside the shock and results in a plasma potential change across the shock. This field is solved

for and substituted into the heat flux equation to alter the value of K_e from the general case. This is in fact done by Spitzer and Haerm and results in their equation (37) for the so modified K_e. Since there are no current fluxes in the present case, then this modified value of K_e is the correct one to be used. Grewal and Talbot used the un-modified value and it is for this reason that their expression differs from that used here. The approximations used by Jaffrin result in a value very close to that of Spitzer and Haerm who used a Fokker-Planck formulation.

An analysis of the problem is carried out below using the correct expression for K_e/k and utilizing many simplifications and insights afforded by recent considerations of similar phenomena.

The normal shock wave will be analyzed using a Navier-Stokes model for the electrons. This model is valid for cases of slightly disturbed equilibrium distribution functions and is thus applicable to the electron gas as discussed in Section III. One dimensional steady flow of a slightly ionized gas with $\alpha \ll 1$ will be considered. The flow will be allowed to be in a non-equilibrium thermal state $S \neq 1$. From the results of the discussion in Section III-C, the flow can be considered frozen and thereby inelastic collisions may be neglected. The only energy source term included

in the electron energy equation will be that describing energy transfer between the heavy particles and the electrons through elastic collisions. No external electric or magnetic fields will be allowed and no currents will flow in the plasma.

From the theory for elastic collisions developed in Section III-C it may be seen that the characteristic time for neutral-ion thermal accomodation is extremely short because of the almost identical masses of the two species. Throughout the flow field the neutral and ion temperatures may be assumed equal and given by a heavy species temperature. From consideration of the ion momentum equation, Jaffrin (1965) shows that if:

$$\left[\frac{m_e}{m_i}\right]^{0.5} \left[\frac{L_{in}}{L_{ii}}\right]_2 << 1$$

then there is negligible ion slip and the ions and neutrals travel at the same velocity. From consideration of the mean free path equations presented in Appendix B:

$$\left[\frac{L_{in}}{L_{ii}}\right]_2 = \frac{256}{25M_1^4} \left[\frac{L_{in}}{L_{ii}}\right]_1 \quad \text{for large M.}$$

Using the data of Table II one sees that ion slip is indeed negligible in the present case.

Every previous analysis of this problem has assumed quasi-neutrality to exist in the flow field. This assumption can be verified upon examination of the electron momentum equation. The inertial and viscous force terms can be shown to be negligible leaving the pressure gradient term to balance the electric force term. This is the definition of Boltzmann equilibrium and the electrons are seen to be in an equilibrium distribution throughout the shock wave. This was theoretically found to be true by Jaffrin and experimentally verified by Kamimoto et al.

An order of magnitude estimate can now be made of the electric field. Using Poisson's equation the degree of charge imbalance can be estimated as:

$$\frac{n_i - n_e}{n_{eo}} \sim \left[\frac{L_{DO}}{L_{nn}}\right]^2 << 1 \qquad \text{(II-2)}$$

the last inequality is verified upon examination of Table II. Therefore quasi-neutrality can be assumed in the plasma.

Assuming that no currents exist in the plasma:

$$j = e(n_i u_i - n_e u_e) = 0 \qquad \text{(II-3)}$$

and that quasi-neutrality prevails one has that

$$u_e = u_i = u_n \qquad \text{(II-4)}$$

From the expressions derived for the coefficients of viscosity for each specie from Equation (B-19)

$$\left(\frac{\mu_e}{\mu_i}\right) \sim \left(\frac{m_e T_e}{m_H T_H}\right)^{0.5} << 1$$

$$\left(\frac{\mu_e}{\mu_n}\right) \sim \left(\frac{m_e T_e}{m_H T_H}\right)^{0.5} << 1 \qquad \text{(II-5)}$$

From Equation (II-4) one sees that all the species will experience the same velocity gradient in the shock. From Equation (II-5) it is seen that the heavy particles will provide the viscous dissipation and therefore will form the shock wave.

Using Equation (B-16) one sees that:

$$\frac{K_e}{K_i} \sim \left(\frac{m_H T_e}{m_e T_H} \right)^{0.5} >> 1$$

$$\frac{K_e}{K_n} \sim \left(\frac{m_H T_e}{m_e T_H} \right)^{0.5} >> 1 \qquad \text{(II-6)}$$

so that the electrons might be expected to provide most of the transport of thermal energy in the problem.

Jaffrin has shown that for weakly ionized gases the heavy particle shock wave is unaffected by the presence of charged particles. This condition uncouples the neutral specie equations from those of the charged particles and allows the neutral particle shock property variations to be solved for separately. Due to the large ion-neutral cross section and the close equality of ion and neutral particle masses, the ions specie property variations tend to follow those of the neutral specie although the ion shock may be slightly more diffuse than the neutral shock. The electrons are bound closely to the ions through strong electrostatic forces. This fact is reflected in the very short Debye lengths experienced in the plasma as was shown in the justification of the quasi-neutrality

assumption mentioned above. The electron density variation, then, is forced to follow the ion density variation through the shock wave and the electrons are compressed. Since the electrons are very subsonic as shown in Section III-A, their flow field cannot support such a jump in all properties across the heavy particle shock and their temperature distribution through the shock wave tends to be very broad. Because of the high electron thermal conductivity the electrons readily transfer energy from the downstream side of the shock upstream, thus raising the electron temperature in the upstream side of the shock wave. This leads to a hot electron precursor region in front of the heavy particle shock wave.

The mathematical problem is thus seen to lie in the consideration of the electron internal energy equation, in which the effect of the shock wave is imposed through an enforced jump in the electron number density and heavy particle temperature. In this manner the electron energy equation will be examined and solutions developed for the response of the electron temperature to a specified jump in properties caused by the shock wave.

The electron energy equation, Equation (III-19) may be written in one dimensional form as follows. Viscous terms are neglected as discussed in Section III-C.

$$\frac{3}{2} nu \frac{dT}{dx} + nT \frac{du}{dx} - \frac{d}{dx}\left(\frac{K}{k} \frac{dT}{dx}\right) = Z/k \quad \text{(II-7)}$$

inelastic energy transfer, H, is neglected under the frozen flow assumption.

As discussed in Appendix B, the effect of electron-neutral collisions may be neglected for the conditions encountered here. Equations (B-21) with unity denominator will be used for K and Equation (B-22) with the characteristic collision time taken as that applying to electron-ion collisions will be used for Z. Since $\ln \Lambda$ does not vary appreciably through the shock process it will be considered to be a constant calculated at its reference value.

The equation may be non-dimensionalized using Equations (III-25) augmented by:

$$\begin{aligned} x &= x/L \\ \tilde{T}_H &= T_H/T_{HO} = ST_H/T_{eo} \end{aligned} \quad \text{(II-8)}$$

For the present analysis the characteristic length L will be taken as the hot electron precursor length.

Using the frozen electron continuity equation:

$$\frac{d\, nu}{dx} = 0 \quad , \quad \tilde{n}\tilde{u} = 1 \tag{II-9}$$

one arrives at the dimensionless electron energy equation.

$$\frac{d}{d\tilde{x}}\left(\tilde{T}^{5/2}\ \frac{d\tilde{T}}{d\tilde{x}}\right) - D\ \frac{d\tilde{T}}{d\tilde{x}} + \frac{2}{3}\ D\ \frac{\tilde{T}}{\tilde{n}}\ \frac{d\tilde{n}}{d\tilde{x}} + G\ \frac{\tilde{n}^2}{\tilde{T}^{3/2}}\left(\frac{\tilde{T}_H}{S} - \tilde{T}\right) = 0 \tag{II-10}$$

where

$$D = \frac{3}{2}\ \frac{n_o u_o L}{K_o/k}$$

$$G = \frac{3}{2}\ \frac{n_o L^2}{t_{coll\ o}\ K_o/k} \tag{II-11}$$

The equation may be brought into even more general form by the substitution

$$\tilde{y} = D\tilde{x} \tag{II-12}$$

resulting in:

$$\frac{d}{d\tilde{y}}\left(\tilde{T}^{5/2}\,\frac{d\tilde{T}}{d\tilde{y}}\right) - \frac{d\tilde{T}}{d\tilde{y}} + \frac{2}{3}\,\frac{\tilde{T}}{\tilde{n}}\,\frac{d\tilde{n}}{d\tilde{y}} + \frac{2.565S}{M_H^{\,2}}\,\frac{\tilde{n}^2}{\tilde{T}^{3/2}}\left(\frac{\tilde{T}_H}{S} - \tilde{T}\right) = 0 \qquad \text{(II-13)}$$

where Equation (III-26) was used for K_o/k and Equation (III-27) for $t_{coll\ o}$. The reference Mach number is defined by:

$$M_H^{\,2} = \frac{3m_H u_o^{\,2}}{5\,k\,T_{HO}} \qquad \text{(II-14)}$$

Thus the whole problem can be non-dimensionalized in such a manner that the solution depends only upon the parameters S and M_H.

Real variables are regained through the non-dimensionalization proceedure Equations (III-25) and (II-8) and the relation:

$$x = \frac{2}{3}\,\frac{K_o/k}{n_o\,u_o}\,\tilde{y} = \frac{9\cdot 10^{12}\,T_{eo}^{\,5/2}}{n_{eo}\,u_o\,\ln\Lambda}\,\tilde{y} \qquad \text{(II-15)}$$

The expression D appearing in Equation (II-12) and in Equation (II-15) is seen to be a Peclet number. The characteristic length of the precursor is scaled with this Peclet number.

Jaffrin's exact analysis has shown that the hot electron precursor extends over a considerably larger region than the width of the shock wave. In this upstream region then one may set:

$$\tilde{n} = 1$$

$$\frac{d\tilde{n}}{d\tilde{y}} = 0$$

$$\tilde{T}_H = 1$$

and the resulting upstream equation for electron temperature is:

$$\frac{d}{d\tilde{y}}\left(\tilde{T}^{5/2}\frac{d\tilde{T}}{d\tilde{y}}\right) - \frac{d\tilde{T}}{d\tilde{y}} - \frac{2.565\,S}{M_H^2}\tilde{T}^{-3/2}\left(\tilde{T} - S^{-1}\right) = 0 \qquad \text{(II-16)}$$

Downstream of the shock the properties may be written as:

$$\tilde{n} = \tilde{n}_2 = \frac{(\gamma+1)M_H^2}{(\gamma-1)M_H^2+2} \simeq 4$$

for $M_H^2 >> 3$ which is certainly valid here; and

$$\tilde{T}_H = \tilde{T}_{H2} = 1 + \frac{2(\gamma-1)}{(\gamma+1)^2}\,\frac{\gamma M_1^2+1}{M_1^2}(M_1^2-1) \simeq \frac{5}{16}\,M_H^2$$

for $M_H^2 >> 16/5$. The electron energy equation may be written in this region as:

$$\frac{d}{d\tilde{y}} \left(\tilde{T}^{5/2} \frac{d\tilde{T}}{d\tilde{y}}\right) - \frac{d\tilde{T}}{d\tilde{y}} - 41.1 \frac{S}{M_H^2} \tilde{T}^{-3/2}\left(\tilde{T} - \frac{5M_H^2}{16\,S}\right) = 0 \qquad \text{(II-17)}$$

To join these two regions it is necessary to integrate the full electron energy equation, Equation (II-13) across the shock wave.

$$\tilde{T}^{5/2} \frac{d\tilde{T}}{d\tilde{y}}\Bigg]_1^2 - \tilde{T}\Bigg]_1^2 + \frac{2}{3}\int_1^2 \frac{\tilde{T}}{\tilde{n}}\, d\tilde{n} + \frac{2.565S}{M_H^2}\int_1^2 \frac{\tilde{n}^2}{\tilde{T}^{3/2}}\left(\frac{\tilde{T}_H}{S} - \tilde{T}\right)d\tilde{y} = 0$$

(II-18)

The integrations can be simplified by the use of some of the results of Jaffrin's analysis. He found that the electron temperature was relatively constant across the shock wave and that the thickness of the shock wave was much smaller than the precursor thickness. These results were experimentally verified by Kamimoto et al. Using the mean value theorem and denoting the mean values of the variables within the shock wave by a subscript s:

$$\tilde{T}^{5/2}\,\frac{d\tilde{T}}{d\tilde{y}}\Bigg]_1^2 + \frac{2}{3}\,\tilde{T}_s \int_1^2 \frac{d\tilde{n}}{\tilde{n}} + \frac{2.565S}{M_H^2}\,\frac{\tilde{n}_s^{\,2}}{\tilde{T}_s^{\,3/2}}\left(\frac{\tilde{T}_{Hs}}{S} - \tilde{T}_s\right)\tilde{y}\Bigg]_1^2 = 0 \qquad \text{(II-19)}$$

Since the shock wave is so much thinner than the precursor characteristic length thickness

$$\tilde{y}_2 - \tilde{y}_1 \sim (x_2 - x_1)/L \ll 1$$

and the last term vanishes. Integrating the second term

$$\frac{d\tilde{T}}{d\tilde{y}}\Bigg]_1^2 = -\frac{2}{3}\,\tilde{T}_s^{-3/2}\,\ln 4 \qquad \text{(II-20)}$$

Although the electron temperature is constant throughout the shock profile, the shock wave causes a discontinuity in its first derivative.

Equation (II-16) is integrated from the "free stream" point $\tilde{y} = 0$ where the boundary conditions are:

$$\tilde{T} = 1$$

$$\frac{d\tilde{T}}{d\tilde{y}} = 0 \qquad \text{(II-21)}$$

up to the shock positioned at $\tilde{y} = \tilde{y}_s$.

Equation (II-17) is integrated from the downstream point $\tilde{y} = +\infty$ where the boundary conditions are:

$$\tilde{T} = \tilde{T}_2 = \tilde{T}_{H2}/S$$

$$\frac{d\tilde{T}}{d\tilde{y}} = 0 \qquad \text{(II-22)}$$

upstream to the shock at $\tilde{y} = \tilde{y}_s$.

Equation (II-20) can be called the jump condition. It enables the two solutions to be matched at the shock and establishes the position of the shock or equivalently the length of the precursor, $\tilde{y}_s$.

The downstream behavior of T_e is found by integrating Equation (II-17) from the point $\tilde{y} = +\infty$ back to the shock position $\tilde{y} = \tilde{y}_s$. Examining the phase plane behavior one writes

$$N = d\tilde{T}/d\tilde{y} \qquad \text{(II-23)}$$

and Equation (II-17) becomes:

$$\frac{dN}{d\tilde{T}} = \frac{N\tilde{T}^{-5/2} - \frac{5N^2}{2\tilde{T}} + \frac{41.1\,S}{M_H^2}\,\frac{\tilde{T} - \tilde{T}_{H2}/S}{\tilde{T}^4}}{N} \qquad \text{(II-24)}$$

At the starting point $\tilde{y} = +\infty$ the boundary conditions are

$$\tilde{T} = \tilde{T}_H/S$$

$$N = \frac{d\tilde{T}}{d\tilde{y}} = 0$$

revealing that it is a singular point which is seen to be a saddle point upon application of Poincare's criteria.

Since the singularity at downstream infinity is a saddle point it is possible to integrate out of it in an upstream direction. A solution is sought in the phase plane resulting in $N = N(\tilde{T})$. From the definition of N, Equation (II-23), one sees that knowing this solution will allow one to find the position of the shock using the jump condition, Equation (II-20). The proceedure is to solve the downstream problem in the phase plane for $N = N(\tilde{T})$ and obtain a sufficient number of data points, say from the starting point

$\tilde{T} = \tilde{T}_{H2}/S$ to $\tilde{T} = 1.5$. Then the upstream solution is calculated from Equation (II-16) in the real plane yielding $\tilde{T} = \tilde{T}(\tilde{y})$ and $\frac{d\tilde{T}}{d\tilde{y}} = \frac{d\tilde{T}}{d\tilde{y}}(\tilde{y})$. Using the jump condition, Equation (II-20) the value $\tilde{y}_s$ is found such that:

$$\left(\frac{d\tilde{T}}{d\tilde{y}}\right)_2 - \left(\frac{d\tilde{T}}{d\tilde{y}}\right)_1 = -\frac{2}{3}\tilde{T}_s^{-3/2} \ln 4$$

and

$$\tilde{T}_1 = \tilde{T}_2 = \tilde{T}_s$$

A solution is started near the downstream saddle point by linearizing Equation (II-17) around the downstream boundary conditions given by Equation (II-22). The linearized solution near $\tilde{y} = +\infty$ is:

$$\tilde{T} = \tilde{T}_{H2}/S + C \exp\left(-b\left(\tilde{y} - \tilde{y}_s\right)\right) \qquad \text{(II-25)}$$

where

$$b = \frac{1}{2}\left(\frac{S}{\tilde{T}_{H2}}\right)^{5/2}\left[\left(1 + 164.4\,\frac{\tilde{T}_{H2}}{M_{H2}}\right)^{0.5} - 1\right] \qquad \text{(II-26)}$$

and C is a constant to be determined later.

Using this linearized solution one can calculate the initial phase plane trajectory slope near the saddle point.

$$\left(\frac{dN}{d\tilde{T}} \right)_{+\infty} = -b \qquad \text{(II-27)}$$

This condition is coupled with the $\tilde{y} = +\infty$ boundary conditions

$$N = 0$$

$$\tilde{T} = \tilde{T}_{H2}/S$$

and the integration is started in the phase plane. This integration was carried out by means of a Runge-Kutta scheme written by the author for CITRAN.

Examining Equation (II-16), the upstream solution, in the phase plane one finds:

$$\frac{dN}{d\tilde{T}} = \frac{N\tilde{T}^{-5/2} - \frac{5N^2}{2\tilde{T}} + \frac{2.565\ S}{M_H{}^2} \frac{\tilde{T} - S^{-1}}{\tilde{T}^4}}{N}$$

at the starting point $\tilde{y} = 0$ the boundary conditions are

$$N = 0$$

$$\tilde{T} = 1$$

and if $S = 1$ one sees that it is a singular point just as Jaffrin found

in his analysis. For the case that is investigated here $S > 1$ and a regular solution can be started from the upstream "free stream" point $\tilde{y} = 0$. The integration of Equation (II-16) was carried out by means of a Runge-Kutta scheme developed by the author for CITRAN.

This upstream solution together with the downstream phase plane solution and the jump condition are sufficient to determine the value of $\tilde{T}_s$ at the shock and the shock position $\tilde{y}_s$ which gives the length of the precursor.

The results of Jaffrin show that the electron temperature is raised to a value very near to its final downstream value of T_{H2} due to heating in the precursor by the time the shock is reached. In this case $T_s \simeq T_{H2}$ and $T \simeq T_{H2}$ everywhere downstream of the shock. Therefore a solution for T linearized about its downstream value of $\tilde{T}_{+\infty} = \tilde{T}_{H2}/S$ may be valid for the entire region downstream of the shock and not only near the saddle point at $\tilde{y} = +\infty$ as mentioned earlier. When this is true it is possible to eliminate the downstream phase plane analysis and solve for the upstream precursor region in a simplified manner. This proceedure is outlined in Appendix D.

This method was used to generate a graph of precursor length versus Mach number M and non-equilibrium parameter S. This graph is shown as Figure (1). The abcissa is given as $\tilde{y}_s S^{5/2}/M_H$ in order to allow comparison to the calculations of Grewal and Talbot. If the value of T_s differed by more than ten percent from its downstream value (the heavy particle temperature behind the shock) the lines are shown as dotted. It is suggested that the downstream phase plane analysis be used to verify calculations in these cases. It may be seen that longer precursor lengths are predicted by the present analysis than those predicted by the analysis of Grewal and Talbot, resulting from the use of a different expression for the electron thermal conductivity in this analysis.

The theoretical electron temperature profile upstream of a one dimensional shock wave was calculated for the conditions corresponding to test 6 of Section V. The initial reference values were taken at the low point in the experimentally measured electron temperature profile:

$$S = 13.2$$

$$T_{eo} = 3300^{o}K$$

$$T_{HO} = 250^{o}K$$

$$n_{eo} = 3.1 \cdot 10^{17}/m^{3}$$

$$M_{H} = 10.5$$

The x axis was transformed from the computer output for $\tilde{y}$ by the application of Equation (II-15). The results are shown in Figure 2.

Further insight may be drawn from this analysis. The results of Kamimoto et al clearly show that even if the electron temperature is initially equal to the final heavy particle temperature, T_{H2}, a precursor exists in which the electrons are heated to a value above their final temperature by the time the shock is reached and then relax downstream to their final temperature. It is of interest to find the boundary above which there is no precursor at all and the electrons relax through the whole process, never being heated up. For any electron cooling to take place

$$\tilde{T}_{S} > \tilde{T}_{H2}/S$$

Writing the integral criterion Equation (D-2)

$$\left(\frac{d\tilde{T}}{d\tilde{y}}\right)^{+} = -b\left(\tilde{T}_s - \tilde{T}_{H2}/S\right) = \left(1 - \frac{2}{3}\ln 4\right)\left(\tilde{T}_s\right)^{-3/2}$$

$$-\left(\tilde{T}_s\right)^{-5/2} + \frac{2.565S}{M_H{}^2\tilde{T}_s{}^{5/2}} \int_0^{\tilde{y}_s} \left(\tilde{T} - 1/S\right)\tilde{T}^{-3/2}\, d\tilde{y}$$

The left hand side of this equation is less than zero. At the initial point $\tilde{y} = 0$, $\tilde{T} = 1$ and the right hand side is equal to $-2/3 \ln 4$ and as the integration proceeds it becomes more and more positive. The border case then is when the left and right hand sides balance at the starting point $\tilde{y} = 0$. In this case the shock takes place immediately and there is no precursor at all. Thus there is no electron heating if

$$b(1 - \tilde{T}_{H2}/S) \geq \frac{2}{3} \ln 4$$

The left hand side of this equation was numerically calculated and the border-line case of equality was found such that

$$\tilde{T}_{H2}/S \leq 0.82$$

or

$$M_H{}^2/S \leq 2.625$$

results in no precursor formation. The regions are shown in Figure 3.

B. The Dark Space

The foregoing analysis has shown that it is theoretically possible for a region of high electron temperature to precede a normal shock wave in a partially ionized gas. It is now necessary to relate this layer of high electron temperature to the appearance of the observed dark region.

Having been ionized in the arc heating process, the plasma is in the process of recombination as it passes through the free jet flow field. For the situation at hand there exist two different processes by which an electron and ion may recombine to form a ground state atom: radiative and three body collisional. In actuality the route of recombination is a combination of these two processes and can be considered as collisional-radiative recombination after Bates, Kingston and McWhirter (1962). The ion density measurements reported in Section V show that the plasma is frozen to recombination to within the sensitivity of the measurement procedure, however, calculations done in Section III-C reveal that a very small amount of recombination is taking place in the flow field which is the source of the radiation emitted by the plasma.

In very dense plasmas the primary recombination process consists of three body collisions in which the third body, an electron, carries off the excess energy. Makin and Keck (1963) have studied this process and shown that the overall rate of recombination is inversely proportional to the nine halves power of the electron temperature. Thus hot electrons tend to inhibit recombination, but this says nothing about the quenching of radiation. In an experimental program Hinnov and Hirschberg (1962) found that the initial capture of a free electron to one of the excited states of the atom did depend upon a three body collision and that subsequent step by step transfers of the electron down to an energy level approximately kT_e below the continuum were effected through the same process. They found that electrons lying in energy levels above this critical quantum level were in Saha equilibrium with the free electron gas. By solving for the rate of transfer through this critical level they also show that the overall rate of recombination is proportional to the inverse nine halves power of the electron temperature. Bates, Kingston and McWhirter (1962) considered both collisional and radiative processes and showed that for transitions between high energy states (large quantum number) the collisional process far overshadowed the

radiative process. Above a certain critical quantum number the electrons will be in Saha equilibrium with the free electron gas. The model suggested by Byron, Stabler and Bortz (1962) was one of three body capture of a free electron to an excited state followed by both collisional and radiative de-excitation to the ground state. They found a minimum in the de-excitation rate at a critical quantum number which served as a "bottleneck" limiting the overall rate of recombination. This rate acts as the slowest rate in a series of chain reactions. Above this critical level the trapped electrons exist in Saha equilibrium with the free electron gas and energy level transitions are controlled by collisional rates while below this critical level transitions are primarily radiative. The critical quantum level is seen to decrease with increasing electron temperature. The overall recombination rate is calculated as the rate of transition through this "bottleneck", and is seen to decrease with increasing electron temperature.

From these researches a general picture of the process of recombination can be drawn. A free electron is captured into an excited state by means of a three body collision and transfers downward to a certain critical quantum level primarily by means

of three body collisions. Below this critical quantum level the transitions to the ground state are primarily radiative, supplying the radiation emitted by the plasma. The quantity of radiation emitted by the plasma depends upon the overall recombination rate, and the quality of radiation emitted depends upon the level of the critical quantum state. The treatment of Hinnov and Hirschberg (1962) assumes that the overall rate of recombination is controlled by collisional processes and is an inverse function of the electron temperature. The theory of Bates, Kingston and McWirter (1962) and Byron, Stabler and Bortz (1962) which was applied specifically to argon by Chen (1969) considers the overall rate of recombination to be controlled by both collisional and radiative processes, however the results also show an inverse dependence upon electron temperature. No matter which model one chooses the overall rate of recombination and with it the quantity of radiation emitted decreases with an increase in electron temperature. This fact alone can explain the relation between the hot electron precursor measured and the dark region observed in this research. Beyond these considerations however are factors controlling the quality of the radiation emitted. All of the previous treatments show that the critical

quantum level moves down with increasing electron temperature and that transitions above this level are primarily collisional. In this manner hot electrons have the effect of removing the continuum and lower energy (visible) lines from the recombination spectrum as well as lowering the overall quantity of radiation emitted. In the rather cursory study mentioned in Appendix A the continuum and red lines of the argon spectrum were found to be absent, upholding this idea. In this manner the hot electron precursor that was theoretically proposed and experimentally verified in this research quenches the recombination radiation of the plasma and moves the existing radiative processes out of the visible region thus causing the observed dark region in front of a normal shock wave.

III. Free Jet Theory

A. The Free Jet Flow Field

Free jet flow fields have been used for a number of different types of studies. One fruitful application has been the use of a free jet as a source of aerodynamically intensified molecular beams. This line of application is exemplified by the work of Bier and Hagena (1963), Scott and Drewry (1963), Fenn and Deckers (1963) and more recently Knuth et al. (1967). Another, perhaps unusual, application of the free jet flow field was a scheme for isotope separation suggested by Zigan (1962). A more usual application is exemplified by the use of a free jet as an experimental facility in which near free molecular flow phenomena are investigated. Such work has been done by Maslach et al. (1966). The physical model for the free jet flow field has also been used to describe exhaust plumes from high altitude rockets as exemplified by the work of Albini (1965) and Hill and Draper (1966).

The free jet flow field was first suggested for use in low density aerodynamic testing by Sherman (1963), because of the

strict limitations imposed on steady state low density wind tunnel facilities. A large Knudsen number for the model tested is desired and there are two ways of obtaining this goal: either with a large mean free path in the test section or a small model dimension. Small models cause instrumentation problems for sophisticated experiments, so the emphasis has been upon the attainment of large mean free paths. A large mean free path for a given body size and desired Mach number implies a low Reynolds number. A low Reynolds number flow in a typical hypersonic nozzle causes the formation of thick laminar wall boundary layers, which leave very little of the cross sectional area of the test section available as isentropic core flow for test use. Thus large nozzles are needed which in turn require large pump capacities. It is desirable to have the largest range of Mach and Reynolds number variation as possible, in particular, to have a large mean free path and at the same time retain a large isentropic core flow.

Free jet testing was advanced as a solution to these problems. The free jet facility consists of a converging nozzle or orifice which accelerates the flow to sonic speed, followed by a free jet expansion into an ambient pressure much less than the reservoir total pressure. It allows isentropic flow development

to a very high Mach number if the ratio of the total pressure to ambient pressure is high enough. The Reynolds number may be adjusted without any appreciable effect on the Mach number distribution, whereas, in the usual hypersonic facility, a lowering of the Reynolds number results in a decrease in the attainable Mach number due to thickening boundary layers.

The flow field of a free jet may be divided into three regions for description: the entry section, the flow field proper, and the bottom shock, as shown in Figure 4.

In the entry section transonic flow exists through a rapidly converging axisymmetric nozzle or orifice in a thin wall. The details of the transonic region have little effect upon the flow field at a distance more than one orifice diameter downstream. This fact was experimentally verified by Ashkenas and Sherman (1966) who showed that the downstream flow was virtually the same in either the case of a sharp edged orifice or a converging axisymmetric nozzle in the entry section. The Reynolds number in the entry section has little effect on the downstream properties in the flow field either. Gregorek and Luce (1966) found no effect on the flow field as reflected in the pitot pressure distribution when the total pressure in the reservior region was varied. Sherman (1963) also

found the same pitot pressure distribution when he operated at two different values of total pressure and both results compared favorably with the Owen and Thornhill (1952) theory (see below). There is, however, a slight boundary layer displacement effect in the throat that is reflected in the nozzle discharge coefficient. In cold flow experiments this effect decreases the effective area of the throat. In hot flow experiments where the stagnation temperature is much higher than the entry section wall temperature, there is a negative displacement thickness effect caused by heat transfer to the wall which increases the effective area of the throat. In high enthalpy applications where real gas effects depending upon rate processes are taking place it is important to make the converging entrance section to the throat as smooth as possible to avoid sharp gradients and to assure the maintenance of equilibrium up to the orifice at the throat.

A rapid expansion begins at the lip of the orifice and the resulting expansion fan turns the flow away from the jet centerline. The condition of constant pressure on the jet boundary causes it to be continuously bent back towards the axis of the jet from its initially large expansion angle. As the flow changes direction

along the boundary, compression waves are formed from the reflection of the initial expansion fan from the boundary. These compression waves coalesce to form a lateral "barrel" shock surrounding the flow field. Any pressure disturbance that travels toward the jet axis from the boundary is of the same family as these compression waves and is gathered up into the barrel shock. Thus the core flow in the free jet is in the "zone of silence" with respect to disturbances taking place on the boundary. An analysis of this flow was carried out in a simple quasi-one dimensional manner by Adamson and Nicholls (1959). An accurate analysis by the method of characteristics for axisymmetric flow carried out by Owen and Thornhill (1952) in which the isentropic properties throughout the flow field are calculated has been used by other authors as a basis for more simplified physical models of the flow field.

A normal shock, Mach disc, or Riemann wave that decelerates the core flow from hypersonic to subsonic and raises the static pressure to a value very near the ambient pressure appears across the free jet flow field, forming a bottom to the barrel shock system. At low values of p_t/p_a the lateral barrel shock curves in and meets on the jet axis forming the familiar shock diamond pattern.

At high values of p_t/p_a the lateral barrel shock does not form a regular reflection at the jet axis but forms a Mach reflection. In the axisymmetric case the normal shock portion of the Mach reflection forms the Mach disc or bottom shock.

Since the Mach number distribution along the jet axis is a function of stagnation conditions only and is independent of the pressure ratio p_t/p_a, this pressure ratio controls only the size of the phenomenon which is determined by the size and position of the bottom shock. Numerous theoretical solutions for the bottom shock position and size have been published. Adamson and Nicholls(1959) use a characteristic solution for the axial pressure distribution along the jet centerline and propose a bottom shock existing at the axial position where a normal shock would bring the static pressure up to ambient. Thus the size and position of the bottom shock are only a function of p_t/p_a and the orifice exit Mach number. The predicted results compare favorably with the experimental measurements of Love and Grigsby (1959). Gregorek and Luce (1966) use the characteristic solution for the Mach number distribution along the jet centerline which they have experimentally verified is independent of p_t/p_a. They also assume that the bottom shock raises the flow static pressure to ambient and thus locates

the shock. The predicted shock position is verified experimentally through schlieren photography. For an axisymmetric jet in a monatomic gas the resulting expression is

$$x_s/D = 0.82\,(p_t/p_a)^{0.476} \qquad \text{(III-1)}$$

Some experimental studies were also carried out yielding empirical data concerning bottom shock position. Sherman (1963) measured the bottom shock position and found good agreement with the semi-empirical predictions of Love and Grigsby (1959). Crist (1965) experimentally examined qualitative effects on the bottom shock location. He found the axial location to be proportional to the orifice diameter, increasing with increases in p_t/p_a and T_t. He noted that there was no γ effect on bottom shock position when using different gases. The diameter or size of the bottom shock, and with it the lateral extent of the whole flow field, was found to increase with p_t/p_a and orifice diameter. Ashkenas and Sherman derived an empirical formula for the bottom shock position from experimental photographic studies, impact pressure surveys and free molecule wire techniques. The expression is

$$x_s/D = 0.67\,(p_t/p_a)^{0.5} \qquad \text{(III-2)}$$

for shock position, independent of γ for values of p_t/p_a between 15 and 17,000.

The existence of the bottom shock will most certainly separate the boundary layer on any body protruding through it. Also it will have a disruptive effect on any wake behind a body in the core of the jet. Gregorek and Luce (1966) report that a model must be placed at least eight orifice diameters ahead of the bottom shock to avoid its effects. It was for this reason that the original idea of the Langmuir tube was considered. As shown above, any disturbance to the barrel shock is not carried into the flow field but is collected in the shear layer that forms the barrel shock and constant pressure boundary of the jet. Thus the Langmuir tube, piercing the barrel shock to reach the core of the jet, is much less likely to disturb the flow field than a Langmuir probe mounted on a sting and piercing the bottom shock. Design for adequate cooling of course was the deciding factor in the choice of the Langmuir tube.

A sketch of the free jet flow field is given in Figure 4.

Upon inspection of the characteristics solution of the free jet flow field done by Owen and Thornhill (1952), Sherman (1963) suggested that the distribution of flow properties might be closely approximated by a source flow physical model. In this model a three dimensional point source is placed at the orifice and a spherical expansion of the working gas results with the density proportional to the inverse square of the radius. In such a rapid expansion the limit velocity of the working gas is quickly reached on rays extending from the source, since the point at which the Mach number reaches a value of about five is only on the order of two and one half orifice diameters downstream of the source. In such a model the loci of constant properties are spheres. This same source flow model has been used by Hill and Draper (1966) and Albini (1965) in their exhaust plume studies, by Gregorek and Luce (1966) and by Mirels and Mullen (1963) in their study of the unsteady expansion of a gas cloud into a vacuum as applied to a hypersonic jet bounded by a vacuum. The discovery and application of such a simplified physical model is indeed very valuable because of the insight that it affords when studying the physical processes occurring in the flow field.

The source flow model was analyzed in detail by Ashkenas and Sherman (1966). Characteristics solutions were curve fitted with this source flow model to give Mach number and impact pressure distributions. Semi-empirical formulas are presented for these two distributions.

In order to develop a full physical model from which all of the property distributions could be calculated, a source flow model will be developed below which is corrected to yield the Mach number and impact pressure distributions presented by Ashkenas and Sherman (1966). With this corrected source flow model one is able to gain physical insight into the processes taking place in the flow field.

Using the coordinate designations shown in Figure 5 a simple mass balance equation is written

$$\rho^* u^* \frac{\pi D^2}{4} = \rho u_{lim} 2\pi R^2 C \qquad \text{(III-3)}$$

where the velocity is the limit velocity in the inertia dominated region and C is a factor to allow for the fact that in reality the flow does not fill the entire half sphere at R. From the consideration

of the energy equation in a chemically frozen flow, the Mach number distribution in the free jet can be expressed as a function of ρ/ρ^*. Since this ratio is expected to be small the relation is expanded in a Taylor series and the above relation for ρ/ρ^* substituted yielding:

$$M = A(\gamma, C)\left(\frac{x}{D}\right)^{\gamma-1} - \frac{1}{\gamma-1}\left[A(\gamma, C)\left(\frac{x}{D}\right)^{\gamma-1}\right]^{-1} \quad \text{(III-4)}$$

where

$$A(\gamma, C) = \left(\frac{\gamma+1}{\gamma-1}\right)^{\frac{\gamma+1}{4}} (8C)^{\frac{\gamma-1}{2}}$$

Equation (III-4) is in the form that Ashkenas and Sherman (1966) present for their curve fitted Mach number distribution. The value of A that they have empirically found best fits the computed data for a monatonic gas is A = 3.26, which gives C = .2705. By rearranging Equation (III-3) for the source flow model and introducing the mass flow rate $\dot{m}$ and the limit velocity given in Equation (III-7) the corrected source flow model for the density distribution is

$$\rho = 1.822 \cdot 10^{-2}\, \dot{m}/(\sqrt{T_t}\, x^2) \qquad \text{(mks)} \qquad \text{(III-5)}$$

along the centerline where R = x.

From this relation, knowing the stagnation conditions and assuming isentropic flow in the core of the jet, the properties can be calculated at any point in the free jet flow field.

When the flow in the jet is assumed chemically frozen to ionization-recombination processes the electron number density distribution is

$$n_e = \frac{\alpha \rho}{m_H} = 1.495 \cdot 10^{25} \alpha \rho \qquad \text{(mks)} \qquad \text{(III-6)}$$

where α is the frozen ionization fraction that exists in Saha equilibrium at the stagnation conditions. The calculation of α is discussed in Appendix E.

The velocity in the jet being the adiabatic limit velocity for the given total temperature is

$$u = u_{lim} = (5kT_t/m_H)^{0.5} = 32.2\,(T_t)^{0.5} \qquad \text{(III-7)}$$

It can easily be shown that for a monatomic gas, u varies by less than 10% from u_{lim} when the Mach number is greater than 5.5.

Using Equation (III-4) or its plot presented in Figure 6 one sees that the source flow model is valid for any point further than about 2.5 diameters from the orifice.

The model of the flow field may be used to locate the approximate position of the bottom shock using the idea first mentioned by Adamson and Nicholls (1959) that the static pressure behind the bottom shock be made approximately equal to the ambient pressure. Actually Crist (1965) reports measurements that show the pressure here to be about 1.3 times the ambient pressure.

The impact pressure in the hypersonic limit for a monatonic gas is:

$$p_{t2} = 0.883\ \rho_1 u_1^2$$

Behind the bottom shock the Mach number is very low and $p_2 \simeq p_{t_2}$ giving

$$p_a = \frac{0.883}{1.3}\ \rho_1 u_1^2$$

Substituting Equation (III-3) for ρu and Equation (III-7) for u and the calculated value of C, one arrives at

$$x_s/D = 0.713 \quad (p_t/p_a)^{0.5} \qquad \text{(III-8)}$$

Ashkenas and Sherman (1966) report the coefficient to be 0.67 as determined experimentally, independent of γ. Gregorek and Luce (1966) report that experimental results correlate well with Equation (III-1) for a monatomic gas. Equation (III-8) overestimates the Ashkenas and Sherman (1966), Equation (III-2) results by 6% and the Gregorek and Luce (1966) results by 2% at the design operating point of $p_t/p_a = 1,000$.

Because of the great disparity in mass between an electron and either an ion or atom, the electron Mach number is always very much less than the heavy particle Mach number. The elevation of electron temperature above the heavy particle temperature that was experimentally measured here further accentuates this difference since

$$M_e^2 = \frac{m_e}{m_H} \quad \frac{T_H}{T_e} \quad M_H^2 \ll M_H^2 \qquad \text{(III-9)}$$

It is interesting to note that the electron Mach number can never become greater than one. Using the definition

$$M_t = u/(\gamma kT_t/m_H)^{0.5}$$

it can be shown that

$$M_e = (m_e T_t/m_H T_e)^{0.5} M_t$$

and for a monatomic gas the largest attainable value of M_t is $\sqrt{3}$.

The experiments show that T_e remains within one order of magnitude of T_t throughout the expansion so that the electrons are necessarily very subsonic.

A computer program was written on CITRAN to calculate the stagnation properties and field properties as derived from the corrected source flow model described in this section. The experimental data input to the program are the stagnation enthalpy, total pressure, measured electron temperature profile distribution, and the ambient pressure. The stagnation properties: T_t, a, ρ_t, n_{et} are calculated by means of the methods described in Appendix E. The bottom shock position is calculated from Equation (III-8). In the flow field the mass density, electron number density and Mach number distributions are calculated using the chemically frozen corrected source flow model that is described in this section.

The static pressure and temperature are calculated in the flow field by assuming isentropic flow. All of the mean free paths as well as the Debye lengths are calculated using the methods described in Appendix B. The output is printed in tabular form with entries at any chosen number of axial stations.

B. Pitot Pressure Distribution

The pitot pressure distribution in the free jet may be derived from the Mach number distribution that is given by Equation (III-4). Assuming that

$$\left[A(\gamma, C) \left(\frac{x}{D}\right)^{\gamma - 1} \right]^2 >> 1 \qquad \text{(III-10)}$$

The second term in Equation (III-4) may be neglected. The resulting expression for M is substituted into the normal shock expression for p_{t2}/p_{t1} given by Liepmann and Roshko (1957). Under the assumption (III-10) the expression for this ratio then reduces to

$$\frac{P_{t2}}{P_t} = A(\gamma, C)^{\frac{-2}{\gamma - 1}} \left(\frac{\gamma + 1}{2\gamma}\right)^{\frac{1}{\gamma - 1}} \left(\frac{\gamma + 1}{\gamma - 1}\right)^{\frac{\gamma}{\gamma - 1}} \left(\frac{D}{x}\right)^2 =$$

$$= 0.662 \left(\frac{D}{x}\right)^2 \qquad \text{(III-11)}$$

The last equality holds for a monatomic gas. The assumption (III-10) is easily satisfied in the inertially dominated region of the free jet since $x/D > 2.5$ in this region and $A(\gamma, C)$ was shown to be 3.26 in Part A of this Section.

This is the form of the pitot pressure distribution that is presented by Ashkenas and Sherman (1966). However, they have found that their data is matched better if a slight offset is introduced in the x measurement. The expression for a monatomic gas that is derived by them is:

$$\frac{P_{t2}}{P_t} = 0.662 \left(\frac{x}{D} - 0.04\right)^{-2} \qquad \text{(III-12)}$$

It is possible to show that this correction offset could arise from the error introduced by the shock wave standoff distance. The

probe is actually sampling the pressure at a point displaced upstream from the probe nose by this amount.

The ratio of the shock detachment distance to the diameter of a blunt nosed cylinder is shown by Liepmann and Roshko (1957) p. 105, to asymptotically approach a value of 0.27 in air as the Mach number increases. Dividing by the hypersonic correction factor

$$\frac{\left(\frac{\gamma - 1}{\gamma + 1}\right)_{\text{argon}}}{\left(\frac{\gamma - 1}{\gamma + 1}\right)_{\text{air}}}$$

to render this ratio independent of γ, the value 0.09 is arrived at. For a probe diameter of 0.125 inches, the shock displacement thickness divided by the sonic orifice diameter is 0.045. The correspondence with the correction factor in Equation (III-12) may be considered fortuitous. However when the same procedure is carried out for a free jet operating in air, the correction factor becomes 0.13 which is also the same as the correction suggested by Ashkenas and Sherman for use in Equation (III-12) in experiments using air.

For comparison with the pitot pressure experiments described in Section IV, Equation (III-11) was used to provide a theoretical distribution.

C. The Electron Temperature Distribution

The flow in the free jet is assumed to be frozen to the recombination reaction. This assumption may be examined through the consideration of the electron continuity equation.

The recombination process may be represented in the right hand side of the electron continuity equation as a (negative) source term

$$- \partial n_e / \partial t = a n_e^2 \qquad \text{(III-13)}$$

where a is the recombination rate constant. From this relation a characteristic time for the recombination rate process may be derived.

$$t_{chem} = (a_o n_{eo})^{-1} \qquad \text{(III-14)}$$

The convective term on the left hand side of the electron continuity equation may be written as:

$$u \; dn_e/dR \qquad \text{(III-15)}$$

since the velocity is constant as discussed previously. From this term, a convective characteristic time may be derived

$$t_{conv.} = R_o/u_o \qquad \text{(III-16)}$$

The ratio

$$t_{conv.}/t_{chem.} = n_{eo}R_o a_o/u_o \qquad \text{(III-17)}$$

gives the relative importance of the two processes: convection and chemistry, in altering the electron density.

For the conditions experienced in the flow field, this ratio varies from a value of $1.3 \cdot 10^{-4}$ using the collisional-radiative rate constant of Chen (1969) to $8.5 \cdot 10^{-5}$ using the three body rate constant of Makin and Keck (1963). Thus the particles traverse the flow field in much less time than it takes for them to chemically react. The flow field can be considered frozen to recombination reactions as far as the continuity equation is concerned and the electron continuity equation may be written as:

$$nu = B/R^2 \qquad \text{(III-18)}$$

where B is a constant.

The electron energy equation in tensor form is derived from the Boltzmann equation for the case of a non-equilibrium plasma by Appleton and Bray (1964). If one makes the assumption that the electrons act as a Newtonian, monatomic gas, this equation reduces to a familiar form. (All species subscripts are omitted.)

$$\frac{3}{2} u_j kn \frac{\partial T}{\partial x_j} + nkT \frac{\partial u_j}{\partial x_j} + \frac{2}{3} \mu \frac{\partial u_k}{\partial x_k} \frac{\partial u_j}{\partial x_j} -$$

$$-\mu \frac{\partial u_k}{\partial x_j} \left(\frac{\partial u_k}{\partial x_j} + \frac{\partial u_j}{\partial x_k} \right) - \frac{\partial}{\partial x_j} \left(K \frac{\partial T}{\partial x_j} \right) = Z + H \qquad \text{(III-19)}$$

where Z and H refer to elastic and inelastic collisional energy source terms respectively.

Comparing the order of magnitude of the viscous terms to the thermal conduction term, one sees that

$$\frac{\text{Viscous Terms}}{\text{Thermal Conduction Terms}} = \frac{\mu_o u_o^2}{L^2} \frac{L^2}{K_o T_o} = \frac{4}{9} M_e^2 \qquad \text{(III-20)}$$

using Equations (B-15) and (B-16).

Since the electron Mach number is much less than one everywhere in the flow field, the effect of the electron viscosity can be neglected in the electron energy equation.

The flow properties along the axis of the free jet follow the distribution given by the source flow model as explained in Part A of this Section. It is appropriate therefore to write the energy equation in spherical coordinates. Using spherical symmetry, the only independent variable is R.

$$\frac{3}{2} B k \frac{dT}{dR} - \frac{kTB}{n} \frac{dn}{dR} - \frac{d}{dR}\left(R^2 K \frac{dT}{dR}\right) = (Z + H)R^2 \quad \text{(III-21)}$$

Elastic collisions supply energy per unit mass to the electron gas at a rate given by Equation (B-25) for Z_e. It is shown in Appendix B that the effect of electron neutral Ramsauer collisions is far overshadowed by the effect of the electron-ion coulombic encounters for the particular situation at hand. Therefore, they will be neglected and the characteristic time $t_{coll,\,i}$ pertaining to the charged particle interaction will be used here.

It is interesting to examine at this point whether or not the electrons and heavy particles have time to approach thermal

equilibrium while traversing the flow field. Thermal equilibrium is accomplished by means of elastic collisions and associated energy transfer so that the appropriate characteristic time would be that given in Equation (B-23).

$$t_{coll.} = 1.02 \cdot 10^{10} T_e^{3/2}/n_e \ln\Lambda \qquad \text{(III-22)}$$

This time should be compared with the characteristic time for convection given by Equation (III-16). For the situation at hand, the ratio of collisional to convective characteristic times lies in the range of 3 to 10. Thus the species should not have sufficient time to equilibrate thermally while traversing the flow field, and this fact is reflected in the great disparity in electron and heavy particle temperatures shown in Figure 24.

Inelastic collisions supply energy to the electron gas through the liberation of the ionization energy in the recombination process. The amount of energy given to the electron gas per recombination event depends upon the particular recombination process. For illustration, consider the quantum mechanical model for recombination proposed by Bates, Kingston and McWhirter (1962) and Byron,

Stabler and Bortz (1962) which is also referred to in Section II. An electron is captured into a highly excited state and transfers downward to the critical quantum level by means of collisional de-excitation in which the electron gas absorbs the excess energy. Transitions below the critical quantum level are primarily radiative and no energy is delivered to electron gas in a optically thin plasma. Thus it is only the energy difference between the continuum and the critical quantum level that is delivered to the electron gas in a recombination event. This difference has been measured to be on the order of kT_e by Hinnov and Hirschberg (1962). The critical quantum level moves down for increasing electron density and temperature thus causing more energy to be delivered to the electron gas per recombination in denser, higher temperature plasmas.

By assuming that the recombination process takes place entirely by a three body de-ionization collision one considers the case when all of the recombination energy is delivered to the electron gas. In this case the maximum possible amount of energy is supplied to the electron gas through inelastic collisions. The rate of energy production per unit mass is then:

$$- \frac{\partial n_e}{\partial t} (I + \frac{3}{2} kT_e) \qquad \text{(III-23)}$$

In this study, the electron temperature was found to be about one-half electron volt which is negligible when compared to the 15.7 electron volt ionization potential. Using the three body rate constant of Makin and Keck (1963) that is discussed in Appendix E, this H then becomes

$$+ a n_e^2 I \qquad \text{(III-24)}$$

The heat conduction coefficient K_e for the electron gas is given by Equation (B-21). As is shown in Appendix B, the effect of the electron-ion encounters far overshadows the effect of the Ramsauer electron-neutral collisions for the conditions experienced in the flow field. Therefore, the electron-neutral collision term in Equation (B-21) will be neglected.

The energy equation is non-dimensionalized using reference quantities

$$\tilde{T} = T/T_o$$

$$\tilde{R} = R/R_o$$

$$\tilde{n} = n/n_o \qquad \text{(III-25)}$$

$$\tilde{K} = K/K_o = \tilde{T}^{5/2}$$

$$\tilde{t}_{coll} = t_{coll}/t_{coll,\,o} = \tilde{T}^{3/2}/\tilde{n}$$

$$\tilde{a} = a/a_o = \tilde{n}/\tilde{T}^{9/2}$$

From the computations in Appendix B:

$$K_o/k = 1.35 \cdot 10^{13}\ T_o^{5/2}/\ln\Lambda \qquad \text{(III-26)}$$

$$t_{coll,\,o} = 1.02 \cdot 10^{10}\ T_o^{3/2}/n_o \ln\Lambda \qquad \text{(III-27)}$$

$$a_o = 2.3 \cdot 10^{-20}\ n_o/T_o^{9/2} \qquad \text{(III-28)}$$

The coefficients of the various terms in the energy equation may be readily examined if one defines certain characteristic times:

$$t_{coll} = t_{coll,\,o} \qquad \text{(III-29)}$$

$$t_{conv} = R_o/u_o \qquad \text{(III-30)}$$

$$t_{chem} = (a_o\, n_o)^{-1} \qquad \text{(III-31)}$$

$$t_{cond} = k\, n_o\, R_o^{2}/K_o \qquad \text{(III-32)}$$

The energy equation now appears as

$$\frac{d}{d\tilde{R}}\left(\tilde{R}^2\,\tilde{T}^{5/2}\,\frac{d\tilde{T}}{d\tilde{R}}\right) - \frac{3}{2}\left(\frac{t_{cond}}{t}\right)_{conv}\left(\frac{d\tilde{T}}{d\tilde{R}} + \frac{4}{3}\,\frac{\tilde{T}}{\tilde{R}}\right) -$$

$$- \frac{3}{2}\left(\frac{t_{cond}}{t_{coll}}\right)\tilde{R}^{-2}\,\tilde{T}^{-3/2}\left(\tilde{T} - T_{HO}\,\tilde{R}^{-4/3}\,T_o^{-1}\right) +$$

$$+ \left(\frac{t_{cond}}{t_{chem}}\right)\frac{I}{kT_o}\,\tilde{R}^{-4}\,\tilde{T}^{-9/2} = 0 \qquad \text{(III-33)}$$

where the source flow solution for T_H developed in Part A of this Section has been substituted in the expression for elastic collisional energy transfer.

The coefficients in front of each term relate the importance of the process represented by the term. A process with a particularly short characteristic time will be the primary process by which the electron energy is determined. Because of the large heat conductivity of the electrons it is expected that conduction will be the predominant process. The first term in Equation (III-33), representing heat conduction, was chosen as the standard by which the importance of the processes represented by the three following terms are gauged. Thus t_{cond} is the common comparison for all of the other characteristic times.

The ratios of the characteristic times may be easily assessed:

$$\frac{t_{cond}}{t_{conv}} = 7.4 \cdot 10^{-14} n_o u_o R_o \ln\Lambda T_o^{-5/2} \simeq 0.074 \qquad \text{(III-34)}$$

$$\frac{t_{cond}}{t_{coll}} = 7.26 \cdot 10^{-24} (n_o R_o \ln\Lambda T_o^{-2})^2 \simeq 0.029 \qquad \text{(III-35)}$$

$$\frac{t_{cond}}{t_{chem}} \frac{I}{kT_o} = 3.12 \cdot 10^{-28} n_o^3 R_o^2 \ln\Lambda T_o^{-8} \simeq 4.8 \cdot 10^{-4} \qquad \text{(III-36)}$$

The values given are for typical operational conditions in the flow field at the axial position x/D = 10.

From this analysis it is easy to see from Equation (III-36) that the flow may be considered frozen even in the electron energy equation. Notice that the condition for frozen flow in the continuity equation was $t_{conv}/t_{chem} \ll 1$ which is less stringent than the above requirement because of the appearance of the factor I/kT_o (or however much energy/mass is given to the electron gas per recombination event). It could easily be imagined that the situation could exist in which the flow field was chemically frozen from the point

of view of mass continuity; however, at the same time, the chemistry of the flow might play a large role in the energy balance. This would allow considerable simplification over the full non-equilibrium problem since it would be possible to solve for the density independently, assuming frozen flow, and then substitute the frozen density distribution into an energy equation in which chemistry is considered. This is what will be done for this case in the following, but from the above analysis, it is clearly permissible to neglect the chemistry altogether.

From the comparison of the characteristic times, it is seen that it may be permissible to ignore all effects other than conduction in this case. Doing this would simplify the non-linear nature of the equation and admit an analytic solution. This was done in order to compare with a later developed full numerical solution .

Considering only the effect of conduction, the electron energy equation can be readily integrated to yield the analytic result:

$$\frac{T}{T_o} = \left(\frac{7}{2}\left(\frac{dT}{dR}\right)_o \frac{R_o}{T_o}\left(1 - \frac{R_o}{R}\right) + 1\right)^{2/7} \qquad \text{(III-37)}$$

This solution was applied by taking an initial value of T_e and dT_e/dx at a given value of x from the experimental data and using these for the reference values. It can be seen that in the case of certain initial conditions it is possible for T to decrease abruptly to zero at a specific value of R. This behavior stems from the idealization involved in considering only non-linear conduction as an energy exchange mechanism. The inclusion of the other terms in the full equation should smooth out this singularity. As was mentioned previously, although these terms look small in Equations (III-34), (III-35), and (III-36) they may become very important in certain regions of the flow field.

The full equation for the electron energy (temperature) distribution was solved by means of a Runge-Kutta integration scheme developed by the author for the CITRAN system. The integration was started at a point near 4 diameters downstream of the orifice in order to minimize the effects of the bottom shock or the body shock on the initial values supplied to the program. The electron temperature and electron temperature gradient were supplied from experimental data taken at this reference point with the Langmuir tube. These initial values together with the operating

parameters of the arc heater, the total enthalpy and total pressure, enabled the solution of the full equation. All of the reference values were computed at this initial point. The integration was performed both upstream and downstream from this initial point to yield an electron temperature profile extending from just in front of the orifice to as far downstream as desired.

By means of a parametric study, the conduction process was found to be dominant as expected. This condition persisted from a point very near the orifice out to a region near the inflection point of the analytic profile for the electron temperature given by Equation (III-37). After this point, the convection, collision, and chemistry processes removed the singular nature of the analytic profile and caused the distribution to decrease smoothly in the downstream direction. It was found that chemistry played a negligible role as was expected. Collisional energy transfer through elastic collisions also played a minor role. The primary process is indeed heat conduction through the electron gas, slightly modified by convection. The theoretical electron temperature profiles drawn on the Figures discussed in Section V were calculated using this theory.

IV. Facility and Tests

A. The Experimental Facility

1. Design

1.1 Arc Heater and Power Supply. The arc heater used in this work is a modified Plasmadyne model SG-1 Arc Plasmatron built by the Giannini Scientific Corporation, Santa Ana, California. The unit was lent to the author by the Space General Corporation of El Monte, California for use in this research. The Plasmatron is a hand-held unit designed for the deposition of refractory materials by plasma spraying.

Initial tests were carried out using a copper anode of the same design as the Plasmatron argon anode but without the refractory powder feed tube. A drawing of the arc heater in this configuration is shown in Figure 7. To eliminate anode attachment instabilities that are described in Appendix A, a short anode was

was designed and utilized which is shown in Figure 8. These design modifications were fully tested and the results are reported in Appendix A.

The original design cathode was used. The cathode is made of a 2% thoriated tungsten rod pointed at the end to control arc attachment and to enhance the thermal emission and field emission of electrons. The thorium reduces the work function of the tungsten which is other wise ideally suited due to its high melting point. The cathode is cooled only at the base to avoid large temperature gradients in the tungsten which have lead to eroding in the past experience of the author. The brazed joint between the tungsten rod and its copper holder must be filed very smooth and polished to avoid anomolous arc attachment there. The joint was then coated with Sauereisen #29 Zircon cement.

Another method of insuring the stability of arc behavior is through gas injection schemes. It is felt by the author that the manner in which the working gas is injected is one of the most important controlling parameters in arc heater design. This point is discussed in Appendix E. The Plasmatron was originally designed with tangential injection. A radial injector was made from

boron nitride rod to fit into the main insulator cavity. This injector protected the micarta main insulator from the radiation of the arc column as well as providing radial injection of the gas.

Originally the Plasmatron starter unit was used to initiate the arc discharge. A capacitor was discharged between a starter electrode and the base of the anode. The discharge was convected upward naturally to form a bridge of ionized argon between the anode and the cathode along which the arc was initiated. The starter electrode is shown in Figure 7. The radial injector had to be recessed to allow clearance for this starter electrode. Later during the test program the starting system was changed. It was felt that the asymetrical shrouding of the cathode with injected argon caused by the recess in the injector for the starting electrode was contributing to the problem of anomalous arc attachment on the cathode. Elimination of the provisions for electrical connections and gap adjustment of the starter electrode would also make the arc head more air tight. The starter electrode was removed and its mounting hole in the main insulator was sealed. A radial injector of the same design but without the recess for the starting electrode was installed. A Miller Model HF-20-1 high voltage

welding starter was installed in parallel to the arc power supply as shown in Figure 9. This unit has internal protection for the arc power supply. A switching arrangement shown in Figure 9 was used to protect the voltmeters and test instrumentation. This unit supplies a high frequency, high voltage momentary discharge between the cathode and anode which provides the initial bridge of ionized argon across which the main arc discharge sustained by the rectifier power supply is immediately initiated. The starter is then disconnected from its 110 volt power source and the arc voltage measurement circuit is closed in one switching operation. This method of starting an arc heater has been recommended above others by Stursberg (1967). A very slight erosion of the anode was sustained in this method of starting; however, the design changes eliminating the starting electrode allowed for much better operation of the arc heater.

Certainly a better method of starting the arc would have been the utilization of the natural high voltage breakdown of the argon in the arc gap caused by field emission from the pointed cathode. This method was used by Witte (1969). However, in order to obtain the high voltages necessary, the welder power supplies

would have to be connected in series. In this configuration it was found that operation at the low power levels desired was not attainable. When set at their lowest settings and connected in series the welders would not supply less than about 200 amperes. The welder power supply was set to provide approximately 500 amperes and connected to the circuit before ignition of the arc. It was found necessary to start the arc at this current in order to minimize sputtering and erosion immediately after ignition. The power was adjusted to the desired level as soon as the arc had started.

The power supply for the arc heater consists of four Westinghouse Silicon Welder Power Supplies Type W-S. Each unit is capable of providing 4 kilowatts of power with amperage continuously adjustable from 80 to 1000 amperes. Two styles are included: style 21N5992 and style 21N5991, in wye and delta configurations. These two configurations were used interchangably in an investigation of the effect on the minimization of arc fluctuations, but no effect was found. For the majority of the test program operation at about 100 amperes and about 25 volts was provided with one welder alone. For the initial facility testing with amperage up to 1000 amperes, a buss board was used which allowed

parallel, series, and series parallel connection of the four welders. The layout of the electrical power supply is shown in Figure 9.

1.2 Settling Chamber. The settling chamber consists of two sections: the settling area and the nozzle area. It was designed so that the length of the settling area was easily changed. The reasons for the use of a settling chamber are discussed in Appendix E. The basic design of the settling chamber follows that of a unit that was previously built by the author in Belgium (Cassady (1965)). A drawing of the unit, which is held together with readily detachable stringer bolts, is shown in Figure 10.

The settling section was fabricated from readily available steel pipe and has an inner diameter of 3.00 inches and an outer diameter of 5.57 inches. A cooling water jacket is provided between. The actual length of the settling area in which the gas was allowed to come to equilibrium was easily changed from 2 inches to 4 inches or 6 inches. A small static pressure tap was brought out through the end plate. Various lengths of stainless steel tubing were placed in this tap to allow the total pressure to be measured at different points along the edge of the settling area.

The nozzle section consists of a throat turned from copper bar stock. The section consists of a 4.0625 inch radius of curvature nozzle cross section. The advantages of this type of design are discussed in Appendix E. The sonic orifice diameter is 0.25 inches.

Coolant water flows through a thermopile and is led into the nozzle area coolant jacket where it is directed toward the throat region by a baffle. It is then led out of the nozzle area coolant jacket and into the settling area coolant jacket through external tubing. It then passes out through a thermopile. All cooling tubes have a section of micarta insulation to allow electrical isolation of the settling chamber and to eliminate paths for heat conduction.

The arc heater is bolted to the settling chamber with 3 bolts. A micarta insulator block with O-ring seals was placed between the heater and chamber to provide a pressure seal and to allow electrical isolation of the two units. The settling chamber is mounted on the vacuum tank by means of a micarta insulator mount. All joints in the settling chamber are provided with O-ring seals which are properly cooled and protected from high temperature degradation.

1.3 Vacuum Pumps and Coolant System. The vacuum facility is shown in Figure 11. It is provided with an Edwards Model 30B5 Speedovac vapor booster pump with a speed of 8,300 liters per second of argon between 10^{-4} and $6.5 \cdot 10^{-3}$ torr. The backing pump is a Beech Russ Model 325-D rotary piston pump with a speed of 8,000 liters per second. The ultimate pressure of the complete system with model, instrumentation, and test gear installed is 0.016 to 0.017 torr.

High pressure water treated to inhibit corrosion was used to cool the arc heater, settling chamber, cooling baffles downstream of the test area, and the booster pump. This water is circulated by a centrifugal pump at approximately 180 psi. through the devices mentioned above which are connected in parallel and then to a closed circuit cooling tower which consists of a bundle of heat exchanger tubes onto which water is sprayed and evaporated. The baffle and booster pump cooling circuits are standard installations. The arc heater and settling chamber cooling circuits are shown in Figure 12. They are instrumented to obtain operational data.

A few special design points should be noted here. The upstream smoothing chamber helps to smooth out any pump fluctuations

in water flow rate. The electrical power for the arc heater is fed in through the cooling water copper tubes. The thermopiles for the arc heater circuit are placed in grounded holders to eliminate spurious signals. The valves controlling the water flowrate are placed downstream of the apparatus to assure the presence of coolant at all points even at very low flow rates. These valves are adjusted so that any cavitation takes place at the valve downstream of the final smoothing chamber thus insulating any fluctuations from the cooling circuit. Steadiness of the cooling water flow rates is of utmost importance as discussed in Appendix E.

2. Facility Instrumentation

All numerical computations and data reduction in this work were carried out on the CITRAN computer system. CITRAN is a time sharing system utilizing a language developed at the California Institute of Technology. It is an on-line system by means of which the operator can interact extensively with an IBM 360 computer through a remote console.

A sketch of the facility instrumentation is given in Figure 13.

Commercial argon in high pressure bottles was utilized as the working gas. Two stages of dome-loaded pressure regulators provided a constant flowmeter pressure of 50 psi which was read from a Bourdon Helix pressure gauge to an accuracy of $\pm$ 0.75 psi. A precision accuracy Fischer Porter Model 10A0735M flowmeter was used whose scale extended from 0.10 to 0.56 grams of argon per second. The argon then passed through a needle valve by means of which the flowrate was adjusted. A mercury thermometer mounted in a Swagelok fitting provided data for the entrance enthalpy of the gas. The gas supply system is shown in Figure 13.

The electrical power supply for the arc heater was passed from the welders through a buss board. Arc current was measured by means of a 750 ampere, 50 mV., shunt placed in the circuit. The arc voltage was measured on a Simpson Model 1700 Voltmeter with an accuracy of $\pm$ 0.15 volts. The arc amperage was measured with a Simpson Model 1701 Ammeter with an accuracy of $\pm$ 3.75 amperes. A voltage divider was constructed from 1% wire wound resistors by means of which the arc amperage and current signals were input to a Brown Model K153X87-C-II-III-107 recorder which has 24 channels, each with 5mV full scale. The channels were so

arranged that continuous readings of the arc voltage, settling chamber coolant temperature rise, arc current, and arc heater coolant temperature rise were recorded. The method of temperature rise measurement is described below. The calibration of the arc voltage and current recordings was carried out during an actual test. Readings taken from the Simpson meters were recorded next to the appropriate traces on the Brown output record. In this manner a calibration factor by which the Brown readings of amperage and current were multiplied to yield the actual power delivered was computed. A diagram of the wiring for the power supply is given in Figure 9.

The experimental apparatus used for pressure measurements is shown in Figure 14. The ambient pressure in the vacuum tank was measured with a McLoed gauge protected by a liquid nitrogen cold trap. With this gauge the ultimate pressure of the facility was recorded before each run in order to warn of any possible leaks in the apparatus. The ambient pressure in the vacuum chamber was measured both with cold argon flowing before arc ignition and with hot argon flowing after the arc had been ignited. The fact that no difference was found in these two measurements is due to the action

of the cooling baffles downstream of the test area which very efficiently bring the test gas back to ambient temperature before it reaches the booster pump.

The total pressure in the settling chamber was measured through an orifice in the settling chamber endplate. A 1/8 inch diameter stainless steel tube of arbitrary length was inserted in this tap to sample static pressure at various points along the length of the settling area. The total pressure was read on a Wallace and Tiernan Model FA 135 mercury manometer. The manometer was referenced to the atmosphere as shown in the Figure. This necessitated the measurement of atmospheric pressure before and after each test.

The cooling water flowrates were monitored with Fischer Porter flowmeters. In the arc heater circuit a tube number FP-$\frac{1}{2}$-21-G-10/80 together with a float number $\frac{1}{2}$-GUSVT-45 was used. In the settling chamber circuit a tube number FP-$\frac{1}{2}$-27-G-10/80 together with a float number $\frac{1}{2}$-GUSVT-40 was used. Since an accurate knowledge of the coolant flow rates is very important in this application, an extensive calibration proceedure was undertaken.

The temperature rise of the coolant water upon passage through the coolant jackets was read by means of copper-constantin thermopiles of two thermocouples each that were made into Swage-lok fittings and placed in the cooling circuit as shown in Figure 12. These thermopiles which gave twice the sensitivity of a single thermocouple pair were wired to read the temperature rise in the coolant continuously on the Brown recorder. Two circuits are used: one for the arc heater and one for the settling chamber. The head thermopiles are placed out of the way of any stray currents and all leads are shielded with grounded shields. These precautions were found necessary in the previous wo rk of the author (Cassady (1965)). It was not found necessary to insulate the thermopiles from the water flow by means of glass enclosures or otherwise. This allowed a much quicker reaction time to temperature changes. The thermopiles were calibrated in hot water and ice baths. A calibration factor of 12.41^{o}K/mV. was measured which varies by 3% from published tables for copper-constantin thermocouples.

The probe actuator used in the facility provides three translational degrees of freedom. It is powered by a Slo-Syn Translator system built by the Superior Electric Company. Three stepping

motors are geared to indicators and lead screws. The indicators read directly in units of 0.001 inches.

The traverse mechanism was aligned to the axis of the nozzle by means of a special jig which held a cathetometer along the nozzle axis. In this manner the x-axis of the probe traverse mechanism was very accurately aligned with the axis of symmetry of the free jet.

The zero point of the traverse system was set using specially designed gauge blocks which fit snugly into the orifice of the nozzle and consisted of a steel rod accurately machined to a point exactly one inch from the plane of the nozzle exit and lying on the axis of symmetry. The various probes were slowly brought up to this point and all of the traverse mechanism indicators were zeroed. In the case of the Langmuir tube in order to avoid damage to the delicate tube a piece of gauge wire was used as a feeler gauge and a small electric current conducted from the nozzle through the gauge block, gauge wire and probe tube signalled contact. Probes were always brought forward into position for all tests to avoid the effects of any backlash in the traverse system.

During the test program described in Section V, a blunt body was placed in the flow field. The body, shown in Figure 17, consists

of a 0.7 inch diameter cylinder aligned along the flow centerline. The front face of the body is flat, normal to the flow. The body was made up of copper soldering fittings and 3/8 inch copper pipe, The front face was made from a copper disc and the threaded portion from a 5/16 inch Swagelok fitting. All joints were silver soldered. The body was constructed to mount on the probe holder that is used for the pitot probes and is cooled by a stream of cold house water in the same manner as the pitot probes. A special mount was constructed to position the body in the flow field. This mount was clamped to the axial positioning tubes of the vacuum tank traverse mechanism. It has three translational degrees of freedom adjusted by means of machine screws to allow the body to be accurately positioned in the jet. The body was positioned using the gauge block method described above and could not be moved without opening the vacuum tank.

3. Development and Preliminary Tests on the Facility

Developmental tests were carried out on the arc heater and cooling chamber configuration in which optimum operating conditions were sought. These tests are described in Appendices A and E.

The results will be summarized here for the sake of continuity.

As described in Section IV-A-1, the arc heater was modified to enable satisfactory operation under conditions different from those for which it was originally designed. A special short anode was incorporated together with a radial working gas injection scheme which eliminated the arc anode attachment instability which appeared when this unit was operated in the regime of 60 torr total pressure instead of its design value of one atmosphere. The original separate starting electrode arrangement was eliminated in favor of a proceedure utilizing the main electrodes of the heater in an effort to eliminate anomolous arc attachment at the base of the cathode. The resulting modified unit performed very satisfactorily and provided a dependable supply of high enthalpy argon for the experiments. Silicon rectifier welder power supplies were found superior to a D. C. motor generator set in providing power for the stable operation of the heater.

Experiments on a variable length settling chamber showed that a two inch length, nominal three inch diameter settling area followed by the gradual subsonic expansion of the working gas through a contoured copper nozzle to a sonic throat provided the

best design. Calculations revealed that this arrangement provided adequate residence time for the working gas to arrive at both thermal and chemical equilibrium before delivery to the free jet flow field. The total pressure in the settling chamber was shown to be relatively constant along its length and across its diameter allowing a wall tap to be used for its measurement. The incorporation of a radiation shield was found to be unnecessary since heat losses due to radiation are negligible at this low total pressure. Most of the heat transfer was found to be concentrated in the nozzle area, causing the choked flow method of total enthalpy calculation to predict values far below those actually produced. For this reason the heat balance method was used to calculate total enthalpy. Facility design and data measuring techniques were refined in order to minimize any error inherent to this method. The percentage of the input power lost to the coolant was found to be relatively constant as the total enthalpy content of the gas was raised.

During initial tests the facility was operated with mass flows between 0.1 and 1.0 grams of argon per second and currents of between 100 and 850 amperes yielding values of h/RT_o between

35 and 500. The design goal of the facility was to obtain operation at low enough enthalpies to allow sufficient diagnostic testing yet at high enough enthalpies to exhibit interesting non-equilibrium effects. This operation was achieved at a mass flow of 0.2 grams of argon per second and a current of approximately 100 amperes yielding values of h/RT_o in the range of 25 to 35. The total pressure in the settling area was measured at near 60 torr and the ambient pressure in the vacuum tank at near 0.06 torr yielding a pressure ratio of one thousand resulting in a five and one half inch long flow field.

B. Pitot Pressure Measurements

1. General

In order to verify that the proposed corrected source flow adequately models the free jet flow field, pitot pressure distributions were experimentally taken. These experimental distributions were then compared with the corrected source flow prediction of the pitot pressure distribution, Equation (III-11). Experiments were carried out in cold flow (arc heater inoperative), and hot flow (arc current of 100 amperes). Two different diameter probes were used to investigate any Reynolds number effects.

The measurement of pitot pressure is the easiest and most straightforward experimental measurement that can be carried out in a free jet flow field. Virtually all of the experimental investigations of cold free jets that are mentioned in Section III have included this measurement. Very few measurements of the pitot pressure distribution in an arc heated free jet have been carried out however. Witte (1969) carried out measurements in such a facility operating at much higher stagnation enthalpies, and

Kirchoff (1969) has carried out measurements in an R. F. heated facility for much lower stagnation enthalpies than those produced here. The latter measurements were done during the same period as those reported here.

2. Probe Design

Two pitot probes were used to investigate the pitot pressure profile in the free jet flow field. The first probe measured the pitot pressure through a 0.125 inch OD, 0.085 inch ID brass tube cut square at the upstream end and placed along the flow centerline. This probe is shown as probe 1 in Figure 15. Probe 2 shown in this Figure was used in the investigation of the pitot pressure distribution in the settling chamber that was described in Appendix E. The second probe used was a hemisphere-cylinder of 0.375 inch diameter aligned with the flow centerline. The collecting orifice was 0.085 inches in diameter. This probe is shown in Figure 16.

Both of these probes were constructed of brass or copper tubes and mounted on a sting by means of a modified Swagelok fitting. The inner collecting tube of the probe extended through the sting mount, through an O-ring and into a connection by means of which

the pressure signal was lead out of the vacuum tank through a 0.25 inch copper tube. The sting mount held another tube which fit between the inner and outer tubes of the probes and directed cooling water to the nose and back along the inner wall of the probe. All joints were provided with O-rings. House water was lead into the vacuum tank to the sting mount to provide cooling for these probes.

3. Instrumentation

The probe pressure signal was brought out through the vacuum tank wall by means of a special Swagelok fitting and lead to a silicon oil U-tube manometer through 0.25 inch copper tubing. The manometer was provided with optical cross hairs and a lead screw which allowed measurements to 0.01 millimeters of silicon oil to be recorded. The reference leg of the manometer was connected to a vacuum pump which maintained a reference pressure of 0.005 torr as measured by a McLoed gauge.

4. Experimental Program

The experimental procedure used is outlined below. The apparatus described above was designed and installed. Leak tests showed that the circuit was well sealed. One of the probes was positioned on the probe mount and indexed using the gauge block procedure described in Section III-A-2. The vacuum facility was pumped down to its ultimate pressure and the probe circuit was allowed to outgas for at least fifteen hours before an experimental run was begun. For the hot flow tests the arc heater was started using the procedure outlined in Appendix A and allowed to settle to operation at 100 amperes of arc current. For the cold tests the argon mass flow was set at 0.2 grams per second and the stagnation enthalpy measured by means of the mercury thermometer shown in Figure 13. The atmospheric reference pressure and the settling chamber pressure were measured for each data point using the apparatus described in Section III-A-2 and shown in Figure 14. Operating data for the hot flow tests were taken with the Brown recorder as described in Appendix A. The pitot probe was moved forward into position for each station at which

data was taken in order to eliminate the effect of backlash in the traverse mechanism.

An investigation was carried out to determine the response time for the probes and associated tubing in the measurement circuit. The probe was positioned at one station for lengths of time up to thirty minutes while the measured pressure was monitored. It was found that the pressure recorded after three minutes did not differ measurably from the final (thirty minute) value. Therefore during the tests the probe was positioned at the desired station and three minutes were allowed before the pressure was measured. The adequacy of this time interval was further verified during the test program by the collection of two sets of data. One set was taken when moving the probe station to station towards the sonic orifice (x/D decreasing) and the other set was taken when moving the probe station to station away from the sonic orifice (x/D increasing). The two data points taken for each station are shown in the Figures mentioned below. The correspondence of these data showed that adequate response time had been allowed before each data point was recorded.

Since the pitot probes were operating in a low Reynolds number regime the question of data correction for hypersonic viscous interaction and rarefaction effects arises. There have been several studies of impact probe operation in this regime; however, no suitable theory describing the necessary correction for operation in supersonic flow has been developed. It has been necessary to rely upon empirical correction factors that have been published by many authors. These correction factors have been calculated for adiabatic probe wall temperatures in flows with low stagnation enthalpies. There have been no investigations of the necessary correction for the conditions experienced in a high enthalpy, ionized, hypersonic flow of a monatomic gas. Both Witte (1969) and Kirchoff (1969) have mentioned this fact and have not made any correction to their pitot pressure data. For the same reason, no correction was made to the present data to account for viscous interaction and rarefaction effects.

4.1 Cold Jet. Measurements of the pitot pressure were carried out in the unheated free jet with a mass flow of 0.2 grams of argon per second. The total temperature as measured by the mercury thermometer shown in Figure 13 did not differ from room temperature

because of the long argon supply lines. The total pressure was recorded for each data point. Figure 18 shows the data taken with the 0.125 inch diameter probe (Probe 1 in Figure 15) as circles and the data taken with the 0.375 inch diameter probe (Figure 16) as squares. The theoretical pitot pressure distribution predicted by the corrected source flow model (Equation (III-11)) is given by the line. It is evident that there is no measurable Reynolds number effect. The standoff correction mentioned in Section III-B is also very small. Figure 18 essentially represents experimental data. The measured pitot pressure distribution follows the corrected source flow model theory quite well until the bottom shock is approached. The position of the bottom shock is represented by line (1) for the 0.125 inch diameter probe and line (2) for the 0.375 inch diameter probe. These values were calculated by means of the equation presented in Section III. The data begin to fall above the theoretical predictions as the bottom shock is approached. This behavior has been noted by other investigators (Ashkenas and Sherman (1966), Witte (1969)) and has been used to locate the position of the bottom shock. However this method of locating the bottom shock is very inaccurate. A much more sensitive measurement can be made with a Langmuir probe as discussed

in Section V. The results of this test program show that the cold free jet is accurately represented by the corrected source flow model.

4.2 Hot Jet. Measurements of the pitot pressure distribution in the heated free jet were carried out with a mass flow of 0.2 grams of argon per second and an arc current of one hundred amperes. The stagnation enthalpy was calculated from the Brown recorder output and the total pressure was recorded for each data point taken. Figure 19 shows the data taken with the 0.125 inch diameter probe (Probe 1 in Figure 15) as circles and the data taken with the 0.375 inch diameter probe (Figure 16) as squares. The theoretical pitot pressure distribution predicted by the corrected source flow model (Equation (III-11)) is shown as a solid line. The small correction for standoff discussed in Section III has been applied to these data. The data follow the theory quite well with the measurements from the two probes bracketing the theoretical prediction.

It can be seen that the theory underestimates the data of the 0.125 inch diameter probe by six percent and overestimates the data of the 0.375 inch diameter probe by fifteen percent at x/D

equal to ten. The error is even less in the region upstream of this station which is of interest in Section V. The measurements are expected to fall below theoretically predicted values since $p_{t2} \sim u_{lim}^2$. Since $u_{lim}^2 \sim T_t$, any loss in total temperature, a fact not accounted for in the theory, will lower the measured value of p_{t2}. The design of the 0.125 inch diameter probe, Probe 1 in Figure 15, allows the possibility of tube expansion due to heating in the hot flow situation. A correction for this effect would be similar to that for shock standoff, moving the data point to the left and thus effecting better agreement with the theory. It can be shown from the corrected source flow model that a ten percent error in pitot pressure is compatible with the experimental error in total temperature mentioned in Appendix E. The results of this test program show that the corrected source flow model adequately represents the flow field in the heated free jet for the region of interest between the start of the inertia dominated region at x/D = 2.5 and the proposed blunt body position at x/D = 10.

V. Langmuir Tube Measurements

A. General

As explained in the Introduction, the measurement of the electron temperature and ion density is necessary in order to gain a full picture of the non-equilibrium situation in the flow field. For this purpose a new type of Langmuir probe known as the Langmuir tube was designed which is admirably suited to the high enthalpy environment and also provides excellent spatial resolution in the measurements. A description of the design of this Langmuir tube is presented in Appendix F together with preliminary tests of its operation.

By means of the Langmuir tube it was possible to place a small cooled collector accurately in the region of interest with a minimum disturbance to the flow field. The novel design of the Langmuir tube necessitated the development of an appropriate theory by means of which its operation could be analyzed. This

theory is developed in Appendix C. The measurement of the electron temperature in the flow field was the primary goal of this research and since the electron specie was everywhere very subsonic, this property was easily obtained from the Langmuir tube characteristic. The consideration of ion collection from the sort of flowing plasma encountered here is considerably more difficult, however a first order heuristic theory was developed which approximated the experimental Langmuir probe characteristic quite well.

A simple electrical circuit was designed with which the Langmuir tube characteristic was recorded on an automatic plotter. It was found that the settling chamber wall served as the best reference electrode through which the probe current could be returned to the plasma, and that for the portion of the probe characteristic investigated, there was negligible depletion of the charged particle population in the plasma.

B. Flow in Empty Free Jet

1. Electron Temperature

The primary goal of this research was to obtain measurements of the electron temperature in the slightly ionized plasma flow field existing immediately upstream of a strong normal shock wave. The hot electron shock precursor described theoretically in Section II is capable of producing the dark region that appears in front of a blunt body shock wave.

In order to determine the existence of this hot electron precursor in front of the blunt body unambiguously, it was first necessary to map the electron temperature profile along the axis of the empty free jet. These profiles then serve as a null from which the effect of any precursor can be measured by comparison. Due to the difficulty in obtaining exactly repeatable operation of the test facility, a theory by means of which the empty jet T_e profiles could be predicted was developed in Section III. Electron temperature profiles were measured in the empty free jet and compared with the theoretically predicted values in order to judge

the adequacy of the theory. After the theory had been shown to be applicable, the profiles in front of a blunt body shock wave could be compared with theoretical predictions for the experimental conditions at hand. In this manner, the appearance of the hot electron precursor could be seen. It is also possible to draw qualitative conclusions from the comparison of the experimental electron temperature profiles in the free jet with and without the blunt body.

Very few similar experimental measurements of the electron temperature distribution have been carried out in the past. Clayden (1963), Sonin (1965), Christiansen (1967), and Kamimoto, Nishida and Yoshida (1967) have used some form of Langmuir probe to study the distribution of electron temperature in plasmas exhausting from contoured nozzles. However, a contoured nozzle was used in these experiments to provide flow fields free of axial gradients in flow properties and the axial electron temperature profiles were consequently found to be level. Kelly, Nerheim and Gardiner (1966) measured the electron temperature distribution in the exhaust of an MPD source. This source corresponds roughly to the presently described facility without

the inclusion of a settling chamber. The flow field of the exhaust of the MPD source corresponds to a free jet although it was not analyzed as such. Uncooled, aligned cylindrical Langmuir probes were used but no data could be taken for $x/D < 15.6$ because of extensive probe heating. Data were taken at only three stations out to $x/D = 62.5$. A pronounced decrease in the electron temperature in the axial direction was noted. Very recently Kirchoff (1969) completed measurements of the axial distribution of the electron temperature in both nozzle and free jet flow fields. This work was unknown to the author during the performance of the experiments reported here. The flow field was generated by a radio frequency arc heater and the experimental conditions differ considerably from the present case. The free jet orifice was 1.75 inches in diameter and two operating conditions were reported. In the first condition the mass flow rate was 1.41 grams of argon per second with a total temperature of $1243^{\circ}K$ and a total pressure of 9.3 torr. In the second condition the mass flow rate was 0.76 grams per second with a total temperature of $1940^{\circ}K$ and a total pressure of 5.3 torr. An aligned cylindrical Langmuir probe was used to take data. Again a drop in the electron

temperature in the axial direction was noted. However in this case, measurements revealed the levelling off and rise in electron temperature caused by the bottom shock. No theoretical calculations were made corresponding to the free jet flow field.

A brief description of the procedure used to measure the electron temperature profiles will be presented here. The Langmuir tube position was first calibrated using the gauge blocks and procedure described in Section IV-A-2. The tube was then drawn out of the jet area by removing it along the jet (x) axis to a point near 40 diameters from the orifice plane. The tube coolant flow was started as described in Appendix F. The arc heater was started with the usual procedure as described in Appendix A and allowed to settle to the desired operating conditions at 100 amperes of arc current and approximately 25 volts arc voltage. The operating parameters were recorded in exactly the same manner as described in Appendix A.

The probe was cleaned by drawing a large electron current at +30 volts probe potential. It was then brought up to the desired test position with the probe traverse mechanism. A probe characteristic was then swept out from a negative potential below

V_f - 10 kT_e/e volts through the floating potential and up to a volt or two above V_f by means of the Kepco power supply. The probe was then biased at +30 volts to clean it of any possible contamination and moved up to the next test station. Six separate characteristic traces were plotted on each sheet of Moseley graph paper. As well as the continuous record of arc heater operation provided by the Brown recorder output, the total pressure and Moseley sensitivity settings were taken at each data point. The total pressure afforded a sensitive, immediate interpretation of the steadiness of the arc heater operation. The Moseley plotter sensitivities had to be changed during a test to keep the characteristic trace at an easily examined size. This change did not affect the operation of the circuit since for this particular recorder the input impedance was the same for all sensitivity settings. In this way, the operation of the facility was continuously monitored and operating parameters were known at all times throughout the test.

The electron temperature at each test station was calculated by the means described in Appendix C. The value at every test station was calculated using the tangent method and semi-log

plots were made for every sixth trace. The semi-log plots exhibited straight line portions thus assuring the existence of a Maxwellian electron distribution. The values of the electron temperature calculated by these two methods always agreed to within ten percent and usually differed by no more than six percent.

The results of representative tests are shown in Figures 20, 21, 22 and 23. The test conditions for these profiles are given in Table I.

Figure 20 shows the electron temperature profile measured during test 1. Data are shown from a point 3.2 orifice diameters downstream of the sonic orifice to a point 24 diameters downstream The sketch in the upper part of the figure depicts the appearance of the free jet. The boundary between the luminous core and the dark region of the jet flow field is drawn where it was observed and the bottom shock position was calculated by the means described in Section III. The initial drop in electron temperature is clearly seen to level off in the observed dark region. This effect is due to the hot electron precursor of the bottom shock. The scatter appearing in the T_e data is not entirely due to error

in temperature measurement. It is primarily caused by slight unavoidable changes in arc heater operation during the performance of a test.

Figure 21 shows the electron temperature distribution to a point 32 diameters downstream of the sonic orifice. This study, test 2, was done to show the electron temperature profile through and downstream of the bottom shock. The calculation of the theoretical electron temperature profile denoted by the solid line is described in Section III-C. The hot electron precursor of the bottom shock, which is not accounted for in the theory of Section III-C, causes the electron temperature to deviate from and rise above the theoretical profile as the bottom shock is approached. The electron temperature does not measurably deviate from the theoretical free jet value until a point further than 10 diameters downstream of the sonic orifice. Therefore any experiment performed at a point 10 diameters downstream of the sonic orifice would not be measurably affected by the hot electron precursor of the bottom shock and the conditions at this point can be assumed to be those existing in the source flow, free-jet flow field described by the theory of Section III.

Figure 22 shows the results of a similar investigation carried out as test 3. The same interpretation may be drawn as for test 2.

Figure 23 is a detailed investigation of the region ahead of the point 12 orifice diameters downstream of the sonic orifice. It is a compendium of three different tests at nearly the same operating conditions listed as test 4. The blunt body was placed at an axial station 10 diameters downstream of the sonic orifice in later tests, and therefore a knowledge of the region upstream of this position was desired in order to investigate the effect of the blunt body shock on the empty jet electron temperature distribution. In this Figure it can be seen that the theoretical electron temperature profile has an inflection point near the proposed blunt body position. As explained in Section III-C, the dominance of electron thermal conduction processes causes this singularity. From Table I it is seen that this test was carried out at a higher stagnation enthalpy than the others. It is shown in Section III-C that electron thermal conduction predominates in the case of a high stagnation temperature, and it is for this reason that the singularity appears. In the light of these

results it was decided to perform the tests with the blunt body in the flow field at a lower level of total enthalpy where the theory of Section III-C more realistically describes the experimental data.

Thus it was determined that the theory of Section III-C adequately describes the experimental data for the empty free jet electron temperature distribution. This theory will suffice to represent the undisturbed electron temperature profile in the following tests in which the blunt body shock wave precursor is examined. It is interesting to note that the theoretically predicted electron temperature at a point one orifice diameter from the sonic orifice lies within 10 percent of the centerline total temperature. This result shows that thermal equilibrium is attained in the settling chamber before the expansion process. Calculations in Appendix E revealed that transit times in the settling chamber should be sufficiently long to enable attainment of such thermal equilibrium as well as chemical equilibrium of the ionization-recombination process at this temperature.

The heavy particle temperature profile and the electron temperature profile are plotted together for test 2 in Figure 24.

The heavy particle profile is calculated by the means described in Section III and the electron profile is experimental data. From this Figure it can be seen that considerable thermal non-equilibrium exists in the free jet flow field. The cause for this thermal non-equilibrium is the great disparity in mass between the heavy and electron species. A physical description by means of pertinent characteristic times is presented in Section III-C.

Some comments can be made on the experimental procedure used in obtaining the results given above. To investigate the degree of reproducibility in electron temperature measurement, six Langmuir traces were taken at the same axial station in the empty free jet while the arc heater operating conditions were held constant. Less than six percent scatter in the resulting calculated electron temperatures revealed that the data was reproducible. The effect of probe cleaning was also examined. No effect was noted if the probe characteristics were taken in immediate succession; however in an amount of time comparable with that necessary to change a Moseley graph sheet, a slight effect of probe contamination was noted occasionally. This effect was entirely eliminated by cleaning the probe with electron

bombardment at potentials of thirty volts above ground (about thirty two volts above V_f). The ion current traces were found linear to well within 10 kT_e/e volts below V_f. At potentials very much lower than V_f the trace was found to break up similarly to its behavior at high electron currents. When the ion current was extrapolated from these regions the semi-log plot method showed that the ion current was incorrectly estimated near V_f. It is felt that at these low potentials, lying more than 20 kT_e/e volts below V_f, the ion collection process is disturbing the plasma flow field and that operation in this region should be avoided. When the ion current was extrapolated from the region near V_f - 10 kT_e/e the semi-log plot method showed that the ion current near V_f was correctly accounted for.

2. Ion Density

The Langmuir tube is a very sensitive instrument with which ion density variations may be measured. In this manner it is possible to determine the point at which the ion density profile begins to deviate from the source flow model at the upstream edge of the bottom shock. Measurements of the actual

ion density can be compared with the profiles computed from the source flow model to investigate whether the flow is indeed frozen to recombination.

Very few similar measurements have been reported in the literature. Most investigators have used nozzle-generated flow fields in which the axial variation of ion density is assumed to be non-existent. Both Clayden (1963) and Kamimoto, Nishida and Yoshida (1967) measured axial ion density variations in the test section of such an apparatus. They attributed these measured decays to volume recombination and used the data to determine a recombination coefficient. Graf (1965) measured ion densities in the subsonic portion of a free jet flow field. Sonin (1965) took axial ion current traces in a nozzle-generated flow field. Since he measured the electron temperature to be constant and utilized aligned cylindrical probes in his experiment, the ion current is directly proportional to the ion density. Only qualitative results were presented, and no profiles were taken in the free jet. Clayden (1964) presents the results of electron density measurements in an arc heated free jet with p_t = 1.3 torr, T_t = 1500°K, D = 1.9 cm. that were taken with an aligned

cylindrical Langmuir probe. Simultaneously with the present measurements, Kirchoff (1969) measured ion densities in a radio frequency heated free jet using an aligned cylindrical Langmuir probe. In Section V-B-1 it was noted that his experimental conditions differed appreciably from those studied here.

Using the data reduction procedure described in Appendix C, the ion density distribution was calculated from the Langmuir tube characteristics taken in the empty free jet flow field. The results of these calculations are shown in Figure 25 for representative test 2 and in Figure 26 for representative test 4. The profile calculated from the source flow model under the assumption that the ionization fraction was frozen at the settling chamber (stagnation) conditions is shown as a solid line. The ion density profile shape closely follows the shape of the frozen source flow profile upstream of the bottom shock. This result experimentally verifies the assumption of frozen flow in the free jet which was advanced on theoretical grounds in Section III.

For the sake of comparison, the ion density corresponding to chemical equilibrium was calculated from a form of the Saha

equation derived for a state of thermal non-equilibrium between the heavy particles and electrons. This equation may be written as:

$$\alpha^{1+S}/(1-\alpha) = (2\rho/m_H)^S (2\pi m_e k T_e/h^2)^{3S/2} \cdot g_i/g_n \exp(-I/kT_H)$$

where $S = T_e/T_H$ and the g's are the internal partition functions of the ions and neutrals.

This 'equilibrium" ion density falls off quite rapidly with x/D reaching a value of the order of $10^7/m^3$ at the station x/D = 8 as compared with the frozen value of approximately $10^{18}/m^3$ at the same station. This comparison further verifies the fact that the flow is frozen to ionization-recombination reactions in the free jet.

The inherent experimental error in the measurement of h/RT_o leads to a rather large error in the predicted initial value of n_i for the source flow model since the degree of ionization as determined by the use of the Saha equation in the settling chamber is very sensitive to the value of the stagnation

temperature as discussed in Appendix E. For typical experimental conditions the maximum error in total temperature determination was shown to be about nineteen percent. Under these conditions n_i can be determined to within a factor of three. This error will be evidenced in a shift of the frozen flow profile upwards or downwards, thus influencing its initial value but not its dependence upon axial distance. The total temperature is apparently overestimated in these tests. Lowering the total temperature will both lower the frozen profile as explained above and raise the measured profile as influenced by the theory of Appendix C. The discrepancy evident here is well within experimental error.

The bottom shock position shown in Figure 25 was calculated by means of the relation described in Section III. The Figure shows that the ion density accurately reflects the neutral particle bottom shock position. It must be noted here, however, that the theory developed in Appendix C applies only to the free jet flow field where the particle velocity is constant and equal to the limit velocity. The investigation is primarily concerned with the region ahead of any shock where this velocity is indeed

constant. As the flow experiences the compression of a shock wave the flow velocity will decrease. By using the theory of Appendix C through the shock wave, the calculated ion density will be too small. Therefore the density profile shown here should not be considered to be the true shock density profile. Since the investigation is only concerned with conditions in the free jet upstream of the bottom shock, this rise in ion density is only used to determine the axial position of the front "edge" of the bottom shock. When the blunt body is placed at an axial position ten diameters downstream of the sonic orifice it is assured that it will be well upstream of the onset of the bottom shock.

This portion of the study showed that the ion density distribution was indeed frozen, following the profile calculated from the source flow model of the free jet very well. It also showed that the ions experience the same bottom shock as the neutrals and that its position is accurately given by the relation derived in Section III. A point ten diameters downstream of the orifice is unaffected by the presence of the bottom shock and any experiment carried out at this point can be assumed to take place in conditions existing in a source flow, free jet flow field.

C. Flow in Front of a Blunt Body

1. Electron Temperature

The blunt body model described in Section IV-A-2 was placed in the flow field to investigate the effect of a strong normal shock on the centerline axial electron temperature distribution in the free jet.

The body was centered and placed at an axial position 2.5 inches (10 orifice diameters) downstream of the sonic orifice. Preliminary tests which were carried out with the body mounted on the movable traverse mechanism had shown that for the design operating conditions the dark region was clearly visible with the body at this axial position. At this position the body is far enough downstream to be well within the inertia dominated region of the free jet and to allow adequate diagnostics of the region in front of it, and yet not so far as to be within the measurable effect of the bottom shock precursor.

The electron temperature distribution was measured in the same manner as in the empty free jet. Limitations imposed by the design of the Langmuir tube did not allow data to be taken closer

than 3.2 diameters from the orifice. However, the source flow model with its inertia dominated flow field was seen to apply no closer than 2.5 diameters in Section III. Therefore the data taken between 3.2 and 10 diameters downstream are well within the "source flow" region and should allow adequate spatial resolution of flow phenomena.

The results of two representative tests, 5 and 6, are shown in Figures 27 and 28. The observed dark region and the observed luminous shock layer are shown in the Figures. The theoretical electron temperature profile for the empty free jet as calculated in Section III-C is shown by the solid line. The electron temperature profile follows the distribution dictated by the source flow model quite well until the observed dark region is approached. In the dark region the profile deviates from the empty jet behavior and begins to rise. This electron temperature rise in the dark region forms the hot electron precursor of the blunt body shock wave. As explained in the Section II, this region of elevated electron temperature quenches the recombination radiation from the plasma and causes the appearance of the observed dark region. The electron temperature continues to rise through

the blunt body shock and then starts to fall as the cold body surface is approached.

In Figure 29 the species temperature distributions are shown for test 6. Considerable thermal non-equilibrium is evident. The highest measured electron temperature is seen to be 1.7 percent above the centerline total temperature and 8.5 percent above the calculated heavy particle temperature T_2 downstream of the blunt body shock. This value was calculated from the Mach number distribution given in Figure 6 and the tables of Mueller (1957).

2. Ion Density

In the previous section it was shown that the observed region of decreased luminosity in front of a normal shock in the argon plasma free jet corresponds to a region of elevated electron temperature, denoted as the hot electron shock precursor. It has been proposed that the primary physical cause for the dark region is only the elevated electron temperature and not any change in the charged particle densities caused by the shock wave. It is now necessary to show that this region of decreased luminosity

and elevated electron temperature does indeed precede the shock wave. The normal shock wave may be defined as that region through which the density of heavy particles deviates from the distribution predicted by the source flow model described in Section III.

Ion density profiles were taken in front of the blunt body stationed ten diameters downstream of the sonic orifice. The experimental procedure was the same as that used in the case of the empty free jet. The statement made there concerning the density profile measured through the shock wave applies here also. Results for representative tests 6 and 7 are shown in Figure 30 and Figure 31. In the region of interest in front of the observed shock layer the profile closely approximates the frozen source flow model distribution as was evident in the empty free jet.

The measured electron temperature profile and ion density profile for test 6 are plotted on the same abscissa in Figure 32. It is seen that the electron temperature profile begins to rise and thus deviate from empty free jet behavior much further upstream than the ion density profile begins to deviate. The electron

temperature profile minimum occurs upstream of the observed dark region and the ion density minimum occurs well within it. A similar position for the n_i minimum was reported by Kamimoto, Nishida and Yoshida (1967). This proves the existence of an elevated electron temperature precursor which precedes the heavy particle shock wave. The observed dark region coincides with this hot electron precursor region in front of the shock.

As shown in Section V-B-1 the hot electron precursor is much larger in the case of the empty free jet where the bottom shock provedes the driving mechanism for electron heating. However, in the case of flow in front of a blunt body, one is much more sure of the shock position and also the luminosity is high enough to enable accurate delineation of the dark region that co-exists with the hot electron precursor. By placing the body in the flow to generate a shock layer one is able to compare a null experiment done in the empty free jet in which there is definitely no precursor to the case in which there is a definite measurable precursor and thereby prove its existence.

VI. Conclusions

This section consists of a review of the experience gained through the design and operation of the facility and equipment together with a description of the results of the measurements taken and their theoretical implications. Some suggestions for future work stimulated by this research will be advanced at the end of this section.

A. Results

A theoretical study of the normal shock wave in a slightly ionized gas was carried out in which the physical processes causing the appearance of a hot electron precursor were examined. In order to examine the problem experimentally, an arc-heated free jet facility was designed and built in which measurements were made of the hot electron precursor to a shock wave in a slightly ionized gas. The free jet flow field was analyzed theoretically and a corrected source flow model was formulated for it. This model provided theoretical predictions of the axial distribution of pitot pressure,

ion density and electron temperature in the free jet to be compared with experimental data.

Through modifications in anode design, gas injection scheme, and starting proceedure, a commercial arc heater was adapted to supply high enthalpy argon to the facility. Experiments and theoretical calculations showed that a two inch length, three inch diameter settling area followed by a gradual subsonic expansion provided the best design settling chamber. It was found that the heat balance method of total enthalpy determination was best suited to this experimental facility.

The design goal of this facility was to obtain operation at low enough enthalpy levels to allow adequate diagnostic testing and yet at high enough levels to exhibit the interesting non-equilibrium effects. This operation was achieved at a mass flow of 0.2 grams of argon per second and a current of approximately 100 amperes yielding values of h/RT_o in the range of 25 to 35. Typical operation parameters are given in Table I. The total pressure in the settling area was measured at near 50 torr and the ambient pressure in the vacuum tank at near 0.060 torr resulting in a five and one half inch long flow field.

Pitot pressure measurements taken along the flow centerline compared very well with the values predicted from the corrected source flow model thus verifying that this model adequately represented the heavy particle flow field.

As explained in the Introduction, Section I, the measurement of the electron temperature and ion density were necessary in order to gain a full picture of the non-equilibrium situation in the flow field. The Langmuir tube was designed to make these measurements. This instrument is capable of providing excellent spatial resolution of measurements taken in a high enthalpy environment. A theory was developed to obtain values of electron temperature and ion density from the Langmuir tube characteristic. It was shown that this instrument is well suited for the measurement of the electron temperature, however, the measurement of ion density was found to be considerably more difficult. The first order, heuristic theory that was developed approximated the experimental Langmuir probe characteristic quite well.

The primary goal of this experimental program was to measure the electron temperature distribution ahead of a strong normal shock wave. To provide a null experiment to which later measurements in the precursor region might be compared, a survey was made of the axial electron temperature distribution in the empty free jet. A theoretical prediction of this distribution was obtained from the corrected source flow model by the consideration of the electron energy equation in which viscous terms were shown to be negligible and the processes of convection, conduction, elastic collisional energy transfer and inelastic collisional energy transfer were examined. It was shown that the effect of collisional energy

transfer between species was very small and that the primary governing process was that of conduction within the electron gas slightly modified by convection. Theoretical profiles of electron temperature were generated which compared well with the experimentally measured distributions. An experimental survey of the axial ion density distribution in the empty free jet showed that the flow was indeed frozen to recombination and well represented by the corrected source flow model. It was also shown that the Langmuir tube served as a sensitive instrument with which the position of the bottom shock could be ascertained.

A cooled blunt body was placed in the flow field to generate a strong normal shock on the flow centerline. The experimental electron temperature profile was found to follow the theoretically predicted profile reasonably well until the dark region upstream of the shock wave was approached. Within the dark region the experimental electron temperature profile began to rise and reached a peak in the luminous shock layer. The dark region was thus shown to be coincident with a layer of high electron temperature. The experimentally measured ion density was seen to follow the frozen flow calculations to a point well within the dark region where it began to rise, signalling the front edge of the heavy particle shock wave. When these data were plotted on the same abcissa as the electron temperature data it was clearly seen that the region of high electron temperature which was coincident with the observed dark

region did indeed precede the shock wave and thereby did form a hot electron precursor to the normal shock wave.

In summary, this research program formulated a physical model for the non-equilibrium phenomenon of a hot electron precursor in a slightly ionized plasma and verified its existence by the means of an experimental study.

B. Discussion of Results

The results of this research have raised many questions that may be resolved in future research programs. The most obvious question concerns the reason why the theory of Section II did not predict the length of the precursor measured in the experimental program reported in Section V. For the experimental conditions corresponding to representative test 6 the precursor length was predicted to be approximately 3 meters as shown in Figure 2. The experimentally measured precursor length shown in Figure 28 is seen to be approximately 2 centimeters. Although the theory was formulated for a one dimensional flow and the experimental situation is one of spherical symmetry it is believed that there are more basic, physical reasons for this failure.

It is certainly possible that all of the mechanisms for energy transfer to the electron gas in the shock layer are not accounted for in the theory. The theory of Section II includes only compressional

heating and elastic energy transfer with the heavy particles as processes through which the heat is supplied to the electrons in the shock layer that is subsequently transferred forward into the precursor region through thermal conduction. An increase in heating rate in the shock layer will steepen the electron temperature profile at the shock and thereby shorten the length of the precursor. An increase of two orders of magnitude is necessary to reconcile the theory with the experiment. With this goal, a preliminary study has been made of possible physical processes through which additional energy may be transferred to the electron gas.

Upon examination of Equation (B-25) it is seen that such an increase in heating rate could be realized by elastic energy transfer with heavy particles if the degree of ionization were to increase by a factor of ten behind the shock wave since this process is proportional to the square of the free electron density. This implies the existence of inelastic, ionizing collisions in the shock layer which were neglected in the theory of Section II. Calculations show that for the conditions corresponding to representative test 6, the equilibrium degree of ionization behind the shock wave is approximately thirteen times the frozen value in front of it. Thus the tendency is to form more free electrons behind the shock wave and thereby enhance the elastic collisional energy source term in the electron energy equation. A study was made to determine whether there were any reactions fast enough to accomplish this. A characteristic flow

time in the shock layer was compared to a characteristic reaction time similar to Equation (III-14) for a number of possible processes.

The processes of ionization through electron-atom collision and atom-atom collision were found to be too slow. Ionization rate data presented by Zeldovitch and Raizer (1966), Nelson and Goulard (1969), Biberman and Yakubov (1964), and Chubb (1968) were used in these calculations. The reason that these reactions are too slow is that their activation energies are too high. A search was made for possible reactions with lower activation energies.

The presence of impurities in the working gas could contribute to an increased ionization rate behind the shock wave. The calculations of Petschek and Byron (1957) pertain to the reaction in which a collision between an impurity atom and an argon atom ionizes the argon atom. In this case the activation energy remains very high and the reaction is too slow to contribute. Morgan and Morrison (1965) examine the alternative process in which the impurity atom is ionized in such a collision. For their suggested value of cross section equal to ten times the atom-atom ionization cross section and an activation energy of 2.2 eV the ratio of characteristic times for conditions existing in representative test 6 is:

$$\frac{t_{conv}}{t_{chem}} = 4.84 \cdot 10^{-3} \left(\frac{1 - \alpha}{\alpha}\right) f$$

where the symbol f refers to the impurity level in the flow.

Although the commercial grade argon used in these experiments was quite pure (99.996%), no particular effort was made to keep the experimental apparatus clean. Impurities such as copper, tungsten, iron and hydrocarbons from O-Ring lubricants and vacuum pump oil are very likely to be present, possibly amounting to one percent of the test gas. Since α is one-tenth percent in test 6, this process may contribute to a small extent in the aggregate production of electrons in the shock layer.

Another means of lowering the activation energy necessary for ionization is to incorporate metastable atoms in the process. The existence of argon atoms excited to their metastable (11.7 eV) level in the exhaust of an arc heater similar to the one employed here was theoretically and experimentally shown by Brewer and McGregor (1963) and Brewer (1964). They have shown that the concentration of metastable states remains essentially at the level populated collisionally in the arc. Measurements of electron temperatures in an arc resembling the one used here were done by Evans and Tankin (1967) which showed temperatures of 24,000°K in the arc region and values as high as 30,000°K in the vicinity of the cathode. Using the values of state degeneracy and partition functions quoted by Brewer (1964) it is easily shown that for an electron temperature of 24,000°K in the arc, the metastable concentration is nearly two percent of the total concentration of argon atoms. This concentration would be high

enough to supply the necessary ten fold increase in the ionization fraction of representative test 6 if a fast enough ionization reaction were available.

Two processes were found capable of producing electrons in the shock layer through collisions with metastable atoms. For the collisional process involving a metastable and an atom in which the metastable is de-excited and the atom is ionized, the data presented by McLaren and Hobson (1968) yield a characteristic time ratio of

$$\frac{t_{conv}}{t_{chem}} = 2.3 \cdot 10^{-3} \quad \frac{1 - \alpha}{\alpha} \quad M$$

for test 6, where M refers to the metastable concentration. It is possible that this reaction contributes to the aggregate production of free electrons in the shock layer. For the collisional process involving a metastable and an electron, the data presented by Zeldovitch and Raizer (1966) yield a characteristic time ratio of:

$$\frac{t_{conv}}{t_{chem}} = 17.5 \, M$$

This reaction is certainly possible but it takes energy from the electron gas. The ratio of this inelastic collisional energy loss to the elastic collisional energy gain can be written:

$$\frac{H}{Z} = 3\,M/\alpha$$

There exists the possibility of direct energy addition to the electron gas through superelastic collisions between metastables and atoms. The data presented by Zeldovitch and Raizer (1966) yield

$$\frac{t_{conv}}{t_{chem}} = 46.8\,\alpha \qquad \text{and} \qquad \frac{H}{Z} = 22.2\,M/\alpha$$

for the conditions of test 6. This reaction may help to counterbalance the energy lost in the previous reaction.

The possibility of potential electron ejection from the face of the blunt body was also examined. The data presented by Kaminsky (1965) showed that an average of less than one electron would be ejected for every ten metastables striking the surface. This process is capable of doubling the ionization fraction behind the shock wave and may also contribute to the aggregate production of free electrons.

This preliminary study has shown that there is a possibility of many ionizing reactions taking place in the shock layer which together might be capable of increasing the number of free electrons to a value near the equilibrium value. If this is done, the increased energy transfer to the electron gas through elastic collisions is capable of shortening the theoretically predicted precursor length to a value corresponding to that measured experimentally.

These reactions were not included in the theory of Section II and this is the reason that the precursor length predicted there did not conform to experimental measurements.

C. Suggestions for Future Research

Drawing upon the experience gained through this research it is possible to suggest some areas in which further research would be worthwhile. From the above discussion it can be seen that the length of the precursor should be very sensitive to the concentration of free electrons in the shock layer. It would be instructive to raise the ionization fraction (total temperature) in the flow field and examine the effect upon measured precursor length. If the reactions suggested above are capable of raising the ionization fraction to its equilibrium value in the shock layer, one would not expect to find any change in measured precursor length when operating at higher stagnation enthalpies. If these reactions are not of importance, the measured precursor length should be sensitive to changes in the frozen ionization fraction in the flow field.

A very valuable contribution to experimental fluid mechanics would be a theoretical study of the operation of pitot probes in low Reynolds number, high enthalpy, supersonic flows particularly in the lowest Reynolds number regions. At the present time there exists no such theoretical study and very few experimental

examinations of the problem including the effects of heat transfer. The facility developed here would be capable of providing flow fields for an experimental program.

Another area deserving further consideration is that concerning the collection of ions from a moving plasma by a Langmuir probe. There have been some theoretical treatments of the problem as mentioned in Appendix C, however they each have their own shortcomings. Using the facility and Langmuir tube developed here it would be possible to pursue a concerted theoretical and experimental effort towards the better understanding of this process.

Finally and perhaps the most interesting suggestion is the possibility of the examination of atomic energy level populations in the flow field and primarily in the dark region by means of a laser. Some of the propositions concerning atomic electronic excitation level populations that are developed in Section II would be very worthy of experimental study. Being an active rather than passive technique, a laser study would allow an examination of this flow field for which spectroscopic techniques do not possess the required sensitivity. Laser techniques would also allow very good spatial resolution in measurements.

These are only a few possibilities for further research that have been suggested by the experience gained in this work and which could be carried out in the facility developed here.

Appendix A

Development and Preliminary Tests on the Facility

Since the Plasmatron arc heater was designed to serve as a hand held refractory spraying tool, the initial tests were performed in the laboratory with the effluent exhausting to the atmosphere. In this set of tests, mercury thermometers were placed in the water lines to monitor coolant temperature rise and house water was plumbed through a flowmeter to measure coolant flow rate. The standard anode was modified by eliminating the powder feed tube present on the commercial model. This configuration is shown in Figure (7). One welder was used as a power supply. Tests were carried out for argon flow rates between 0.1 and 1.0 grams per second. In this configuration, it was found that steady operation could not be obtained for values of h/RT_o less than about 37. A graph of the energy content of the working gas as a function of the input power for various

flow rates is given in Figure (A-1). The arc voltage varied from 17 to 30 volts, the higher values appearing at high currents and high flow rates. The current was varied from 190 amperes to 850 amperes. The lower limit was imposed by the unstable operation mentioned above and the upper limit was imposed by the high current density on the anode which resulted in high heating rates and subsequent erosion.

It was seen that the heating rate at the anode also was dependent upon the working gas mass flow rate, so that much higher currents could be maintained for high mass flow rates. However, the maximum obtainable enthalpy in the gas dropped off with increasing mass flow rates. The percent of input electrical power delivered to the gas varied from 12% to 34%. Lower power levels were less efficient in transferring energy for a given mass flow rate and lower mass flow rates were less efficient in absorbing energy from a given input power level. These efficiencies can easily be calculated from the data given in Figure (A-1). A practical lesson learned from this series of tests was the necessity of eliminating all traces of cooling water from the arc region during operation. A small water leak can very quickly cause rapid erosion of both anode and cathode. Such a leak is evidenced by a red tinge to the

effluent jet.

The arc heater was mounted on the settling chamber which was equipped with the 4 inch settling section and the chamber was positioned on the vacuum tank end plate.

The proceedure followed during the performance of a typical test will be outlined here. The vacuum tank was closed and pumped down and the ambient pressure was measured with the McLoed gauge to assure that no leaks existed in the apparatus. This ultimate pressure was always very near 0.016 torr. The argon and coolant water flows were initiated and allowed to stabilize at the desired levels as read on the flowmeters. The ambient pressure was again read on the McLoed gauge. The atmospheric pressure was read by referencing the mercury manometer to the tank ambient pressure. This pressure was recorded again after each test was completed. The total pressure for cold flow was read by switching the mercury manometer over to the total pressure tap. (Refer to Figure (14)). The welder power supply was set to provide 500 amperes and was connected into the circuit. The arc was ignited and the power was adjusted to the desired level. For these tests, the original starting electrode design was retained and the arc was started using the commercial capacitive discharge starter. The tank ambient pressure was again measured with the McLoed gauge to assure that

no leaks had formed. All flowmeters were checked and re-adjusted if necessary and their readings were recorded on the Brown recorder output paper. These readings were recorded again at the end of each test. Readings were also taken at random times throughout the test to assure that the flowrates remained constant. The total pressure was continuously monitored throughout the test and recorded on the Brown output paper. For this set of tests, the arc amperage and voltage was continuously monitored on the Simpson meters and recorded on the Brown output paper. Thus, the Brown output paper supplied a continuous record of the time history of the test parameters. The data reduction for this set of tests was programmed on the CIT-RAN system. The data supplied to the program were: the argon mass flow rate, the two coolant water mass flow rates, the two coolant temperature rises, the total pressure together with its reference atmospheric pressure, the arc amperage and the arc voltage. The output of the program consisted of: the input electrical power in kilowatts, the percent of the power lost to the arc heater coolant circuit, the percent of the power lost to the settling chamber coolant circuit, the percent of the power delivered to the gas, h/RT_o computed by means of the heat balance method, h/RT_o computed by means of the choked flow method, and the percent difference between the two. For a discussion of the two methods and a comparison, see Appendix E.

Preliminary tests were carried out on the facility to test the data reduction procedure and to find the most stable operating conditions for the arc heater. Low mass flow rates of argon are desirable because then the existing vacuum pumping facility can maintain a large pressure drop between stagnation and ambient pressures and a physically large flow field can be assured, as is discussed in Section III. Investigations were carried out with argon mass flows varying from 0.1 to 0.5 grams per second and arc currents of 250 to 1000 amperes. Arc voltages ranged between 15 and 18 volts. The optimum point for a large flow field and stable arc heater operation was found to be at 0.2 grams of argon per second. For this value of mass flow rate, the ambient pressure was 0.060 torr and the cold flow total pressure was 16.5 torr for the room temperature argon supplied. At these test conditions, the dark region upstream of a blunt body shock wave was clearly visible for all power levels of operation. The total pressure varied from about 52 torr to 68 torr as the arc amperage was varied from 250 to 1000 amperes. The arc voltage remained relatively constant between 15 and 17 volts showing a very slight decrease as the arc amperage was raised. Thus, the design goal of $p_t/p_a \cong 1000$ was achieved and, using the equation for the base shock position that is derived

in Section III, the flow field is seen to be between 5 and 6 inches long for these operating conditions. The enthalpy delivered to the gas ranged from h/RT_o = 35.3 to 164. Analysis of the cooling water losses showed that: the power lost to the arc heater coolant is a strong function of the input power, and the higher the arc voltage at a given power, the higher the power losses to the coolant of the settling chamber.

An investigation of cathode grounded versus anode grounded configurations was carried out. It was found that the anode grounded configuration produced more stable arc heater operation.

A radiation shield was fabricated from a piece of stainless steel tubing of 2 3/8 inch I. D. and a wall thickness of 1/16 inch. Its length was equal to the length of the settling area of the chamber and it was held centered in the chamber by means of 3 spacers at each end. The purpose of this radiation shield is to help reduce radiative heat losses by placing a hot boundary between the body of the gas in the settling area and the cooled walls. The gas then sees the glowing shield at its outer boundary and thus the heat losses due to radiation are decreased.

As described in Section IV-A, the settling chamber was so constructed as to enable the length of the settling area to be changed

readily. Pieces were machined to afford three different lengths of the settling area: 2 inches, 4 inches and 6 inches.

Tests were carried out for the three lengths of settling chamber with and without the radiation shield. The data from these tests were reduced in the manner described previously and the results are shown in Figure (A-2) and (A-3).

When the radiation shield is used the arc heater absorbs a slightly larger percentage of the power and the chamber a slightly smaller percentage. However, this effect is very small. At total pressures in this region around 0.1 atmosphere total pressure, the amount of heat lost to the confining walls due to radiative heat transfer is a very small fraction of the total heat loss. This is most definitely not the case in high pressure arcs, as is described by John and Bade (1961). There was no discernable effect caused by the heat shield on the total enthalpy delivered to the gas.

The chamber length was also found to have a very small effect on percentage losses of total power to the heater and chamber cooling circuits. The 2 inch chamber was slightly better with respect to the amount of enthalpy delivered to the gas when compared to the longer length chambers.

A few overall conclusions can be drawn from this series of tests. Almost all of the chamber cooling losses are taking place in the nozzle area of the chamber since the length of the settling area and the presence of the heat shield in the settling area are seen to have little effect on the percentage of the total power lost to the chamber coolant. As the input power increases, the percentage loss to the cooling of the heater increases and at the same time the percentage loss to the cooling of the chamber decreases. The overall effect is a relatively constant total percentage loss of power to coolant as the input power level increases.

Two design modifications were instituted as a result of the experience gained in this series of tests. The heat shield was discarded. Since the arc heater seemed to operate more stably with the 2 inch chamber length, this configuration was adopted.

Another test program was undertaken to study the effect of chamber length. A longer chamber should allow rate processes effects to more completely approach equilibrium. As discussed in Appendix E, at enthalpy levels below $h/RT_o = 100$ argon behaves essentially as an ideal monatomic gas. Thus it was decided to determine whether a longer settling area would help to minimize the difference that was always present between the stagnation enthalpy

values calculated by the heat balance method and by the choked flow method. The effect of the radiation shield was also examined in this sense. The tests were carried out for the 6 inch and 2 inch chamber lengths, with and without the radiation shield. The results are shown in Figure (A-4) in which the stagnation enthalpy calculated by means of the ideal gas choked flow method is represented by the solid line and the values calculated by the heat balance method for various configurations are represented by the symbols.

The stagnation enthalpy computed by means of the heat balance method is seen to lie increasingly above the choked flow result for higher enthalpies in the gas and the attendant higher heat transfer to the chamber walls. This result substantiates the conclusions reached in Appendix E stating that the choked flow method of determining the stagnation enthalpy is erroneous primarily due to heat transfer effects. It is apparent that much higher enthalpies covering a much broader range are available with the 2 inch chamber length. For the cases where the regimes of attainable enthalpy overlap the 2 inch length seems to allow slightly closer agreement with the choked flow result; however its superiority in this sense is very slight. This supports the conclusions found in Appendix E

and in the previous set of tests, that most of the heat transfer is taking place in the nozzle area. The effect of the heat shield is seen to increase the difference between the two methods of enthalpy calculation to a slight degree. The results of this test program further support the design conclusion to use the 2 inch chamber length without the radiation shield. Calculations in Appendix E show that the residence time in the 2 inch chamber is sufficient to allow the attainment of a high degree of both chemical and thermal equilibrium.

In order to further quiet high frequency fluctuations in the arc voltage the "short" anode described in Appendix E and shown in Figure (8) was installed. However, an asymmetry was noticed in the flow field which was clearly caused by rotation of the arc column. The arc heater was modified for radial injection to eliminate gas swirl as described in Appendix E. These design changes indeed eliminated much of the high frequency fluctuation voltage and allowed a much steadier flow as evidenced by the luminosity. The results of tests on this configuration similar to the original facility tests are shown in Figures (A-5) and (A-6).

It can be seen from a comparison of the corresponding Figures that the power lost to the arc heater coolant was decreased by the incorporation of the short anode; however, that the power lost to the chamber coolant was increased. The overall enthalpy delivered to the gas was increased slightly by the use of the short anode. The most important beneficial effect of the short anode and radial injection scheme was the elimination of the high frequency fluctuation of the arc voltage.

At this time the circuit for the automatic recording of arc voltage and arc amperage on the Brown recorder was designed and installed. The circuit is described in Section IV-A-2. With this modification, it was only necessary to hold the gas and water flow rates constant throughout a test and to record the flow meter readings along with the notations of the total pressure read from the mercury manometer on the Brown output paper, and this Brown output paper gave a continuous record of arc heater operation. The 24 channels of the Brown recorder were connected to read the arc voltage, chamber coolant temperature rise, arc current, and heater coolant temperature rise in repeating cycles.

An investigation of a motor-generator power supply was carried out in order to compare with operation using the welders. The two generators are General Electric Models 27625, 7 and 8 each supplying 240 amperes at 250 volts D. C. Their fields are separately excited with 125 volts and they are driven by a 440 volt 3 phase motor of 175 horse power. The operating characteristics of the set were plotted using a variable resistance water ballast resistor as a load. It was found that the motor-generator set was unable to produce as steady operation of the arc heater as the welders did. Low power operation was not attainable without danger of swallowing the arc. Starting characteristics were very bad leading to much sputtering and erosion. Therefore, the use of the motor-generator power supply was abandoned in favor of the welder power supply.

The design goal of the facility was to obtain operation at very low power levels in order to minimize the hostility of the environment in the flow field and thus allow precise diagnostic testing and yet high enough levels to exhibit the interesting non-equilibrium effects. An investigation of low power operation was carried out. The goal was to obtain stable, dependable operation and to retain the presence of a clearly defined dark region ahead of a blunt body shock layer.

It was found that the most stable operation resulted when both the anode and the chamber were grounded. With one welder satisfactory operation was achieved at 100 amperes of arc current. By placing the blunt body shown in Figure (17) on the probe traverse mechanism and moving it into the flow field it was found that the dark region was clearly defined at this power level so that this power level was chosen as the operation point for all subsequent tests.

The greatest problem that arose concerning arc heater stability throughout the test program outlined above was with anomalous arc attachment on the cathode. This phenomenon caused an easily discernable, long period (10 minutes) voltage oscillation of about 20% amplitude. It was characterized by a slow buildup of arc voltage to a point about 10% above the operating point followed by an almost instantaneous drop to a value about 10% below. The effect was usually not present during a test; however, when it did appear it was easily detected by a close monitoring of the total pressure level. When the effect appeared, all testing was halted until the test parameters returned to the desired operating point and stabilized there. The effect was more common at lower power levels so design changes were instituted in order to eliminate it.

After particularly erratic runs, there was evidence of melted copper around the brazed joint between the tungsten cathode and its copper holder. It was surmised that the cathode attachment point of the arc was wandering and anomolously attaching to this joint. The joint was filed and polished and coated with Sauereisen #29 Zircon cement. The edge of the conical entrance region of the anode was rounded with a 1/16 inch radius in order to eliminate arc attachment at this point. Finally, the starting arrangement was completely changed since the recess in the radial injector which allowed clearance for the starting electrode also had the effect of destroying the symmetry of the smooth shrouding of the cathode with radially injected argon, and allowing a region through which anomolous arc attachment could take place to the cathode. The starting electrode was removed and a new radial injector without this recess was installed. Starting was then accomplished using the Miller starter and the procedure outlined in Section IV-A-1. These design changes helped to eliminate this anomolous arc attachment and allowed for superior operation of the arc heater.

During the developmental test program on the facility, a preliminary investigation of the dark space appearing upstream of

a blunt body shock was carried out. The initial visual investigation was made with the arc heater operating at 350 amperes to increase the flow luminosity.

The first tests showed that a luminous shock layer was clearly visible around the nose of the body. A clearly definable dark region existed in front of this shock layer which moved with the body and shock layer as the axial position was changed.

The free jet flow field was examined with a small hand held spectroscope. The normal continuum radiation from a recombining argon plasma was found to be absent from the whole flow field. This situation would result from the effect of high temperature electrons on the recombination process when this process is of the collisional-radiative type of Bates, Kingston and McWhirter (1962). This model is discussed in Section II.

Appendix B

Collisional Effects - Mean Free Paths and Transport Properties

1. Mean Free Paths

There are three types of particles present in the flow: atoms, ions, and electrons. Each of these has three mean free paths associated with the three possible collision partners. In order to investigate the relative importance of the various equilibration processes in the flow field and in order to estimate the Knudsen number of the Langmuir tube these various mean free paths are calculated in a manner outlined below.

Neutral particles

A hard sphere model was used for neutral-neutral collisions. The radius of the hard sphere was taken from the data presented on

page 149 of Kennard (1938). A temperature dependent cross section was not used because the viscosity coefficient from which the cross section is extracted is not very well known at the low values of heavy particle static temperature expected in the free jet expansion. Assuming a Maxwellian velocity distribution for the neutrals and chemically frozen flow in the free jet

$$L_{nn} = 1.135 \cdot 10^{-7}/(1 - \alpha)\rho \qquad \text{(B-1)}$$

The neutral electron cross section is affected by the Ramsauer-Townsend effect. This phenomenon is discussed in Section 4.4 of McDaniel (1964). An analytic form for the Ramsauer cross section was obtained for $T_e < 10,000^{\circ}$ K from Jaffrin (1965)

$$Q_{en} = (0.39 - 0.551 \cdot 10^{-4} T_e + 0.595 \cdot 10^{-8} T_e^2) \cdot 10^{-20} \ (m^2) \qquad \text{(B-2)}$$

When plotted on the graph of experimental measurements given in Figure (9-11) of Shkarofsky (1966) it is seen that this form closely approximates the data of Townsend and Bailey. Assuming chemically frozen flow in the free jet

$$L_{ne} = 6.68 \cdot 10^{-26}/(a\rho Q_{en}) \qquad \text{(B-3)}$$

The neutral-ion cross section includes the effects of charge exchange encounters and elastic scattering collisions. This total cross section is found to be a slowly varying function of temperature. Jaffrin (1965) suggests a value of 140 square angstroms for this quantity. The work done by de Voto (1965) on this subject substantiates this value for the momentum transfer cross section. However, the total cross section as measured by ion beam scattering experiments, ion mobility measurements and theory amounts to one half of the momentum transfer cross section. For the energies considered here (see de Voto (1965) Figure 7) the value will be taken as

$$Q_{in} = 70 \cdot 10^{-20} \qquad (m^2) \qquad \text{(B-4)}$$

and will be considered independent of temperature.

Under the assumption of chemically frozen flow in the free jet

$$L_{ni} = 9.55 \cdot 10^{-8}/a\rho \qquad \text{(B-5)}$$

Charged Particle Collisions

It is shown by Holt and Haskell (1965) in their Section 9.3 that if $\ln\Lambda > 1$ then the collective effect of multiple distant charged particle encounters outweighs the effect of any binary coulombic collision. The expression for this parameter may be written

$$\ln\Lambda = 16.33 + \frac{1}{2} \ln (T_e^3/n_e) \qquad \text{(mks)} \qquad \text{(B-6)}$$

For the experimental conditions presented here this parameter is sufficiently large to require the use of the Fokker-Planck description rather than the binary coulombic description for charged particle encounters.

Spitzer (1962) has presented an analysis of the dynamics of collective encounters between charged particles in separate Maxwellian distributions by means of the Fokker-Planck description. His results may be written in the form of a mean free path as

$$L = \frac{2\pi\epsilon_o^2 \, m \, w^4}{n_f e^4 \ln\Lambda \, (\phi - G)} \qquad \text{(mks)} \qquad \text{(B-7)}$$

where the term $(\phi - G)$ is a function of $w/(2kT_f/m_f)^{0.5}$ tabulated in his Table 5.2 and w is the root mean square speed of the test particle.

Ions

The ion-neutral cross section is given in Equation (B-4). The mean free path for ion-neutral collisions is then

$$L_{in} = 9.55 \cdot 10^{-8}/(1 - \alpha)\rho \qquad \text{(B-8)}$$

The ion-ion mean free path is calculated using the Spitzer mean free path given in Equation (B-7). Using the root mean square ion speed the argument of the function $(\phi - G)$ is $\sqrt{3/2}$ and the value of the function is found to be 0.714.

$$L_{ii} = 1.2 \cdot 10^{-16} T_H^2/\alpha\rho \ln\Lambda \qquad \text{(B-9)}$$

In the calculation of the ion-electron mean free path, the Spitzer formula is used again. The field particles are electrons in this case and using the root mean square ion speed, the argument of $(\phi - G)$ is found to be much less than one. Taking the limit of the expression given by Spitzer for $(\phi - G)$ for small values of the argument, it can be shown that

$$(\phi - G) \simeq 0.754 \left(3 m_e T_e / 2 m_H T_H\right)^{0.5}$$

in this case.

Using this limit it can be shown that

$$L_{ie} \simeq 209 \, (T_e/T_H)^{0.5} \, L_{ii} \qquad \text{(B-10)}$$

and since $T_e > T_i$ throughout the flow field, this mean free path is much larger than the ion-ion mean free path.

Electrons

The electron-neutral cross section is calculated using the Ramsauer cross section given in Equation (B-2). The result is

$$L_{en} = 6.68 \cdot 10^{-26}/(1 - \alpha)\rho\Omega_{en} \qquad \text{(B-11)}$$

The electron-electron mean free path is calculated using the Spitzer formula in which thermal electrons are colliding with a field gas of electrons. The argument of $(\Phi - G)$ is again $\sqrt{3/2}$ yielding a value of 0.714. Thus the mean free path is

$$L_{ee} = 1.2 \cdot 10^{-16} \, T_e^{\,2}/\alpha\rho \ln\Lambda \qquad \text{(B-12)}$$

The electron-ion mean free path again uses the Spitzer formula in which the thermal electrons are colliding with a field of ions. The argument of (ϕ - G) is then very much larger than one and in the limit the value of this function approaches one. Thus the mean free path is

$$L_{ei} = 8.6 \cdot 10^{-17} Te^2/\alpha \rho \ln\Lambda \qquad \text{(B-13)}$$

2. Electrical Parameters

The Debye length is another important parameter in the plasma. This length is a measure of how far two oppositely charged particles can separate under the influence of their thermal energies and thus violate quasi-neutrality or charge balance. It also depicts the radius around a charged particle beyond which its coulombic potential is effectively shielded by neighboring charged particles. A small ratio of Debye length to the pertinent characteristic dimension of a phenomenon constitutes the definition of the plasma state of an ionized gas. For small values of the ratio of the Debye length to the dimensions of flow phenomena as reflected in the lengths of the associated mean free paths one expects that the ionized gas

remains essentially charge balanced or quasi-neutral throughout the course of the phenomenon in question.

The Debye length may be written as

$$L_D = 69 \, (T_e/n_e)^{0.5} \qquad \text{(mks)} \qquad \text{(B-14)}$$

Another important electrical parameter is the logarithm of the ratio of the Debye length to the critical impact parameter. This quantity is denoted by $\ln\Lambda$ and is given in Equation (B-6). Its importance is discussed there. The numerical size of this quantity does not vary to a great extent in any given situation. Therefore it is often assigned a value calculated at reference conditions and considered to be a constant throughout the analysis. For the calculations of the mean free paths it was computed at each point. However, in the treatment of the electron energy equation in Section III and the normal shock wave in a slightly ionized gas in Section II, the value of $\ln\Lambda$ was held constant at reference conditions in order not to further complicate the numerical integration of non-linear equations.

3. Transport Properties

In general all of the transport properties are calculated using the Fay mixture rule (Fay (1962)).

$$\mu_j = \frac{5\pi}{32} n_j m_j c_j^2/\nu_j \qquad \text{(B-15)}$$

$$K_j/k = \frac{75\pi}{128} n_j c_j^2/\nu_j \qquad \text{(B-16)}$$

where the collision frequency is modified to account for the existence of many species

$$\nu_j = \sum_k n_k Q_{jk} (c_k^2 + c_j^2)^{0.5} \frac{2m_{jk}}{m_j} \qquad \text{(B-17)}$$

and m_{jk} is the reduced mass.

Using the Spitzer cross sections derived from Equation (B-7)

$$Q_{jk} = \frac{8\pi}{9} \left(\frac{e^2}{4\pi\epsilon_o}\right)^2 \frac{\ln\Lambda}{(kT_j)^2} (\phi - G) \qquad \text{(B-18)}$$

$$Q_{ee} = 0.714\ Q_{ei}$$

the transport properties for the electron gas may be calculated.

Assuming $T_e m_H / T_H m_e$ is much greater than one and that m_H/m_e is much greater than one, Equation (B-15) becomes

$$\mu_e = \frac{5}{32} (2\pi m_e k T_e)^{0.5} \left(\frac{1 - \alpha}{\alpha} Q_{en} + \frac{2 + 0.714(2)^{0.5}}{2} Q_{ei} \right)^{-1} \tag{B-19}$$

where Q_{en} is the Ramsauer cross section, Equation (B-2) and Q_{ei} is the Spitzer cross section, Equation (B-18), with the function $(\phi - G) = 1$ as explained above Equation (B-13).

Under the same assumptions given above Equation (B-16) becomes

$$K_e/k = \frac{75}{128} \left(\frac{2\pi k T_e}{m_e} \right)^{0.5} \left(\frac{1 - \alpha}{\alpha} Q_{en} + \frac{2 + 0.714(2)^{0.5}}{2} Q_{ei} \right)^{-1} \tag{B-20}$$

Although this model for transport properties gives a heuristically correct portrayal of the physical processes it may lack quantitative accuracy to the extent that the constant appearing in the expression may have to be slightly adjusted to allow agreement with the results of more accurate treatments. Because of the large effect of charged particle encounters as compared to

electron-neutral collisions even in relatively weakly ionized plasmas, caused by the Ramsauer effect, it was considered more realistic to adjust the constant in Equation (B-20) to conform in the limit of negligible electron-neutral collisional contribution which corresponds to the fully ionized result given by Spitzer and Härm (1953). The resulting expression is:

$$K_e/k = \frac{1.35 \cdot 10^{13}\, T_e^{5/2}/\ln\Lambda}{1 + 2.36 \cdot 10^{9}\, \frac{1-\alpha}{\alpha}\, \frac{T_e^2}{\ln\Lambda} \cdot Q_{en}} \qquad \text{(B-21)}$$

where the expression for Q_{en} is given in Equation (B-2).

4. Energy Transport through Elastic Collisions

The term appearing on the right hand side of the electron energy equation representing the addition of energy to the electron gas by means of elastic collisions with the neutrals and ions may be derived from the collision term in the Boltzmann equation. It may be written in the form:

$$Z_{ej} = \frac{n_e}{t_{coll,\, j}} \left[\frac{3}{2}\, k(T_j - T_e) + \frac{1}{2}\, m_j (u_j - u_e)^2 \right] \qquad \text{(B-22)}$$

The second term in the bracket vanishes because quasi-

neutrality coupled with the absence of currents and appreciable ion slip assure that all species travel with the same velocity.

The term $t_{coll,\ j}$ is a characteristic time for energy transfer by means of elastic collisions between the electrons and specie j.

In the case that all species are assumed to be in Maxwellian distributions around a specific mean velocity, as is assumed here, the work of Morse (1963) is applicable. Particularly since the "diffusion Mach number" relating to the difference in specie mean speeds which he requires to be small is identically zero here, his method of calculation of $t_{coll,\ j}$ will be used here. A considerable number of typographical errors were found in Morse (1963) and it is suggested that the reader refer to his reference (21) to compare the form of the equations. All results used here were derived from basic principles using his method of calculation and were thoroughly checked and verified.

There are two types of elastic collisions by means of which energy may be transfered to the electron gas. The ion-electron collision depends upon a coulombic potential field and the collision time may be written as:

$$t_{coll,\ i} = \frac{3}{2} \frac{m_e m_i}{(32\pi)^{0.5}} \left(\frac{kT_e}{m_e}\right)^{3/2} \left(\frac{4\pi\epsilon_0}{e^2}\right)^2 \frac{1}{n_i \ln\Lambda} \qquad \text{(B-23)}$$

The neutral-electron collision depends upon the Ramsauer cross section. The curve fit expression for the Ramsauer cross section, Equation (B-2) was used in a derivation using the same kinetic theory approach as that of Morse (1962) and the necessary integrations were carried through. The resulting expression for $t_{coll,\ n}$ is

$$t_{coll,\ n} = \frac{3\pi}{16} \frac{m_n}{n_n m_e} \left(\frac{m_e}{2\pi kT_e}\right)^{0.5} \cdot$$

$$(0.39 - 1.10 \cdot 10^{-4} T_e + 3.18 \cdot 10^{-8} T_e^{\ 2})^{-1} \cdot 10^{+20}$$

(B-24)

Since both the heavy particles are assumed to possess the same temperature the two contributions given by Equation (B-22) may be added to yield the total energy transferred to the electron gas through elastic collisions

$$Z_e = 2.04 \cdot 10^{-33} \frac{n_e^2 \ln\Lambda}{T_e^{3/2}} (T_H - T_e)$$

$$\left[1 + 2.48 \cdot 10^{9} \frac{1-\alpha}{\alpha} \frac{T_e^2}{\ln\Lambda} \cdot 10^{-20} \cdot \right.$$

$$\left. (0.39 - 1.10 \cdot 10^{-4} T_e + 3.18 \cdot 10^{-8} T_e^2)\right] \qquad \text{(B-25)}$$

5. Approximations

Both K_e/k and Z_e are written in a form in which the effect of electron-neutral collisions can be easily compared to the effect of electron-ion encounters. In both cases the terms representing the effect of electron-neutral collisions is non-dimensionalized and compared to unity. This dimensionless number represents the ratio of the effect of electron-neutral collisions to the effect of electron-ion encounters in the electron transport properties. This ratio was calculated for the conditions arising in this experiment and it was found that at no location did the electron-neutral collisions contribute more than 10 percent to either of these transport properties. The largest contribution is seen to be in the regions of high electron temperature near the jet orifice and behind the blunt body shock. In the region of interest for this study in

front of the blunt body shock the contribution was found to be less than 3 percent. Thus it can easily be seen that except in the case of very small ionization fraction and very high electron temperature the plasma may be treated in its fully ionized limit as far as electron transport properties are concerned. Furthermore, a quantitative evaluation of the adequacy of this assumption can be calculated from the forms of K_e/k, Equation (B-21) and Z_e, Equation (B-25), that are presented here.

Appendix C

Langmuir Probe Theory

1. General

A Langmuir probe consists of a small, current-collecting electrode which is immersed in the plasma to be studied. Various voltages are applied to the electrode in a slow enough manner to avoid transient effects, and the resulting collection currents are measured. The diagram of applied voltage versus collected current is known as the probe characteristic. Analysis of the probe characteristic yields certain plasma properties, notably the electron temperature and ion density in the plasma.

The Langmuir probe may be more accurately defined as an electrostatic probe operating in the free-molecule flow regime. Its use by Langmuir in 1924 was one of the earliest experimental techniques developed for the study of plasmas. From an experimental

standpoint it is very easy to use, but the theoretical analysis of the characteristic may be very difficult. It affords a truly local measurement of plasma properties whereas spectroscopic and microwave techniques yield averaged results.

The basic theory of operation of the Langmuir probe will not be discussed here. There are three review articles which cover the general theory of operation: De Leeuw (1963), Chen (1965) and Schott (1968). However some important parameters affecting probe behavior will be listed here. They will be discussed further at the appropriate point in this Appendix.

The ratio L_D/d_p characterizes the extent of the electrical disturbance to the plasma caused by the probe. A small value of this parameter assures that this effect is small and that the probe yields a truly local measurement.

The probe Knudsen number (with respect to any specific mean free path) characterizes the effect of particle collisions upon the probe operation.

The ratio T_e/T_H characterizes the extent to which residual electrical fields penetrate into the plasma and affect ion collection. This point will be further considered in the discussion of ion collection below.

The ratio u/v characterizes the effect of mass motion of the plasma upon ion collection. The ion acoustic speed represented here is written as:

$$v = (kT_e/m_i)^{0.5} \qquad (C\text{-}1)$$

Although the theory of operation of a Langmuir probe in a stationary plasma is reasonably well understood, the application of this diagnostic tool to flowing plasmas remains the subject of considerable theoretical effort. The understanding of stationary probe operation has reached such a stage of refinement (e.g. Laframboise (1966)) and reliability that experimental programs have been designed in such a way that the effect of plasma mass motion is minimized and this stationary probe theory can be utilized. Sonin (1965), Kamimoto and Nishida (1965), Graf (1965) among others have utilized long cylindrical probes aligned with the flow velocity vector to eliminate the effect of plasma mass motion. In these researches however the stagnation enthalpy level was much lower than in the present investigation. It was possible to utilize a very fine wire with a large l/d ratio and retain a fair degree of spatial resolution. In the present application the probe must be cooled

externally and the Langmuir tube was designed to satisfy this requirement. Therefore, the theory of a cylindrical Langmuir probe with its axis normal to the plasma mass flow velocity vector is considered here. With such a theory, the characteristic of the Langmuir tube described in Appendix F can be analyzed to yield the electron temperature and ion density distributions.

2. Electron Temperature

Both French (1961) and Clayden (1963) found experimentally that the shape of a probe and its orientation with respect to the streaming motion of the flow field had little effect on electron temperature measurements because of the fact that the electron Mach number is so small. Since the directed speed of the electrons is so much smaller than their thermal speed, the retarding field portion of the probe characteristic is relatively unaffected by the mass motion of the plasma. The same conclusion was reached on a theoretical basis by Kanal (1964). Dunn and Lordi (1969) have shown experimentally that the determination of the electron temperature is independent of the ion mean free paths also. Sonin (1965) verified that the determination of electron temperature was independent of the cylindrical probe axis and flow velocity orientation.

Thus it can be assumed that the determination of electron temperature by means of the retarding field technique used for stationary probes is valid for any shape and orientation of the probe as long as the electron Mach number is very small and the electron mean free paths are large enough to assure that the probe is in free molecular flow with respect to the electrons. The orientation of the probe has a large effect on the process of ion collection however. This point is discussed later in this Appendix.

Since the primary goal of this work was to measure electron temperature distributions, the Langmuir tube described in Appendix F was designed to best accomplish this end and the problem of the interpretation of ion density was relegated to secondary importance. For the measurement of electron temperature distributions in a free jet flow field, the transverse cylinder orientation of the probe has three advantages: it allows very good spatial resolution, it minimizes the disturbance to the flow field by piercing the barrel shock rather than the bottom shock, and it allows the probe to be adequately cooled.

Thus in the Langmuir tube, one has a diagnostic tool that is not only experimentally easy to use but also one whose results are easily analyzed theoretically to yield the electron temperature.

For the Maxwellian electron velocity distribution that is assumed here the total current to the probe is given in the retarding field region as:

$$j = j_e - j_i = j_{eo} \exp \left[e(V_p - V_\infty)/kT_e \right] - j_i \qquad (C\text{-}2)$$

where V_∞ is the plasma potential.

It may be seen from the electron current portion of this expression that

$$\frac{kT_e}{e} = \left[\frac{d \ln j_e}{d V_p} \right]^{-1} \qquad (C\text{-}3)$$

The electron temperature may thus be evaluated from the slope of a graph of $\ln j_e$ versus V_p.

The ion current must be eliminated from the total current as given by the probe characteristic in order to arrive at the electron current. In practice this is accomplished by means of a linear extrapolation of the ion current beyond the floating potential as shown by line 1 in Figure (C-1). From Equation (C-2) it is seen that for values of V_p more than 10 kT_e/e below V_∞ the contribution of the electrons to the total current is entirely negligible.

As shown below the floating potential V_f is below V_∞ and kT_e/e as measured did not exceed 0.7 eV, therefore the point of tangency of this line 1 can be safely taken at about five volts below floating potential. In all cases the probe characteristic was clearly linear to a point much closer to V_f than this so that there was no difficulty in positioning line 1.

The vertical distance between line 1 and the probe characteristic then represents the electron current. The logarithm of this value is plotted on the ordinate versus the potential on the abcissa. The slope of this plot then yields the electron temperature by means of Equation (C-3). This method of electron temperature calculation is known as the semi-log plot method. The linearity of the data so plotted reveals the existence of a Maxwellian electron velocity distribution and thus serves as a check upon the assumptions underlying the method. The experimental data proved to be linear in this manner.

A method for the determination of the electron temperature which is much easier to apply was developed by Sonin (1965). This method is especially valuable in the present situation where great resolution affords copious data whose reduction by means of the semi-log plot method would be such a formidable task as to seriously limit

the benefits gained by the attainment of such great resolution.

The method is known as the tangent method and is easily explained with reference to Figure (C-1). The line 1 is drawn as explained above, and the line 2 is drawn tangent to the probe characteristic as it crosses the voltage axis at the floating potential. Equation (C-3) may be rewritten

$$\frac{kT_e}{e} = j_e \left[dj_e/dV_p \right]^{-1} \qquad \text{(C-4)}$$

Equation (C-2) may be differentiated to yield

$$d\, j_e/d\, V_p = dj/d\, V_p + d\, j_i/d\, V_p \qquad \text{(C-5)}$$

Evaluating all quantities at $V = V_f$ where the total collected current vanishes results in:

$$\frac{kT_e}{e} = \frac{j_{if}}{(dj/dV_p)_f + (dj_i/dV_p)_f} \qquad \text{(C-6)}$$

In Figure (C-1) one can identify:

$$(dj/dV_p)_f = (b + c)/a$$

$$(dj_i/dV_p)_f = -c/a$$

$$j_{if} = b$$

Thus

$$kT_e/e = a \qquad (eV) \qquad (C\text{-}7)$$

To use this method one need only draw line 1 on the probe characteristic, the same as when using the semi-log plot method, and the tangent line 2. The distance "a" is then merely measured directly from the characteristic in volts, directly giving the electron temperature in electron volts.

Another advantage to this method beyond its ease of application is its "local" character. Notice that the probe is required to operate only near to its floating potential in order to yield results using this method. Often operation of the probe in the region well above its floating potential seriously depletes the free electron density in the flow field since electron currents can be very large. This effect of course disturbs the phenomena being investigated

and limits the use of the probe as a diagnostic tool. Operation in this region is necessary when using the semi-log plot method in order to minimize any errors caused by the approximation of the ion current. The use of the tangent method avoids this problem.

In the investigations carried out here the tangent method was used to reduce all data. In addition three or four traces per test were analyzed using the semi-log plot method to serve as a continuous check on the data. In all cases the results agreed to within 10% and more often to within 6%.

3. Ion Density

Since by definition a state of quasi-neutrality exists in the body of a plasma, either a measurement of the ion density or a measurement of the electron density would yield the charged particle density distribution. In order to measure either particle density the probe is biased far into the attracting region of the characteristic so that the collection current represents only the flux of the particle whose density is to be measured. However when this is done, the possibility of large collection currents which excessively deplete the flow field of charged particles arises. A qualitative measure of this effect can be formulated. Assuming frozen flow one can

calculate the number of charged particles per second delivered to the flow field through the sonic orfice if one knows the total density, temperature and ionization fraction. If one assumes that this current is uniformly distributed across the cross section of the free jet, then an estimate of the free jet area will give an average current density flowing in the jet. Since the area of the probe is known, the amount of current that would ideally be swept up by the probe is calculable. This value can be compared to the actual current collected by the probe and an "effective" collection area can be assigned to the probe. By comparing this "effective" area with the actual probe area, one can get an idea of how local the effect of the probe collecting charged particles actually is. A value of ten for the ratio of effective to actual probe area might not cause trouble in the light of the simplicity of this criterion. However a ratio of one hundred is considered to be an upper limit beyond which the disturbance to the plasma becomes unacceptable.

For the collection of ions this ratio of "effective" to actual probe area was calculated to lie between one and ten for all conditions. The portion of the retarding field characteristic above V_f that was taken as data required electron currents of a magnitude

such that this ratio was near ten. However, when the probe was biased positively above V_f far enough to reach plasma potential, this ratio reached well over one hundred. For this reason, it was felt that probe operation in the vicinity of the plasma potential was excessively depleting the flow field of electrons and thus destroying the local nature of the measurement.

Since the determination of the electron density requires probe operation above the plasma potential, it was decided to measure instead the ion density in order to investigate the charged particle density distributions. This is the commonly acceptable practice for just the reason mentioned above. Both Sonin (1965) and Graf (1965) arrive at the same conclusions. This limitation seriously complicates the theoretical analysis of the probe characteristic however. As shown above, for small electron Mach numbers, the collection of electrons by the probe is not affected by the plasma mass motion. This mass motion strongly affects the collection of ions, however, since they are travelling at hypersonic speeds. Thus a theory must be developed for the collection of ions by a Langmuir probe from a moving plasma.

Several theories have been developed for this situation (Smetana (1963), Kanal (1964), Lam and Greenblatt (1966)). The existing theories were inapplicable to the situation at hand, or were

too complicated to be amenable to this type of experimental application. These various theories will be mentioned during the development below.

The problem is to measure the ion density in a flowing plasma with a free molecular probe whose diameter is much larger than the Debye length. An exact theory would express this current as the directed flux of ions modified in some manner to account for their thermal motion. A heuristic theory is developed here which considers the contribution of the directed flux together with the diffusive flux of the ions and neglects any interaction between these two.

It is instructive to first consider the diffusive ion flux that is collected by a probe in a stationary plasma. The various applicable theories are described by French, Sonin and DeLeeuw (1963). In the free molecular flow situation that is present here, the electron flux to the probe in the electron collection region of probe operation is given by the expression

$$j_{eo} = -0.398\, e\, n_e (kT_e/m_e)^{0.5} \qquad \text{(C-8)}$$

In the retarded collection region of probe operation this value is

modified by the Boltzmann factor which accounts for the dimunition of electron density in a potential gradient. The resulting expression for the electron current is

$$j_e = j_{eo} \exp \left[e(V_p - V_\infty)/kT_e \right]. \qquad \text{(C-9)}$$

The flux of ions in the stationary plasma case is accompanied by many more difficult theoretical considerations. The equation describing the phenomenon may be written as:

$$j_{io} = 0.607\, e\, n_i\, (kT_e/m_i)^{0.5} \qquad \text{(C-10)}$$

The numerical coefficient in the expression differs in the various theoretical treatments. The author believes that the choice presented here is the best one. This point is discussed by French, Sonin and DeLeeuw (1963), and by Clayden (1964). It should be especially noted that the electron temperature appears in this expression rather than the ion temperature which would appear if the current flux were merely supplied by free molecular diffusion. When T_e is much greater than T_i the electric field of the probe extends far out into the plasma and accelerates the ions to the ion

acoustic speed before they enter the sheath region of the probe. The qualitative effect of the ratio T_e/T_i upon this phenomenon is easily seen. For values of this ratio much greater than one, more electrons are expected to be able to diffuse into the sheath region than when its value is near one. This can be seen upon examination of the Boltzmann factor in Equation (C-9). Since the sheath region is one in which charge-balance is violated, this increased diffusion will tend to reduce the net charge density there. From Poisson's equation this reduction causes a flattening of the potential distribution and for a given potential drop the potential field of the probe will extend further out into the plasma. The quantitative effect of this residual field acceleration is discussed by Bohm (1949) and Allen, Boyd and Reynolds (1957). Kamimoto and Nashida (1965) experimentally tested and verified this effect in a flowing argon plasma by the use of an aligned cylindrical probe. Thus the characteristic speed for static ion collection is the ion acoustic speed given by Equation (C-1) and not the ion thermal speed.

The total "static" charged particle flux to the probe may be written as:

$$j = j_e - j_{io} = e\, n_i \left[0.40\, (kT_e/m_e)^{0.5} \cdot \right.$$

$$\left. \exp\, (e(V_p - V_\infty)/kT_e) - 0.61 (kT_e/m_i)^{0.5} \right] \qquad \text{(C-11)}$$

where the current sign convention of the probe characteristic is maintained and the area needed to convert this to current flow is taken as the total wetted area of the probe $2\pi r_p l_p$.

This is a very simplified treatment of the static probe characteristic; however in the light of simplifications made in the treatment of the effect of mass flow on the probe characteristic, it is felt that its use is justified. A valuable asset of this treatment is the fact that it allows an analytic evaluation of probe operation. A numerical approach such as the excellent treatment by Laframboise (1966) would unnecessarily complicate the calculations and would not allow the simple physical interpretation that is sought in this heuristic, first order approach. Scharfman et al (1967) have attempted to develop a more accurate theory in this manner at the expense of analytic simplicity and experimental usefulness.

The collection of flowing ions by the probe forms the remaining part of the total collection current received by the probe.

As mentioned earlier the mass flow of the plasma has little effect on electron collection so that the total electron current is included in Equation (C-11)

In the case of hypersonic ion flow that occurs here there is a temptation to apply the "swept area" idea of Clayden (1963) to ion collection. Since the ions have little lateral spread of velocity as compared to their large directed flow component it might be expected that their flux on the probe would be just that swept out of a uniform stream moving at the adiabatic limit velocity. The problem with this idea is that in the case considered here the *ions* are not "hypersonic" in the correct sense. Because T_e/T_i is much greater than one, the correct "diffusion" speed with which the directed flow velocity is to be compared is not the ion thermal speed but the acoustic speed of the ions. This is evidenced by the appearance of the acoustic rather than thermal speed in the expression for the "static" ion collection current, Equation (C-10). In the case of hot electrons such as encountered here, the ion acoustic Mach number may be very near one and the "hypersonic" swept area concept can not be used. This is the main problem with the theoretical approaches of both Kanal (1964) and Smetana (1963).

Both of these treatments apply only to the case where T_e/T_i is very near one and the residual fields mentioned above do not appear. In this case the ion thermal and acoustic speeds are nearly the same and when these theories are applied to the present case the computed collection is that predicted by the swept area concept and the results do not compare at all with the experimental characteristic. Clayden modified his theory in a heuristic manner to account for this inadequacy. In the present treatment the author uses a different approach which approximates the probe characteristics obtained experimentally very well.

Since the collection of charged particles is divided into "diffusive" and "directed" contributions, it is assumed that these two types of collection are completely independent, having no effect upon each other. The directed collection of electrons is easily dealt with. The "diffusion" speed for static collection is seen to be the electron thermal speed in Equation (C-8) and since the electrons are very subsonic the contribution to the probe collection current due to their directed velocity is negligible compared to the contribution due to diffusion. Thus the total electron current will be assumed to be supplied by diffusion as in the static case.

For the ions, however, the directed speed is very nearly equal to their "diffusion" acoustic speed. In this case, the contributions of both collection mechanisms will be considered separately and added. The diffusive contribution is included in Equation (C-11), and the directed contribution will now be considered.

The field of the probe will be assumed to be unaffected by the mass flow motion and therefore will be a central force field. Thus the probe affects the particle motions through its field but the particles do not affect the field through their motions. In this sense, the theory may be considered as a sort of first order treatment. The theories of Kanal (1964) and Smetana (1963) are based on a similar assumption.

The field is considered central although not necessarily coulombic. The presence of sheaths caused by the diffusive collection of charged particles will alter the coulombic character of the field near the probe but the potential will remain only a function of the radial distance measured from the probe.

Since the potential field decays to the plasma potential at infinity, the conservation of energy and angular momentum gives an expression for the radial velocity of a particle in the potential field:

$$u_r^2 = u_\infty^2 - s^2 u_\infty^2 / r^2 - 2e(V(r) - V_\infty)/m_i \qquad \text{(C-12)}$$

where s is the impact parameter.

In order for the particle to reach the probe its radial velocity must be directed towards the probe during its whole journey to the probe surface. The boundary case between collection or not occurs when the radial velocity vanishes just at the probe surface. The shape of the potential distribution caused by the space charge in the diffusion sheath may alter this criterion so that if the radial velocity vanishes at a point outside the probe surface and the potential distribution is such that any particle reaching this point falls into the probe, the particle may be collected. This phenomenon is called the appearance of an absorption radius and is discussed by Allen, Boyd and Reynolds (1957), Bernstein and Rabinowitz (1959) and Laframboise (1966). The shape of the potential distribution inside the sheath may also give rise to the appearance of potential barriers through which a particle is unable to penetrate. In the region outside the sheath, however, the requirement of quasi-neutrality requires that the potential assume a coulombic character.

Laframboise (1966) has shown that in such a potential field barriers do not appear. The extent of the diffusion sheath may be characterized by the Debye length in the plasma. In the present case, the Debye length is much smaller than the probe radius, and any absorption radius must be very nearly equal to the probe radius. It can also be shown that any potential barrier appearing this close to the probe has very little effect for the case considered here.

Setting the radial velocity equal to zero at the probe radius results in the collection criterion:

$$s/r_p = (1 - 2e(V_p - V_\infty)/m_i u_\infty^2)^{0.5} \qquad \text{(C-13)}$$

Any particle starting from infinity with an impact parameter less than or equal to this critical value will be collected. Projected on the uniform stream at infinity the collection area of the probe is therefore increased due to this increase in the effective radius of the collector.

This formulation will lead to a directed ion current that is proportional to the square root of the probe potential. The experimental probe characteristic clearly shows that this current grows directly proportionally to the probe potential. There is another

effect to be considered. The above derivation applies to an infinitely long cylindrical collector placed normal to the uniform stream. in the present case, the cylindrical collector was made only seven and one-half times as long as its diameter to allow good spatial resolution of measurements. Therefore the finite length of the collector should be taken into account. In exactly the same manner the effective collection length of the probe is increased by the field. The relation is

$$1/1_p = (1 - 2e(V_p - V_\infty)/m_i u_\infty^2)^{0.5} \qquad \text{(C-14)}$$

The total collection area projected onto the free stream is now proportional directly to the probe potential and the collection of ions from the directed stream may be written as:

$$j_{id} = n_i e u_\infty (1 - 2e(V_p - V_\infty)/m_i u_\infty^2) \qquad \text{(C-15)}$$

The area needed to reduce this to a current is taken as the frontal area of the probe $2r_p l_p$.

The total charged particle flux on the probe is written as

$$j_t = j_e - j_{io} - j_{id} \tag{C-16}$$

where the sign convention is that on the experimental characteristic. This expression may be expanded as:

$$j_t/n_i = 2.685 \cdot 10^{-14} (kT_e/e)^{0.5} \left[\exp W - 0.00563 - \right.$$

$$\left. - 0.00656 (T_t/T_e - 0.4W)(T_e/T_t)^{0.5} \right] \tag{C-17}$$

where

$$W = e(V_p - V_\infty)/kT_e = e(V_p - V_f)/kT_e + X \tag{C-18}$$

and X is defined below.

Since at plasma potential it was felt that the high electron current drawn was affecting the plasma, this theory was used to determine the plasma potential from the easily measured floating potential of the probe. At the floating potential the probe draws no current from the plasma. Since the electrons are much more energetic than the ions there is a preponderant electron current when the probe is at plasma potential. In order to balance this

with an equal and opposite ion current the probe must be biased at a potential below plasma potential. This potential difference both enhances ion collection and retards electron collection. As expected, the presence of a directed ion flux decreases the potential drop necessary to reach floating potential. When one sets $j_t = 0$ and solves Equation (C-16) for $(V_f - V_\infty)$ the result is

$$\exp(X) = 0.00563 + 0.00656(T_t/T_e - 0.4X)(T_e/T_t)^{0.5} \quad \text{(C-19)}$$

where

$$X = e(V_f - V_\infty)/kT_e \quad \text{(C-20)}$$

This equation was solved on CITRAN yielding a table of values for X for each chosen value of T_t/T_e.

The probe characteristic, Equation (C-17) can now be written as:

$$j_t/n_i = j_t/n_i\,(T_t,\ T_e,\ V_p - V_f,\ X(T_t,\ T_e)) \quad \text{(C-21)}$$

The quantities T_e, T_t and $V_p - V_f$ are measured experimentally and $X(T_t, T_e)$ is calculated. The probe characteristic given by

Equation (C-21) was calculated for many cases and compared with the probe characteristic taken directly from the Moseley plotter. An example is given in Figure (C-2). The dashed line represents the contribution of the static or "diffusion" ion current. It can be seen that reasonable agreement was obtained considering the simplicity of the theoretical treatment.

Using this theory the ion density was calculated in the following manner. The total collection area $A_p = 2\pi r_p l_p$ was calculated. The total collection current I was measured at a chosen potential $(V_p - V_f)$ below the floating potential. From these two quantities a measured value of $j_t = I/A_p$ was calculated. The total temperature and electron temperature were experimentally measured. Using the same value of $(V_p - V_f)$, Equation (C-17) was solved for a theoretical value of j_t/n_i. The ion density is then the ratio of the two.

$$n_i = (I/A_p)/(j_t/n_i)_{theo.} \qquad (C\text{-}22)$$

The value of n_i calculated in this manner is to be compared with the ion density calculated by assuming frozen flow in the free jet.

An examination of the effect of varying the value of $V_p - V_f$ at which I was measured was carried out. It was found that varying the value between $-4 \leq V_p - V_f \leq -1$ volts resulted in less than a two percent spread in the calculated distributions of n_i in the free jet. This result reflects the fact that the whole probe characteristic is very well modelled by this theory. This is the type of test that is suggested by Scharfman et al (1967) in order to investigate the applicability of such a theory for ion collection.

4. Collisions

The various mean free paths for the experimental conditions existing during the Langmuir probe tests are presented in Table II. It is appropriate to discuss here the effect of the probe Knudsen number upon probe operation during these tests. The diameter of the Langmuir tube is 4.57×10^{-4} meters.

The probe is easily seen to be well within the free molecule flow regime with respect to neutral-neutral collisions. The appropriate probe Knudsen number varies monotonically from about 2.5 at a point 3.2 diameters downstream of the orifice to about 260 at a point 32 diameters downstream. The lowest value here is about 10 times the lowest value to which Scharfman et al (1967) found

a free-molecule theory applicable.

The measurement of electron temperature was found to be relatively independent of the ion mean free paths by Dunn and Lordi (1969); however, operation in this retarding field region of the characteristic is very sensitive to the electron mean free path length. Due to the Ramsauer effect, the electron-neutral mean free paths are very long. The associated probe Knudsen number is very large so that electron-neutral collisions should not affect probe operation at all. The probe Knudsen number associated with electron-electron collisions varies from about one at a point 3.2 diameters downstream of the orifice to a value of nearly one hundred further downstream. The variation is not monotonic because the mean free path depends strongly on the measured electron temperature distribution which is not monotonic . For these values of probe Knudsen number, the theory presented here for electron collection is certainly suitable. In fact, French, Sonin and DeLeeuw (1963) found that even for a probe operating in the continuum regime with respect to electron-electron collisions the theory developed here could safely be used to calculate the electron temperature.

The appearance of collisional effects is usually associated with a small ion-neutral mean free path. The resulting operation

in the ion collecting region must then be modified to account for collisional diffusion. Descriptions of this type of correction can be found in Chen (1965) and Schott (1968). Experimental considerations are described by Dunn and Lordi (1969). For the experimental situation at hand, the probe Knudsen number associated with these collision partners varies from about one to one hundred monotonically from 3.2 to 32 diameters downstream of the orifice. Therefore this type of correction should not be necessary for the interpretation of ion collection by the probe.

Upon examination of Table II it is seen that the ion-ion mean free path is very short in this experimental situation. This is due to the inverse square dependence of the ion-ion cross section upon the ion temperature which is very low for the assumed isentropic expansion in the free jet. However ion-ion collisions in the body of the plasma itself are not very important so far as the process of ion collection by the probe is concerned. What is important are collisions between ions in the free stream and ions which have already contacted the probe and have assumed the probe temperature. This type of collision can affect the ion collection process, but its occurence is very unlikely since the "probe" ions must escape from the potential well of the probe in order to interact with

the free stream. This argument was used by Clayden (1963) and Sonin (1965) to justify their neglect of ion-ion collisional effects. French (1961) and French, Sonin and DeLeeuw (1963) also concluded that such collisions do not affect the ion collection region of the probe characteristic in either the stationary or flowing plasma application. But even assuming that some ions manage to escape the probe potential well and enter the free stream region with about the probe temperature, the collision cross section between oncoming ions with velocity u_∞ and a "thermal" ion is

$$Q \sim \left(\frac{1}{2} m_i u_\infty^2\right)^{-2} \ll Q_{ii} \sim (kT_i)^{-2}$$

Therefore the pertinent mean free path is much longer than that corresponding to collisions between thermal ions and operation in the ion collection region should not be affected by ion-ion collisions.

Appendix D

The Computational Details

This Appendix describes the actual method of computation used to generate the graph of precursor length, Figure 1.

The results of Jaffrin show that the electron temperature is raised to a value very near to its final downstream value of T_{H2} due to heating in the precursor by the time the shock is reached. In this case $T_S \simeq T_{H2}$ and $T \simeq T_{H2}$ everywhere downstream of the shock. Therefore a solution for T linearized about its downstream value of $T_{+\infty} = T_{H2}$ may be valid for the entire region downstream of the shock, not only near the saddle point. This solution is given by Equation (II-25), and in this case the constant may be evaluated at the position of the shock where $\tilde{T} = \tilde{T}_S$ yielding

$$\tilde{T} = \tilde{T}_{H2}/S + (\tilde{T}_s - \tilde{T}_{H2}/S) \exp(-b(\tilde{y} - \tilde{y}_s)) \qquad \text{(D-1)}$$

When this linearized downstream solution is valid a simplified method of determining the shock position can be used. The full energy equation, (II-13), is integrated from $\tilde{y} = 0$ to a point just downstream of the shock denoted by $\tilde{y} = \tilde{y}_s^+$. Compared to the length of the integration, the precursor length, the shock appears very thin and step functions may be substituted for the shock property profiles $\tilde{n}(\tilde{y})$ and $\tilde{T}_H(\tilde{y})$ in the last integral. The fact that $\tilde{T} = \tilde{T}_s$ and is constant across the shock wave is also used in the integration. The upstream boundary conditions,

$$\tilde{T} = 1$$

$$\frac{d\tilde{T}}{d\tilde{y}} = 0$$

are applied at $\tilde{y} = 0$. At the point $\tilde{y} = \tilde{y}_s^+$ the conditions are:

$$\tilde{T} = \tilde{T}_s$$

$$\frac{d\tilde{T}}{d\tilde{y}} = \left(\frac{d\tilde{T}}{d\tilde{y}}\right)^+ = -b(\tilde{T}_s - \tilde{T}_{H2}/S)$$

where the last condition is obtained from Equation (D-1). The integration yields:

$$\frac{\tilde{T}_{H2}/S - \tilde{T}_s}{2} \left(\tilde{T}_s S/\tilde{T}_{H2}\right)^{5/2} \left((1 + 164.4 \frac{\tilde{T}_{H2}}{M_H^2})^{0.5} - 1\right) +$$

$$+ 1 + \tilde{T}_s \left(\frac{2}{3} \ln 4 - 1\right) = \frac{2.565\, S}{M_H^2} \int_0^{\tilde{y}_s} \left(\tilde{T} - \frac{1}{S}\right) \tilde{T}^{-3/2} d\tilde{y} \qquad \text{(D-2)}$$

The criterion is applied during the upstream integration. Each value of $\tilde{T}(\tilde{y})$ calculated by the Runge-Kutta scheme was substituted as a trial value of $\tilde{T}_s$ in the left hand side of Equation (D-2). The integral on the right hand side was continuously calculated using a Simpson integration. The calculated value of the left hand side was compared with the accumulated integral at each point. When the equality was satisfied the integration was stopped on the coordinate corresponding to the shock position. Thus when the linearized downstream solution was valid, the shock could be automatically found during the upstream integration scheme. The validity of the linearized downstream solution was tested by comparing the so calculated value of $\tilde{T}_s$ with the final downstream value of $\tilde{T}_{H2}/S = 5M_H^2/16S$. In the cases of interest here the difference was usually less than ten percent showing that the linearized downstream solution was indeed applicable.

Appendix E

Conditions in the Arc Head and Settling Chamber

1. The Arc Head

Experimental evidence supported by theoretical calculations (Wheaton and Deane (1961), McHale (1964)) has suggested that the anode attachment point of the arc in a plasma generator is not stationary but is in constant motion axially. The cool, high density layer of gas next to the anode wall is pierced locally by the arc column to form a high temperature conducting path for the arc current. This attachment point moves down the anode channel under the influence of aerodynamically and convectively generated forces, all the while increasing its total potential drop until minimum energy principles require that the arc restart near the cathode or along another path between the arc column and the anode surface. This cycling process was found to cause periodic changes in arc voltage without affecting the temporal distribution of arc current.

These instabilities of anode attachment are a common problem in arc heater applications. Their effect has been mentioned in the reports of Lai et al (1958), Weltmann (1962) and Makin (1962). Clayden (1961) specifically mentions the cyclic nature of this arc instability and attributes it to the mechanism mentioned above.

Two specific anode design parameters affect this phenomenon. A low pressure existing in the arc attachment region causes the filament of the arc column to become relatively diffuse, thereby partially eliminating the local nature of the anode attachment point. When this occurs the movement of the localized attachment point and the resulting voltage fluctuations are avoided. However, there is an optimum value to be sought here, for although a diffuse arc column tends to heat the working gas more uniformly, the attendant low densities may not allow full equilibrium to be reached within the arc column. Thus for stable operation one should operate at low total pressures and utilize a settling chamber to assure that equilibrium is attained.

The second parameter is the geometric design of the anode, through which the arc-anode attachment point may be controlled and located spatially. This can be accomplished by means of a sudden

change in anode geometry such as that afforded by a conical entrance section followed by a constant area throat. The arc usually attaches at the point where the wall slope changes abruptly because of the singularity in the potential field and the local hot region which causes increased plasma conductivity near this point. In the interest of flow steadiness, a constant curvature anode might be preferred, but in this case stability is decreased because the arc-anode attachment point is not fixed. In this work the conical entrance-constant area throat design was used. In order to further limit the excursion of the arc attachment point, the axial length of the throat was decreased resulting in the "short" anode shown in Figure (8). The use of a settling chamber serves to damp out any flow unsteadiness caused by this design.

By these means arc stability and flow steadiness were enhanced in the design described here. In all of the tests carried out, the time necessary to take any measurement was considerably longer than the characteristic time measured for this type of voltage fluctuation. Thus, any such fluctuations that existed were effectively averaged out in the data. Since the arc voltage is primarily affected by this type of anode attachment instability, the electron temperature

would be expected to display the largest effect experimentally. The temporal resolution of the Langmuir tube output was much better than that of any of the other data collected; however, any fluctuations that were evident were always very small and an average curve was easily fitted through them.

The experimental tests on the arc-heater facility in which this type of high frequency instability was examined and in which the effects of the design parameters mentioned above were studied are described in Appendix A.

Another type of arc-instability experienced in this work was that of anomolous arc attachment on the cathode. A similar problem was reported by Witte (1969) in his design of arc heater. The explanation of the basis for this phenomenon is closely tied to specific arc-heater design. Therefore, the description of the phenomenon together with the design changes and experimental tests carried out to eliminate it are best described in Appendix A.

One of the critical parameters in arc-heater design is the manner in which the working gas is injected into the region of the arc column. Two injection schemes are evident: tangential and radial. Tangential injection delivers the working gas to the region

of the arc column with a definite swirling motion. This swirl tends to move the arc attachment point on the anode and thus avoid the problem of intense local heating and failure. The vortex motion also serves to lengthen the arc column and thereby improve the heat transfer from the arc column to the working gas. The thermal loading on the anode is lowered since the dense, colder gas is centrifugally spun into the outer layers which are in contact with the anode wall. For the same power, a longer arc-column also results in a higher voltage drop and therefore less current and associated heat loading on the anode.

However, tangential injection also results in a large radial temperature gradient as well as a residual tangential velocity in the working gas stream. This makes the use of a settling chamber mandatory. At low pressures, this swirling motion has been seen to extend through the settling chamber and into the test section. Both Becker and Heyser (1967) and Stursberg (1967) report that the expected increases in efficiency and electrode life when this scheme was utilized could not be clearly seen. As reported by John and Bade (1961) in their review of arc technology, the self induced or natural motion of the arc column and the electrode spots is sufficient to allow satisfactory operation at relatively low total

pressures (less than one atmosphere) and arc power. It is the high pressure, high power arc heaters that require that this motion be augmented either by tangential injection or an applied magnetic field. (Boatwright et al (1962), Boldman (1963)). The anode attachment point tends to be relatively diffuse at low pressures and low power levels. French and Muntz (1960) found that they could obtain more stable, less contaminated operation if the total pressure was lowered. There have been some attempts at obtaining diffuse anode attachment at higher pressures by drawing the arc column through the aerodynamic throat and allowing attachment in the supersonic, low pressure region downstream. With this scheme, of course, the settling chamber must be eliminated and the attainment of uniform heating or chemical equilibrium in the working gas is doubtful.

In this investigation radial injection was utilized. The injector is described in Section III-A-1 and some of the effects are discussed in Appendix A. Radial injection eliminated any possible swirl in the test section. The design of the injector caused a layer of cool argon to flow over the length of the cathode and thus afford better cooling and less contamination. The relatively high speed flow of cool gas over the base of the cathode as compared to

conditions at the tip tends to discourage anomolous arc attachment on the cathode. The arc-heater was tested with both radial and tangential injection. The results of these tests are described in Appendix A. It was concluded that the radial injection indeed was a superior scheme.

2. Calculation of the Total Enthalpy

One of the most important properties necessary to describe the state of a real gas flow is the total enthalpy. In the free jet flow field it is especially necessary, in order to determine the particle velocity and density distribution by means of the methods described in Section III. In experimental facilities utilizing arc heaters the total temperature is so high that an indirect means of measurement is mandatory. Two such methods are considered here; the heat balance method and the choked flow method.

The heat balance method determines the energy per unit mass in the working gas by subtracting cooling water power losses from the electrical power supplied and dividing by the gas mass flow rate. The method is very easy to use and is free from theoretical uncertainties. Any errors introduced from heat leaks were minimized by the insulation of all conduction paths from the

apparatus. Since the power lost to the cooling water is a large fraction of the total electrical power supplied there is a large inherent error in this method because it depends upon the difference between two large quantities. This error has been minimized by the very careful calibration of all involved measurement proceedures. The maximum possible error at typical operating conditions was found by error analysis to be 19 percent.

The analysis of the adiabatic, reversible flow of a perfect gas of a given chemical composition through a sonic orifice shows that the total enthalpy is proportional to the square of the total pressure for a given mass flow and sonic orifice area. This method of determining the total enthalpy will be called the choked flow method. It can be generalized to either equilibrium or frozen flow of a real gas.

The equilibrium choked flow method was developed using the tables of Witte (1964) for equilibrium properties of argon. In the desired region of operation of h_t/RT_o less than 100, it was found that the ideal gas results were indistinguishable from the equilibrium flow results. This same conclusion has been reached by Becker and Heyser (1967) and Sherman and Talbot (1962). The

equilibrium choked flow method for determination of the stagnation enthalpy was used by Potter et al (1963) notably among others.

In chemically frozen flow the enthalpy given by the choked flow method is the translational and thermal energy of the atoms and ions. The energy bound up in chemistry is considered frozen in and does not affect the formulation. Goodwin (1963) examined this relation for dissociating nitrogen and found that the enthalpy determined by the heat balance method agreed well with stagnation point heat transfer measurements and that the choked flow method gave much lower enthalpies. He concluded that the discrepancy amounting to 2/3 of the total energy in the gas represented that portion of the energy frozen into the chemistry of dissociation. Pope (1968) was able to account for this much energy difference by assuming that the dissociation-recombination reaction was frozen at conditions existing immediately at the arc-heater exit.

The amount of energy tied up in ionization at the low ionization fractions experienced in the flow under study was calculated and found to be very small when compared to the total enthalpies generated. Thus the appearance of a discrepancy between the two methods of enthalpy determination could not be ascribed to the

freezing-in of chemical energy. A similar conclusion was reached by Sherman and Talbot (1962). Thus, the flow may be considered as that of a high enthalpy, perfect monatomic gas.

Large discrepancies were found, however, between the results calculated by the heat balance and choked flow methods. The choked flow method generally yielded results between 20% and 40% below the results of the heat balance method. Makin (1962) reports a similar discrepancy between the two methods and notes that the choked flow method may give too low a result due to non-ideal gas effects. Boatwright et al. (1962) also noted large differences between the two methods in a high pressure arc. Some of the non-ideal gas flow effects contributing to the inaccuracy of the choked flow method are: non-equilibrium and non-uniformity of the gas flow in the settling chamber; changes in the nozzle discharge coefficient caused by viscous shear, diabatic flow and orifice erosion; and the depletion of the total enthalpy while traversing the nozzle due to heat transfer to the cooling water.

The first point may be neglected for low enough ionization fractions as discussed above and for a settling chamber long enough to afford adequate mixing of the effluent from the arc heater. This statement was substantiated by Potter et al. (1963)

in their studies of the effect of chamber length. The use of radial injection in the arc heater to eliminate swirl in the effluent is also expected to help in this respect.

The orifice erosion mentioned in the second point was virtually non-existent in the facility designed here.

The effect of irreversible, diabatic flow on the nozzle discharge coefficient can be examined. Frictional shear stresses reduce the discharge coefficient by decreasing the velocity near the wall. Heat transfer to a cold wall increases the discharge coefficient by increasing the density near the wall. These two processes tend to counteract each other in their effect upon the discharge coefficient and the mass flux distribution may be very flat across the orifice as a result, giving a discharge coefficient very near one. Calculations by Winovitch (1964) show this to be the case, and he advises that the discharge coefficient be taken as unity. The small deviations that he found possible were far overshadowed by the effects caused by normal experimental error in the measurement of other quantities necessary to the theory. It should be noted here that caution should be exercised when using the particularly simple method of ratios derived from the choked flow method and used by many authors: Kamimoto et al. (1965),

Clayden (1961). For the same mass flow rate and sonic orifice area the stagnation enthalpy for heated flow may be related to the easily measured stagnation enthalpy in cold flow and the total pressure in both cases

$$h_{t,\,hot} = h_{t,\,cold}\,(p_{t,\,hot}/p_{t,\,cold})^2$$

The balancing effect of heat transfer is absent in the cold flow case and viscous shear effects may lower the discharge coefficient below unity and thus invalidate the assumption of equal sonic orifice area in hot and cold flow. In order to account for this effect, the discharge coefficient was measured in cold flow in the present apparatus. The cold enthalpy was measured with a mercury thermometer as shown in Figure (13). For cold flow at a mass flow rate of 0.2 grams per second the total pressure was measured as 16.5 torr. Within experimental accuracy the cold flow discharge coefficient was found to be unity.

The third point mentioned above is very important. Diabatic flow caused by heat transfer to the cold wall invalidates the assumption of isentropic flow that is basic to the theory of the choked flow method. The shear energy dissipated by viscous

forces is dwarfed by the large heat transfer found in such an apparatus. The parameter

$$\frac{\text{Power lost to wall cooling water}}{\text{mass flow rate} \cdot \text{total enthalpy/mass in gas}}$$

is of importance here. In the investigations of Winovitch (1964) and Pope (1968), this parameter was less than 10% so that this effect could be ignored. In this case, good agreement was found between the choked flow method, properly modified for frozen-in chemical energy, and other methods of determining the stagnation enthalpy. In the case examined here, the values of this parameter range from 100% to 200% so that this is a very important effect.

For the low Reynolds numbers existing in the chamber and nozzle (see later in this Appendix for their calculation) it was decided not to utilize the boundary layer analysis used by Winovitch (1964) and Potter et al. (1963). Instead a simple one dimensional flow analysis was developed in which averaged properties are considered in order to estimate the effect of this process and see whether it could be blamed for the discrepancy mentioned above. The total pressure increases along the axis of the nozzle according to:

$$\frac{dp_t}{p_t} = -\frac{\gamma M^2}{2} \frac{dT_t}{T_t}$$

Thus, the effect of heat being lost to the wall would be to raise the total pressure above that measured in the chamber. This relation reveals why the enthalpy computed by the choked flow method based on the chamber pressure would be too low. Since the total enthalpy is proportional to the square of the total pressure, a small change in total pressure can have a large effect on the enthalpy. In the settling area of the chamber the Mach number is very small and thus heat transfer there does not change the total pressure very much. As described in Appendix A, it was experimentally determined that the heat transfer to the walls in the settling area was very small compared to that in the nozzle, and also that the total pressure did not vary measurably along the length of the settling area. The length of the chamber was not found to affect the choked flow method result so that the major effect was expected to be caused by heat transfer in the nozzle.

An integration was carried out along the nozzle using the Mach number distribution derived from the nozzle area distribution. Since it was possible to measure only the total heat transfer rate to

the walls, a rough approximation to the heat transfer distribution was assumed. The calculated correction raised the results of the choked flow method to within the experimental scatter of the results derived from the heat balance method. Thus the effect of heat transfer to the nozzle wall, which invalidates the isentropic flow assumption, is the reason that the choked flow method cannot be used in this application. A corrected choked flow method could be used to estimate the stagnation enthalpy; however, since the correction still requires the measurement of cooling water losses in the nozzle as well as many other assumptions that are weak theoretically, the heat balance method was employed in this work to determine the stagnation enthalpy. Good results using the heat balance method have been reported in the literature, most notably by Arney and Boylan (1963), who found that this method checked to within 3% of the results measured with a total calorimeter. Weltmann (1962) found an agreement to within 10% between the heat balance method and measurements of total enthalpy taken immediately downstream of the nozzle exit.

Since measurements were carried out along the centerline of the free jet, there remains the problem of a non-uniform enthalpy distribution across the jet profile. Pope (1968) found that the ratio

between the centerline total enthalpy measured in the test section and the mass averaged total enthalpy gained from the heat balance method varied from 1.25 to 2.07. Total enthalpy profiles across the free jet were measured at Cal Tech in a similar flow field by Witte (1969) using a total enthalpy probe. The data from these experiments were statistically curve fitted and integrated to give a value of

$$\frac{h_{t,\,centerline}}{h_{t,\,average}} = 2.079$$

and this number was multiplied by the mass average total enthalpy calculated by means of the heat balance method to determine the centerline values of total enthalpy used in this work.

Entrance enthalpy of the working gas before heating was measured using the mercury thermometer in the entrance gas line. Because of the long gas lines connecting the high pressure argon storage bottles to the apparatus this temperature was always very near room temperature. Compared to the amount of enthalpy added during the arc heating process this additional small amount was in all cases entirely negligible. The total enthalpy of the working gas was taken as that amount added during the arc heating process.

3. The Settling Chamber

The purpose of a settling chamber is to allow the decay of any aerodynamic unsteadiness generated in the arc heater as well as to allow the attainment of thermal and chemical equilibrium in the working gas before the sonic region is reached. The flow from the arc heater consists of particles with disparate energies caused by the arc heating process. The non-diffuse, filamentary arc column heats only the portion of the gas which passes through the arc column. The settling chamber affords a mixing area in which this non-uniform heating is equalized and thermal equilibrium is attained. Chemical equilibrium is assured if particle transit times through the chamber are longer than the characteristic times associated with the relevant chemical processes.

Another purpose served by the settling chamber is the separation of the arc heating process from the test area. A geometrical area enlargement after the anode assures arc attachment at the anode. The arc heater can be considered solely as a supply of high enthalpy working gas and its interaction in any other way with the test area can be ignored.

Settling or mixing chambers are used in most experimental facilities using arc heaters except in some high power installations. The inclusion of a settling chamber reduces the overall efficiency of the heating process. In this case, for example, the power lost to the chamber cooling water amounted to about 40% of the total electrical power supplied. The ability of the settling chamber to assure the uniformity of the heated test gas overshadows efficiency considerations in low power installations.

Various sizes of settling chambers have been used. Arney and Boylan (1963) carried out an experimental study of the effect of chamber length in assuring chemical equilibrium in the settling chamber. They found that dissociational equilibrium in nitrogen at a total pressure of one atmosphere was assured for lengths between 5 and 7 inches for a 3 inch diameter settling chamber. This figure of course depends upon the flow residence time in the settling chamber as compared to the rate process time for the specific chemical reaction taking place in the gas as it approaches equilibrium. To calculate these two characteristic times, conditions must be known in the settling chamber.

Conditions existing in the settling chamber are calculated from the directly measured total pressure and the indirectly measured total enthalpy by assuming that the working gas is in equilibrium. The degree of chemical equilibrium can be characterized by the ratio of the characteristic time for convection of the reacting species to the characteristic time for the ionization-recombination reaction taking place. Writing the steady one dimensional continuity equation including recombination for the electrons yields

$$\frac{d(n_e u)}{dx} = -a n_e^2$$

where a is the recombination coefficient. By non-dimensionalizing this equation, the characteristic times may be written

$$t_{conv} = L_o/u_o$$

$$t_{chem} = (a_o n_{eo})^{-1}$$

where reference states refer to conditions in the settling chamber.

Makin and Keck (1963) give

$$a = 2.3 \cdot 10^{-20} \, n_e / T_e^{9/2} \qquad \text{(mks)}$$

for three body recombination. The ratio of t_{conv}/t_{chem} was calculated to lie between the limits of 10 for low power tests and 100 for high power tests. Thus the species have enough time to complete rate reactions while traversing the settling chamber and chemical equilibrium can be assumed to exist there.

The same calculation was carried out using the recombination coefficient for collisional-radiative recombination in argon published by Chen (1969) which was calculated using the quantum mechanical theory of Bates, Kingston and McWhirter (1962). The calculated ratio is very close to the ratio reported above, thus substantiating the conclusion.

The degree of thermal equilibrium in the settling chamber can also be estimated. Thermal equilibrium will be obtained by means of energy transfer through elastic collisions between the various species. Since the ions and neutrals have approximately the same mass, they attain thermal equilibrium very quickly. It is the electrons which are of interest here. A characteristic time

can be written for energy transfer by means of elastic collisions between electrons and the heavy particles. This process was discussed in Appendix B. Equation (B-25) allowed one to compare the effects of the two collisional processes; electron-neutral and electron-ion. For the conditions in the flow field it was shown that charged particle encounters were by far the predominant mechanism; however, for the condition existing in the settling chamber both processes are of importance. The charged particle encounters remain the most important mechanism, but here the electron-neutral collisions contribute about 25% of the total effect. The characteristic times for these two processes are given in Equations (B-23) and (B-24). For the typical test conditions in the settling chamber, the ratio of the flow characteristic time L_o/u_o and the characteristic time for energy transfer by elastic collisions is greater than 10. Thus, the electrons and heavy particles have sufficient time to equilibrate their temperatures as they flow through the settling chamber and the temperature of all species is the total temperature existing in the settling area.

From the definition of Reynolds number and the continuity equation

$$Re = 1.272 \dot{m}/\mu d$$

where d is the chamber diameter or the orifice diameter. The viscosity was calculated from data found in Kennard (1938) using the Sutherland model for cold flow cases and from the data of Arave and Huseby (1962) for the equilibrium properties of high temperature argon.

For the typical hot flow case of 0.2 grams per second argon mass flow at 8,000°K stagnation temperature, the chamber Reynolds number is 20 and the nozzle Reynolds number is 235.

For cold flow conditions at 0.2 grams per/second of argon mass flow and the stagnation temperature of 26°C, the chamber Reynolds number is 144 and the nozzle Reynolds number is 2240.

Since the Mach number in the settling area of the chamber is so low the total pressure is approximately equal to the static pressure. The total pressure was therefore measured by means of a wall tap into the settling area. Various lengths of stainless steel tubing were placed in the end wall tap hole shown in Figure 10. to measure the total pressure at various points along the length of the settling chamber wall. No change was found in the

measured total pressure. A length of tube was chosen which allowed the pressure to be measured just before the nozzle expansion was started.

In order to investigate the flow field existing inside the settling chamber, a pitot pressure probe with a long (6 inch) 0.125 inch diameter tube to run through the orifice and into the settling area was built. The probe is shown in Figure (15) as probe number 2. The instrumentation and test proceedure was the same as that used for the pitot tests described in Section IV-B. The pitot pressure was measured with this probe along the centerline of the chamber from the nozzle entrance up to the face of the arc heater. Since this test could only be carried out in cold flow, the chamber Reynolds number is about 7 times that for the hot flow case with an equal mass flow of 0.2 grams per second. Therefore, the cold mass flow was lowered in order to more closely match the hot Reynolds number. The lowest rate to which the argon flow meter was calibrated was 0.1 grams per second for which the cold flow chamber Reynolds number is 72. In order to examine the effect of chamber Reynolds number, tests were performed for mass flow varying between 0.1 and 0.2 grams per second. The pitot pressure was recorded and compared with the static pressure measured at

the wall tap. No measurable difference was found for any value of the Reynolds number. The pitot pressure remained constant for all axial positions up to a point very close to the arc heater exit. Although it was not possible to exactly match the hot and cold flow Reynolds numbers it is felt that since these results were invariant to changes in Reynolds number as measured, they could safely be extended to the lower value present in the hot flow situation. Thus, it was experimentally verified that the wall tap does indeed indicate the total pressure in the chamber and that the total pressure does not vary axially along the chamber length.

The second point was verified in the hot flow situation by the experimental observation that the length of stainless steel tube inserted in the pressure tap had no effect on the value of measured total pressure. Weltmann (1962) measured the crosswise static pressure profile in the settling chamber for hot flow. This profile was found to be constant thus substantiating the conclusion that the centerline pressure is equal to the wall pressure that was arrived at here. Potter, et al. (1961) measured the total pressure profile in the settling chamber in hot flow and also concluded that the wall tap recorded the true total pressure.

Typical total pressures measured here were 17 torr for cold flow and 50 torr for hot (100 A) flow. The mass flow rates were always held at 0.2 grams per second of argon as explained in Appendix A.

The stagnation density was computed from the equation of state for equilibrium argon using the measured total pressure and temperature. Typical stagnation densities were $4 \cdot 10^{-3}$ kg/m^3.

The mean velocity in the settling area was computed from the measured mass flow rate, total pressure, and total temperature. Typical mean velocities were 10 m/sec. The Mach number corresponding to this is $6.3 \cdot 10^{-3}$.

The ionization fraction existing in the settling chamber was calculated from the equilibrium relations for argon. As mentioned above, the species have sufficient time to reach chemical and thermal equilibrium during their transit of the settling chamber. The Saha expression derived by Witte (1964) is:

$$\frac{\alpha^2}{1-\alpha^2} = 4.97 \cdot 10^{-4} \frac{T_t^{5/2}}{p_t} e^{-182900/T_t} \cdot \left[\frac{4 + 2e^{-2060/T_t} + 2e^{-156200/T_t}}{1 + 12\, e^{-13500/T_t}} \right]$$

where T_t is measured in degrees Kelvin and p_t is measured in torrs.

Unfortunately, the ionization fraction is a very strong function of the temperature. As mentioned previously, the method of computing the total temperature has a very large inherent error and this error is compounded many times over in the calculation of the ionization fraction. By differentiating the above expression, one finds that at the typical operating conditions a 10% error in total temperature leads to a 125% error in the ionization fraction. Thus the ionization fraction and with it the charged particle densities can be considered to be known at best only to within a factor of two or three.

Appendix F

Langmuir Tube Design and Preliminary Tests

1. Mechanical Design

The theory of the operation of the Langmuir probe is given in Appendix C. For the present application the most stringent criterion for probe design is the method of solution of the cooling problem. This problem does not arise in transient applications such as side or end wall probes in shock tubes. For steady state operation provisions must be made to insure adequate cooling of the probe. One solution has been to mount the probe on a swing arm arrangement in such a manner that the collecting surface is capable of being swung rapidly through the hot plasma. The voltage sweep of the probe characteristic is then applied by means of a pulse generator and the characteristic itself is photographed on an

oscilloscope. This method presents obvious problems with sequence timing. Furthermore, as mentioned in Appendix C, it is necessary to perform the probe characteristic voltage sweep slowly enough to avoid the effects of transients. Certain transients in arc heater operation that are mentioned in Appendices A and E have characteristic times equal to or longer than the time allowed for the voltage sweep using this method. For these reasons, this method was discarded. Water cooling of the probe necessitates a return circuit for the water. If the probe is to be sting mounted the design must be of a concentric tube type which results in a large probe. The Langmuir tube design overcomes these difficulties.

The Langmuir tube consists of a length of very small diameter tubing which is passed normal to the jet axis, through the barrel shock, into the flow field and out through the barrel shock on the other side. The tube is provided with an insulating coating everywhere except at a small cylindrical collector section at the center. Cooling water need only make one transit through the flow field allowing the probe size to be much smaller than the sting mounted type. By piercing the barrel shock rather than the bottom shock, the probe will cause much less disturbance to the flow field.

This point is discussed in Appendix C. Furthermore, with this design it is possible to place a blunt body downstream of the probe without the presence of the probe affecting the flow around the body. The Langmuir probe was therefore built in the form of a tube as shown in Figure (F-1). This configuration will be referred to as a Langmuir tube.

The Langmuir tube is cooled by means of a high pressure distilled water. Calculations revealed that for a 0.018 inch OD, 0.010 inch ID tube, 11 inches long, adequate flow rate of water to assure sufficient cooling of the probe would be provided by a 100 psi pressure drop.

The Langmuir tube arrangement was fashioned in the form of a bow as shown in Figure (F-1). The numbers in this Figure will be referred to below. The body of the bow (1) was fabricated from one-half inch thick aluminum plate. The Langmuir tube which forms the "bow-string" (2) was made from a length of 0.018 inch OD, 0.010 inch ID tempered stainless steel hypodermic tubing. Two sleeve insulators made of 0.031 inch OD, 0.020 inch ID alumina tubing (3) were slipped on the stainless steel tube leaving a 3.5 millimeter long collecting area in the center uninsulated (4).

Slotted fittings on the ends of the arms of the bow allowed the tube to be aligned normal to the jet centerline. Nylon insulators (5) threaded for 5/8 x 18 standard thread pass through these fittings. These nylon insulators were drilled and tapped to accept a Swagelok #200-1-1 fitting (6) on the inside and a Swagelok #400-2-1 fitting (7) on the outside. The ends of the nylon insulators were turned down to the thread root diameter and provided with steel compression bands (9) to eliminate expansion of the internal threads. "Leak-Lock" brand joint sealant was used on all threaded joints. Nuts on threaded nylon insulators (8) allowed the "bow-string" to be tightened in tension.

The Langmuir tube itself was fabricated under a 30X binocular microscope. A piece of the hypodermic tubing was cut off to the desired length and the ends were squared up on a Carborundum stone by hand. A piece of 0.008 inch diameter tungsten wire was passed through the tube so that it protuded from both ends. Two pieces of alumina insulator tubing were then placed on the tube. The ends of the tube were cleaned with acid with care not to get any acid in the tube. The area approximately one-half inch from the end of the tube was tinned with soft solder and a 5/8 inch long piece of 1/8 inch copper tubing was carefully soft soldered

on each end so that the stainless steel tubing just protruded from the copper tube. The tungsten wire, which kept the tube bore free from solder as well as material deposited during heating, was then removed. The 1/8 inch tubes were placed in the Swagelok #200-1-1 fittings (6). The "bow-string" was tightened by means of the large nuts (8). The end fittings were then covered with a layer of P-78 Sauereisen ceramic compound applied with a fine brush (11).

The bow was attached to the probe traverse mechanism described in Section IV-A-2 at point (12). It is positioned so that the blunt body lies in the area between the bow and the "bow-string". The Langmuir tube then passes through the barrel shock to the bow which is entirely outside the free jet flow field. The collection area (4) can be positioned anywhere between a point 3.2 diameters downstream of the orifice (the inertially dominated flow region is discussed in SectionIII) and the face of the blunt body. The probe positioning system was indexed in the manner described in Section IV-A-2.

Electrical connection to the Langmuir tube was made through heavy copper wires (13) soldered to the fittings (6). These wires were protected with grounded co-axial shields to eliminate any electrical interference.

The cooling circuit for the Langmuir tube is shown in Figure (F-2). Distilled water is passed through the tube with a 100 psi pressure drop. The circuit was designed so that the direction of water flow through the tube was easily reversed. A sintered metal filter was placed at each end of the tube ((14) in Figure (F-1)). Distilled water was placed in the collector jar and drawn into the water storage tank by means of an aspirator until the level reached the clear tube shown. Valves were positioned and the water storage tank pressurized to 100 psi with nitrogen from a high pressure bottle. This pressure was maintained throughout the test by means of a gas regulator on the nitrogen bottle. The valve was opened and water flow through the tube into the collector jar was allowed to stabilize before the arc heater was started. The run time with this apparatus was approximately three and one half hours before recharging with fresh distilled water.

2. Electrical Circuit Design

The electrical circuit by means of which the potential bias on the Langmuir tube was swept and the probe characteristic was recorded is shown in Figure (F-3). All electrical leads were made

of heavy stranded copper wire protected with a grounded co-axial shield to eliminate electrical interference. As described above the connection to the Langmuir tube was made at both ends through the Swagelok #200-1-1 fittings. The wire was then led out through the vacuum tank wall by means of a special connector constructed of a 1/4 inch copper tube filled with teflon and having a 1/16 inch diameter copper rod through the center. This tube was passed through Swagelok fittings in the vacuum tank wall. Co-axial microphone connectors were used at all connection points in the wiring.

The probe collection current was then passed through a 100 ohm precision wire wound resistor across which the current (ordinate) of the probe characteristic was read. A Kepco Model ABC-30-0.3M adjustable power supply provided continuously adjustable bias voltage for the probe. Voltage sweeps from 40 volts above reference potential to 40 volts below were possible with this unit. Such a range was more than sufficient to cover the necessary portion of the probe characteristic. The probe reference potential was that of the grounded vacuum tank wall, settling chamber and arc-heater anode. The probe characteristic was printed on a Moseley Autograph Plotter, Model 7001-A. Probe collection current (ordinate)

was read across the resistor R and probe bias voltage (abcissa) was measured between the probe and the ground reference potential.

An analysis of possible read-out errors was carried out for this circuit. Some of the collection current may pass through the Moseley Y axis input impedance which is parallel to the 100 ohm measuring resistor. This model of Moseley has a one megohm input impedance for any sensitivity setting. The percentage error in current measurement is found to be less than 0.01 percent. Some of the collection current may pass through the Moseley X axis input impedance which is parallel to the measuring resistor and the Kepco power supply. The percentage error calculated is also very near 0.01 percent. In order that the measurement of voltage does not affect the operation of the probe, the Moseley X axis input impedance must be much larger than the plasma impedance as measured from the probe characteristic. The measured plasma impedance was at most 10,000 ohms in the ion collection region, therefore the voltage measurement will not affect probe operation. From this analysis it can be seen that using this circuit, the output plot of the Moseley will be a true representation of the probe characteristic.

3. Preliminary Tests

The theory of Langmuir probe operation usually considers the situation in which the probe is immersed in a plasma of infinite extent and does not consider the circuit by means of which the charge carriers collected by the probe are returned to the plasma. In the usual stationary probe experiment the plasma is in contact with the boundaries of the apparatus and a portion of this boundary is used as the reference electrode through which the probe current is returned to the plasma. In the present case the plasma is not in a stationary condition and the possibility arises that the manner of returning the probe current to the plasma could affect the operation of the probe. The design of the experimental facility allowed an investigation of this effect to be carried out. There are three possible locations through which the probe current may be returned to the plasma: the anode, the settling chamber wall, and the vacuum tank wall (ground). These areas are electrically insulated from each other so that eight different hookups are possible as shown in Table III.

For the study of the manner in which the probe current is returned to the plasma it is necessary to differentiate negative probe operation (ion collection) from positive probe operation (electron collection).

For negative probe operation there exist three important criteria for the return circuit:

1. Does the probe circuit include the anode sheath in the arc heater ? Since electrons must be taken from the plasma at the return electrode, it is of interest whether the anode sheath is in this circuit.

2. Is the current of ions and electrons balanced or unbalanced far downstream in the flow field ? After the streaming plasma passes the probe and ions are neutralized at the probe surface, the charge balance of the plasma is destroyed in the wake of the probe. Of course, this effect is of importance only if the probe collects an appreciable portion of the charged species supplied by the arc heater. The result of this effect is the formation of a net current through the vacuum tank walls.

3. Does this wall return current flow through the probe circuit?

The eight probe hookups are shown in Table III along with the criteria pertaining to each. All tests were carried out with reference to: stability of operation, effect on ion current slope or "impedance" as read from the probe characteristic, and effect the electron temperature as calculated by the semi-log plot method described in Appendix C.

Hookups IV and VII as well as III and VI were compared to explore the effect of the inclusion of the anode sheath in the return circuit. Hookups V and VI were compared to see whether the net wall return current returning through the probe circuit had any effect on probe operation. The results showed a seven to eight percent decrease in ion impedance when the circuit included the anode sheath as compared to the case when the electrons had to be drawn into the cold chamber wall. This effect was considered small enough to be neglected. The possibility of net wall return currents flowing through the probe circuit had no effect on ion collection.

The effect of these eight hookups on electron collection by a positive probe was also examined. In this regime the effect on electron temperature was evaluated. Again three criteria were considered.

1. Does the return circuit contain the cathode sheath? In this case, electrons must be supplied at the return electrode. The inclusion of the cathode sheath will also place the arc heater power supply into the circuit.

2. Can a net return current exist through the vacuum tank walls?

3. Does the possibility of this net wall current flowing through the probe circuit affect probe operation?

The first criterion was tested by comparing hookups III with VI, IV with VII, and II with V. The second criterion was examined by comparing hookups III with IV and VI with VII. The effect of the third criterion was investigated by comparing hookups II with III and V with VI.

The results of these tests showed that the inclusion of the cathode sheath in the probe circuit had no effect on probe operation. Any possible net wall return current flowing through the probe had no effect on its operation. The electron temperatures calculated using the semi-log plot method (see Appendix C) yielded almost identical results for all of the hookups tested.

In all of the above tests hookup VIII yielded unreliable data for two reasons. First, as mentioned in Appendix A, the arc heater did not operate in a very stable manner if the anode was not grounded. This unstable operation was minimized during these tests; however, it is suspected that it contributed to the problems with hookup VIII. Second, in hookup VIII the return circuit is limited to the vacuum tank wall as its reference electrode. In this case all of the probe

current is necessarily net wall return current and the electrons collected by a positive probe are ultimately drawn from outside the boundaries of the free jet plasma flow field. The effect of this was very evident in the non-Maxwellian electron velocity distribution found when calculating the electron temperature for this hookup. In fact when the Brown recorder sampled the arc current or voltage signal it simultaneously supplied a current flow path between the anode and ground which caused a pronounced perturbation upon the probe characteristic output. This result further reveals the unsuitability of the use of the tank wall as a reference electrode as described in the following set of tests. Due to these shortcomings hookup VIII was discarded.

The floating and plasma potentials measured for each of the hookup configurations were referred to the anode, the settling chamber wall, and the vacuum tank wall in an attempt to discover which of these areas was in closest contact with the plasma. The operating conditions in the facility were held constant and the hookups were varied. Potential differences between parts of the apparatus were measured with a Simpson 20, 000 ohm per volt voltmeter. If the potential difference between floating or plasma potential and one of the reference area potentials was relatively constant

throughout the test sequence then this reference area could be considered in best contact with the plasma itself. The results showed that the vacuum tank wall was not suitable for use as a reference point. This is to be expected since the plasma is seen to be not in good contact with these walls by the nature of the experiment. The anode was found to be slightly better than the settling chamber wall in service as a reference electrode.

Earlier tests on the facility that were described in Appendix A showed that in order to insure stable operation of the arc heater, the anode should be grounded. Hookup I was found to deliver a steadier Langmuir probe characteristic as well as a more satisfactory linear semi-log plot for the determination of the electron temperature. Therefore hookup I was used throughout the test program.

LIST OF REFERENCES

1. Adamson T. and Nicholls J. (1959): "On the Structure of Jets from Highly Expanded Nozzles into Still Air", Journal of the Aerospace Sciences, 26, pp. 16-24.

2. Albini F. (1965): "Approximate Computation of Under-expanded Jet Structure", AIAA Journal, 3, pp. 1535-1537.

3. Allen J., Boyd R., and Reynolds P. (1957): "The Collection of Positive Ions by a Probe Immersed in a Plasma", Proc. Phys. Soc. (London) B70, pp. 297-304.

4. Appleton J. and Bray K. (1964): "The Conservation Equations for a Non-Equilibrium Plasma", Journal of Fluid Mechanics, 20, pp. 659-672.

5. Arave R. and Huseby O. (1962): "Aerothermodynamic Properties of High Temperature Argon", Document No. D2-11238, Boeing Company (Feb. 1962).

6. Arney G. and Boylan D. (1963): "A Calorimetric Investigation of Some Problems Associated with a Low Density Hypervelocity Wind Tunnel", AEDC TDR-63-19, Arnold Engineering Development Center, U. S. Air Force.

7. Ashkenas H. and Sherman F. (1966): "The Structure and Utilization of Supersonic Free Jets in Low Density Wind Tunnels," Rarefied Gas Dynamics, Supplement 3, Vol. 2, pp. 84-105, Academic Press Inc., New York.

8. Bates, D., Kingston A. and McWhirter R. (1962): "Recombination between Electrons and Atomic Ions," Proc. of Royal Soc., 267 A, pp. 297-312.

9. Becker M. and Heyser A. (1967): "Der DVL Plasmawindkanal, eine Anlage fuer hypersonische Geschwindigkeiten, geringe Dichten und hohe Temperaturen," DLR F. B. 67-66, Deutsche Versuchsanstalt fuer Luft-und Raumfahrt, Germany.

10. Bernstein I. and Rabinowitz I. (1959): "Theory of Electrostatic Probes in a Low Density Plasma," Physics of Fluids, 2, pp. 112-121.

11. Biberman L. and Yakubov I. (1964): "Approach to Ionization Equilibrium Behind the Front of a Shock Wave in an Atomic Gas," Soviet Physics-Technical Physics, 8, pp. 1001-1007.

12. Bier K. and Hagena O. (1963): "Influence of Shock Waves on the Generation of High Intensity, Molecular Beams by Nozzles," Rarefied Gas Dynamics, Supplement 2, Vol. 1, pp. 478-496, Academic Press, New York.

13. Boatwright W., Stewart R. and Grimaud J. (1962): "Description and Preliminary Calibration of a Small Arc Heated Hypersonic Wind Tunnel:, NASA TN D-1377, National Aeronautics and Space Administration.

14. Bohm D. (1949): "Minimum Ionic Kinetic Energy for a Stable Sheath", The Characteristics of Electrical Discharges in Magnetic Fields, p. 77-86, Ed. Guthrie and Wakerling, McGraw Hill, 1949.

15. Boldman D. (1963): "Performance Evaluation of a Magnetically Spun D. C. Arc Operating in Nitrogen", AIAA Journal 1, pp. 802-805.

16. Brewer L. (1964): "Spectroscopy of a Supersonic Plasma: I, Excitation Mechanism", AEDC-TDR-64-151, Arnold Engineering Development Center, U. S. Air Force.

17. Brewer L. and McGregor W. (1963): "The Radiative Decay of Metastable Argon Atoms in a Low Density Argon Plasma Stream", AEDC-TDR-63-5, Arnold Engineering Development Center, U. S. Air Force.

18. Byron S., Stabler R. and Bortz P. (1962): "Electron-Ion Recombination by Collisional and Radiative Processes", Physical Review Letters 8, pp. 376-379.

19. Cassady P. (1965): "High Enthalpy Free Jet Testing Utilizing an Arc Heater", Project Report 65-123(2), von Karman Institute for Fluid Dynamics, Rhode-St.-Genese, Belgium.

20. Chen C. (1969): "Collisional Radiative Electron-Ion Recombination Rate in Rare Gas Plasmas", Journal of Chemical Physics, 50 , p. 1560.

21. Chen F. (1965): "Electric Probes", Chapter 4 of Plasma Diagnostic Techniques, Eds. Huddlestone R. and Leonard S., Academic Press, 1965.

22. Christiansen W. (1967): "Study of Shock Waves in a Non-equilibrium Plasma", Physics of Fluids 10, pp. 2586-2595.

23. Chubb D. (1968): "Ionizing Shock Structure in a Monatomic Gas", Physics of Fluids, 11 , pp. 2363-2376.

24. Clayden W. (1961): "Recent Research with the ARDE Low Density Wind Tunnel with a Plasma Jet Heater", Rarefied Gas Dynamics , Supplement 1, p. 715-740, Academic Press, New York.

25. Clayden W. (1963): "Langmuir Probe Measurements in the RARDE Plasma Jet", Rarefied Gas Dynamics, Supplement 2, Vol. 2, pp. 435-470, Academic Press, New York.

26. Clayden W. (1964): "Development and Use of an Ion Mach Meter to Calibrate an Arc-Heated Low Density Wind Tunnel", AGARD ograph 84, pp. 981-1011, AGARD-North Atlantic Treaty Organization.

27. Crist R. (1965): "Experimental Study of the Shock Structure of a Highly Underexpanded Jet Exhausting from a Sonic Nozzle", AIAA Student Journal, Vol. 3, pp. 43-48.

28. De Leeuw J. (1963): "Electrostatic Plasma Probes", Physico-Chemical Diagnostics of Plasmas, pp. 65-96. Ed. Anderson, Springer and Warder, Northwestern University Press, 1963.

29. De Voto R. (1965): "Argon Plasma Transport Properties", Sudaer Report No. 217, Stanford University.

30. Dunn M. and Lordi J. (1969): "Thin Wire Langmuir Probe Measurements in the Transition and Free-Molecular Flow Regimes", CAL No. AI-2187-A-14, Technical Report, Cornell Aeronautical Laboratory, Inc., Buffalo, New York.

31. Evans D. and Tankin R. (1967): "Experimental Measurement of the Emission and Absorption of Radiation by an Argon Plasma", ARL-67-0157, Aerospace Research Laboratories, U. S. Air Force.

32. Fay J. (1962): "Hypersonic Heat Transfer in the Air Laminar Boundary Layer", Avco Everett Research Laboratory Report AMP-71, ASTIA AD No. 283503.

33. Fay J. (1962): "Plasma Boundary Layers", Magneto-hydrodynamics, p. 337-348, Proc. of the 4th Biennial Gas Dynamics Symposium, Ed. Chambel et. al., Northwestern University Press, 1962.

34. Fenn J. and Deckers J. (1963): "Molecular Beams from Nozzle Sources", Rarefied Gas Dynamics, Supplement 2, Vol. 1, pp. 497-515, Academic Press, New York.

35. French J. (1961): "Langmuir Probes in a Flowing Low Density Plasma", UTIA Report No. 79, University of Toronto.

36. French J. and Muntz E. (1960): "Design Study of the UTIA Low Density Plasma Tunnel", UTIA TN-34, University of Toronto.

37. French J., Sonin A., De Leeuw J. (1963): "The Use of Langmuir Probes in Low Density Plasma Flows", Rarefied Gas Dynamics, Supplement 2, Vol. 2, pp. 471-494, Academic Press, New York.

38. Goodwin G. (1963): "Production and Diagnostics of Hypervelocity Low Density Streams", Rarefied Gas Dynamics, Supplement 2, Vol. 1, pp. 388-401, Academic Press, New York.

39. Graf K. (1965): "The Determination of Spatially Non-Uniform Electron Density Distribution", UTIAS Rept. No. 108, University of Toronto.

40. Gregorek G. and Luce R. (1966): "Axisymmetric and Planar Free Jets for Hypersonic Low Density Facilities", ARL 66-0068, Aerospace Research Laboratories, U. S. Air Force.

41. Grewal M. and Talbot L. (1963): "Shock Wave Structure in a Partially Ionized Gas", Journal of Fluid Mechanics, 16, pp. 573-594.

42. Hill J. and Draper J. (1966): "Analytical Approximation for the Flow from a Nozzle into Vacuum", Journal of Spacecraft, 3 , pp. 1552-1554.

43. Hinnov E. and Hirschberg J. (1962): "Electron Ion Recombination in Dense Plasmas", Physical Review, 125 , pp. 795-801.

44. Holt E. and Haskell R. (1965): Foundations of Plasma Dynamics, Macmillan, New York.

45. Jaffrin M. (1965): "Shock Structure in a Partially Ionized Gas", Physics of Fluids, 8 , pp. 606-625.

46. Jaffrin M. and Probstein R. (1964): "Structure of a Plasma Shock Wave", Physics of Fluids 7, pp. 1658-1674.

47. John R. and Bade W. (1961): "Recent Advances in Electric Arc Plasma Generation Technology", ARS Journal 31, pp. 4-17.

48. Jukes J. (1957): "The Structure of a Shock Wave in a Fully Ionized Gas", Journal of Fluid Mechanics, 3, pp. 275-285.

49. Kamimoto G., Kimura T., Teshima K. (1965): "Performance of the Kyoto University Low Density Plasma Jet Wind Tunnel:, Dept. of Aero. Eng. C.P. 7, Kyoto University, Japan.

50. Kamimoto G. and Nishida M. (1965): "Langmuir Probe Measurements in an Argon Plasma Flow", Dept. of Aero. Eng. C. P. 8, Kyoto University, Japan.

51. Kamimoto G., Nishida M., Yoshida K. (1967): "The Behavior of the Charged Particles Across the Normal Shock Wave in a Partially Ionized Gas", Dept. of Aero. Eng. C.P. 17, Kyoto University, Japan.

52. Kaminsky M. (1965): Atomic and Ionic Impact Phenomena on Metal Surfaces, Academic Press, New York.

53. Kanal M. (1964): "Theory of Current Collection of Moving Cylindrical Probes", Journal of Applied Physics, 35, pp. 1697-1703.

54. Kelly A., Nerheim N., Gardiner J. (1966): "Electron Density and Temperature Measurements in the Exhaust of an MPD Source", AIAA Journal 4, pp. 291-295.

55. Kennard E. (1938): The Kinetic Theory of Gases, McGraw Hill Book Company, New York.

56. Kirchoff R. (1969): "An Experimental Study of the Shock Structure in a Partially Ionized Gas", Rept. No. AS-69-8, College of Engineering, Univ. of Calif., Berkeley.

57. Knuth E., Kuluva N., Callinan J. (1967):"Densities and Speeds in an Arc Heated Supersonic Argon Beam", Entropie No. 18, November-December 1967, pp. 38-46.

58. Laframboise J. (1966): "Theory of Spherical and Cylindrical Langmuir Probes in a Collisionless Maxwellian Plasma at Rest", UTIAS Rept. No. 100, University of Toronto.

59. Lai W., Gustavson J., Talbot L. (1958): "Design Considerations and Initial Evaluation of Model B Plasma Generator", University of California at Berkeley, Institute of Technical Research Technical Report HE-150-161.

60. Lam S. and Greenblatt M. (1966): "On the Interaction of a Solid Body with a Flowing Collisionless Plasma", Rarefied Gas Dynamics, Supplement 3, Vol. 2, pp. 45-61, Academic Press, New York.

61. Li H. and Mathieu R. (1961): "Shock Wave Structure in a Fully Ionized Gas Based on a Multi-Component Fluid Theory", Dept. Aer. Eng. Tech. Rept. 14, Pennsylvania State University.

62. Liepmann H. and Roshko A. (1957): Elements of Gasdynamics, John Wiley, New York.

63. Love E., Grigsby C. et. al. (1959): "Experimental and Theoretical Studies of Axisymmetric Free Jets", NASA TR-R6, National Aeronautics and Space Administration.

64. McDaniel E. (1964): Collision Phenomena in Ionized Gases, John Wiley and Sons, New York.

65. McHale R. (1964): "Modes of Operation of Confined K. W. D. C. Arc Jets in Helium or Argon", Univ. of Calif. at Berkeley, Inst. of Eng. Res. Rept. As-64-2.

66. McLaren T. and Hobson R. (1968): "Initial Ionization Rates and Cross Sections in Shock Heated Argon", Physics of Fluids, 11 , pp. 2162-2172.

67. Makin B. (1962): "Progress Report on the University of Southhampton Low Density Arc Heated Wind Tunnel", Univ. of Southampton AASU Report 227. U. K.

68. Makin B. and Keck J. (1963): "Variational Theory of Three Body Electron-Ion Recombination Rates", Physics Review Letters 11 , pp. 281-283.

69. Maslach G., Willis D., Tang S., Ko D. (1966): "Recent Experimental and Theoretical Extensions of Nearly Free Molecular Flow", Rarefied Gas Dynamics, Supplement 3, Vol. 1, pp. 433-443, Academic Press, New York.

70. Mirels H. and Mullen J. (1963): "Expansion of Gas Clouds and Hypersonic Jets Bounded by a Vacuum", AIAA Journal 1 , pp. 596-602.

71. Morgan E. and Morrison R. (1965): "Ionization Rates Behind Shock Waves in Argon", Physics of Fluids, 8, pp. 1608-15.

72. Morse T. (1963): "Energy and Momentum Exchange between Non-equipartition Gases", Physics of Fluids, 6, pp. 1420-1427.

73. Mueller J. (1957): "Equations, Tables and Figures for Use in the Analysis of Helium Flows at Supersonic and Hypersonic Speeds", NACA TN 4063, National Aeronautics and Space Administration.

74. Murty S. (1968): "Shock Wave Structure in a Partially Ionized and Radiating Gas", Dept. Aero. Eng., Indian Institute of Science, Bangalore, Rept. No. AE-RP-177A.

75. Murty S. (1969): "Electron Temperature Distribution Across a Shock Wave in a Partially Ionized Gas", Dept. Aero. Eng., Indian Institute of Science, Bangalore, Rept. No. AE 178-A.

76. Nelson H. and Goulard R. (1969): "Structure of Shock Waves with Non-Equilibrium Radiation and Ionization", Physics of Fluids, 12, pp. 1605-1617.

77. Owen P. and Thornhill C. (1952): "The Flow in an Axially Symmetric Supersonic Jet From a Nearly-Sonic Orifice into a Vacuum", R&M No. 2616, Aeronautical Research Council, U. K.

78. Petschek H. and Byron S. (1957): "Approach to Equilibrium Ionization Behind Strong Shock Waves in Argon", Annals of Physics, 1, pp. 270-315.

79. Pope R. (1968): "Measurements of Enthalpy in Low Density Arc Heated Flows", AIAA Journal 6, pp. 103-110.

80. Potter J., Arney G., et. al. (1963): "Gasdynamic Diagnosis of High Speed Flows Expanded from Plasma States", AEDC-TDR-63-241, Arnold Engineering Development Center, U. S. Air Force.

81. Scharfman W. et. al. (1967): "The Use of Langmuir Probes in Diagnosing Ionized Flow Fields", Proc. of the Third Symposium on Plasma Sheath, AFCRL 67-0280, SR 64, Vol. II, pp. 125-167, USAF.

82. Schott L. (1968): "Electrical Probes", Plasma Diagnostics, pp. 668-731, Ed. Lochte-Holtgreven, W., North Holland Publishing Co. Wiley Interscience.

83. Scott J. and Drewry J. (1963): "Characteristics of Aerodynamic Molecular Beams", Rarefied Gas Dynamics, Supplement 2, Vol. 1, pp. 516-538, Academic Press, New York.

84. Sherman F. and Talbot L. (1962): "Diagnostic Studies of a Low Density Arc Heated Wind Tunnel Stream", Progress in Astronautics and Rocketry, Vol. 7, Hypersonic Flow Research, Ed. F. Riddell, Academic Press, New York.

85. Sherman F. (1963): "A Survey of Experimental Results and Methods for the Transition Regime of Rarefied Gas

Dynamics", Rarefied Gas Dynamics, Supplement 2, Vol. 2, pp. 228-260, Academic Press, New York.

86. Shkarofsky I., Johnston T. and Bachynski M. (1966): The Particle Kinetics of Plasmas, Addison Wesley.

87. Smetana F. (1963): "On the Current Collected by a Charged Circular Cylinder Immersed in a Two Dimensional Rarefied Plasma Stream", Rarefied Gas Dynamics, Supplement 2, Vol. 2, pp. 65-91, Academic Press, New York.

88. Sonin A. (1965): "The Behavior of Free Molecule Cylindrical Langmuir Probes in Supersonic Flows and Their Application to the Study of the Blunt Body Stagnation Layer", UTIAS Rept. No. 109, University of Toronto.

89, Spitzer L. (1962): Physics of Fully Ionized Gases, 2nd Edition, No. 3 of Interscience Tracts on Physics and Astronomy, Interscience Publishers, New York.

90. Spitzer L. and Härm R. (1953): "Transport Properties in a Completely Ionized Gas", Physical Review 89, pp. 977-981.

91. Stursberg K. (1967): "Lichtbogen-Brennkammern neidriger Leistung fuer Hypergeschwindigkeits-Vakuum-Windkanaele", DLR Mitt. 67-10, Deutsche Versuchsanstalt fuer Luft-und Raumfahrt, Germany.

92. Weltmann R. (1962): "The Design and Calibration of an Arc Heated Hypersonic Low Density Wind Tunnel", NASA TN D1169, National Aeronautics and Space Administration.

93. Wheaton J. and Dean R. (1961): "On Anode Gas Sheath Electrical Breakdown in a High Pressure Arc Plasma Generator", Res. Rept. Thayer School of Engineering, Dartmouth College, Hanover, New Hampshire.

94. Winovitch W. (1964): "On the Equilibrium Sonic Flow Method for Evaluating Electric Arc Air Heater Performance", NASA TN D-2132, National Aeronautics and Space Administration.

95. Witte A. (1964): "Analysis of One Dimensional Isentropic Flow with Tables for Partially Ionized Argon", Tech. Rept. No. 32-661, Jet Propulsion Laboratory, Calif. Institute of Technology.

96. Witte A., Kubota T., Lees L. (1969): "Experimental Investigation of a Highly Ionized Arc-Heated Supersonic Free-jet", AIAA Journal 7, pp. 870-878.

97. Zeldovitch Y. and Raizer Y. (1966): Physics of Shock Waves and High Temperature Hydrodynamic Phenomena, Academic Press, New York.

98. Zigan F. (1962): "Gasdynamische Berechnung der Trenndueseneentmischung", Z. Naturforsch. 17a , p. 772.

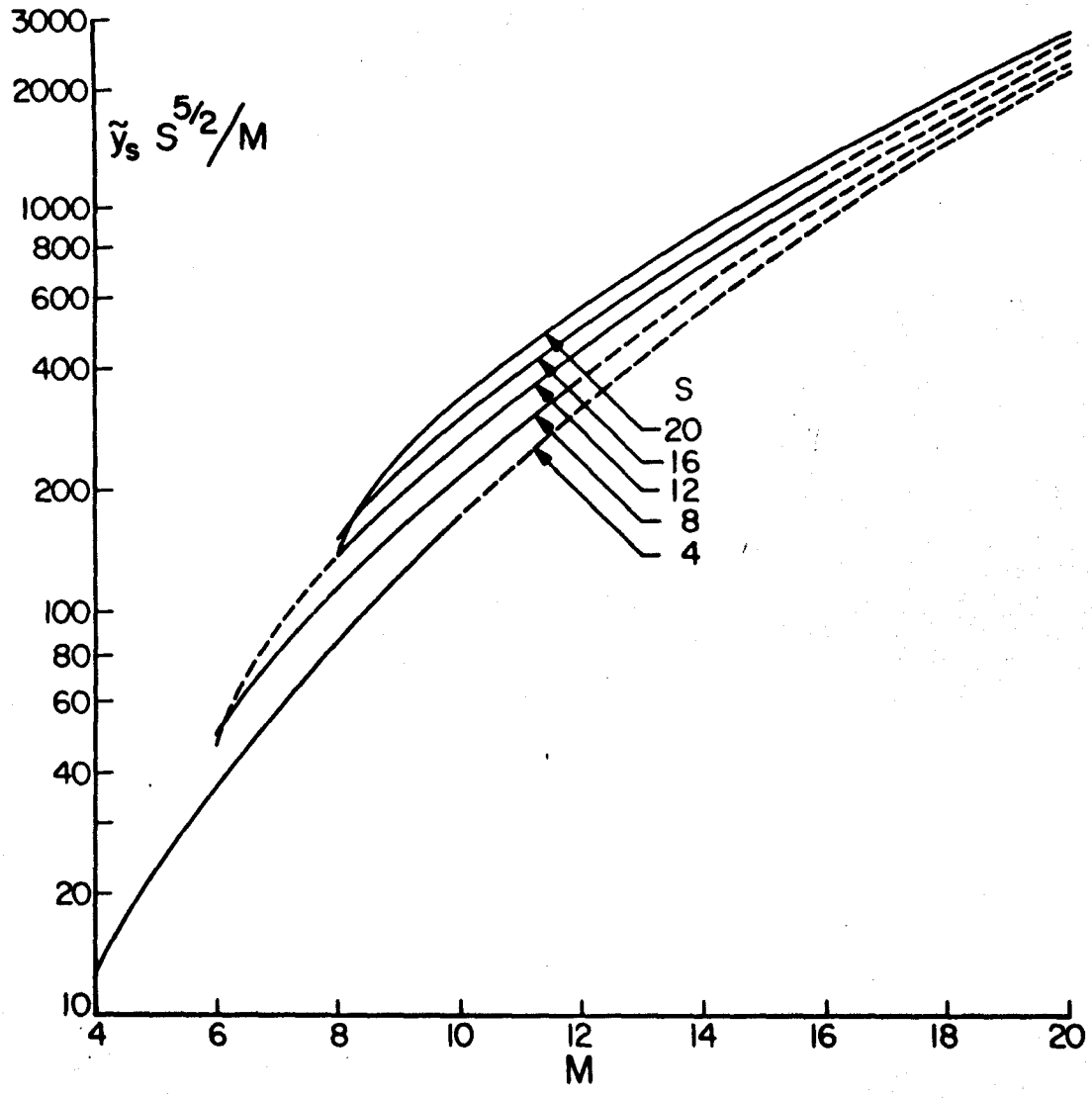

FIG. 1 PRECURSOR LENGTH

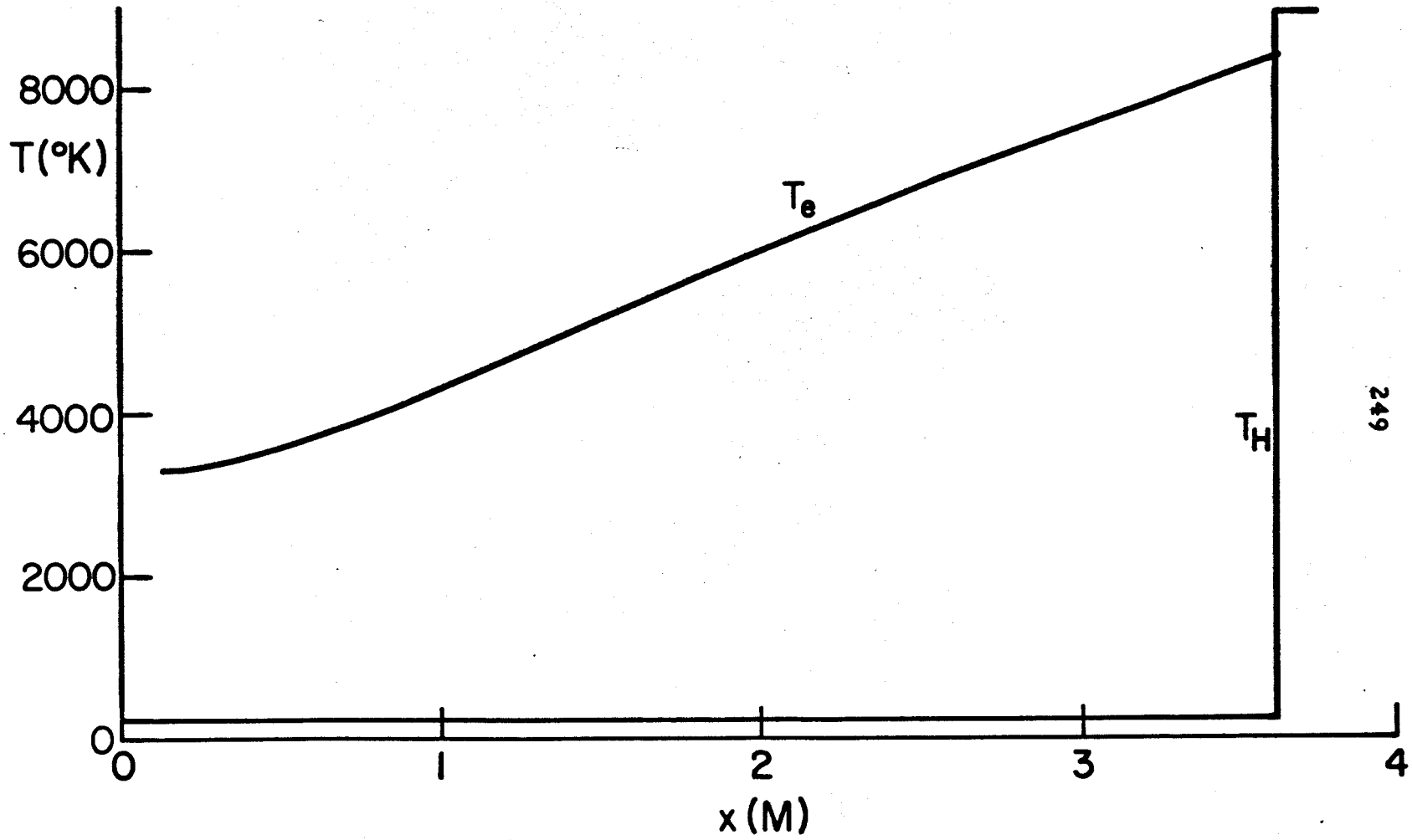

FIG. 2 HOT ELECTRON PRECURSOR

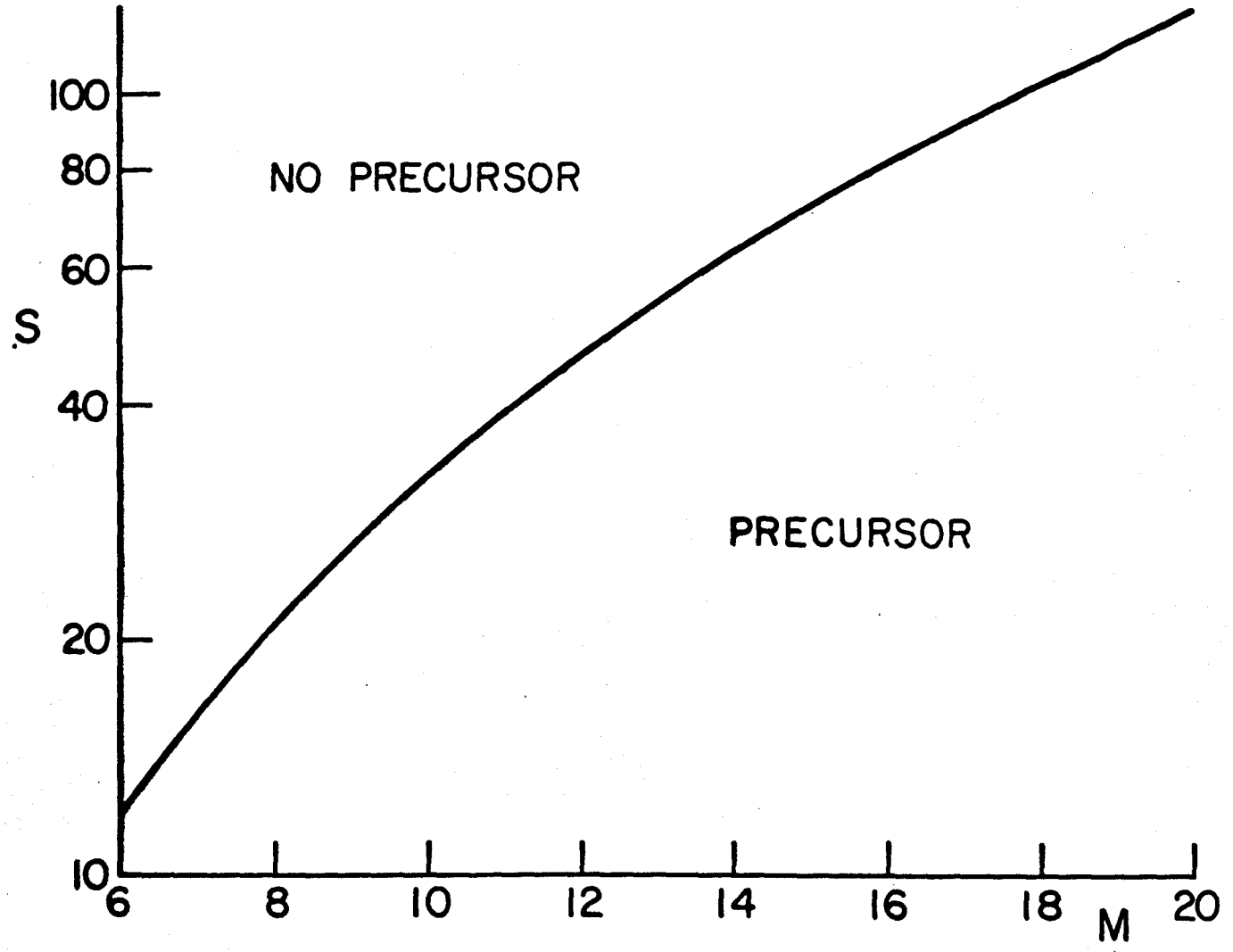

FIG. 3 EXISTENCE OF PRECURSOR

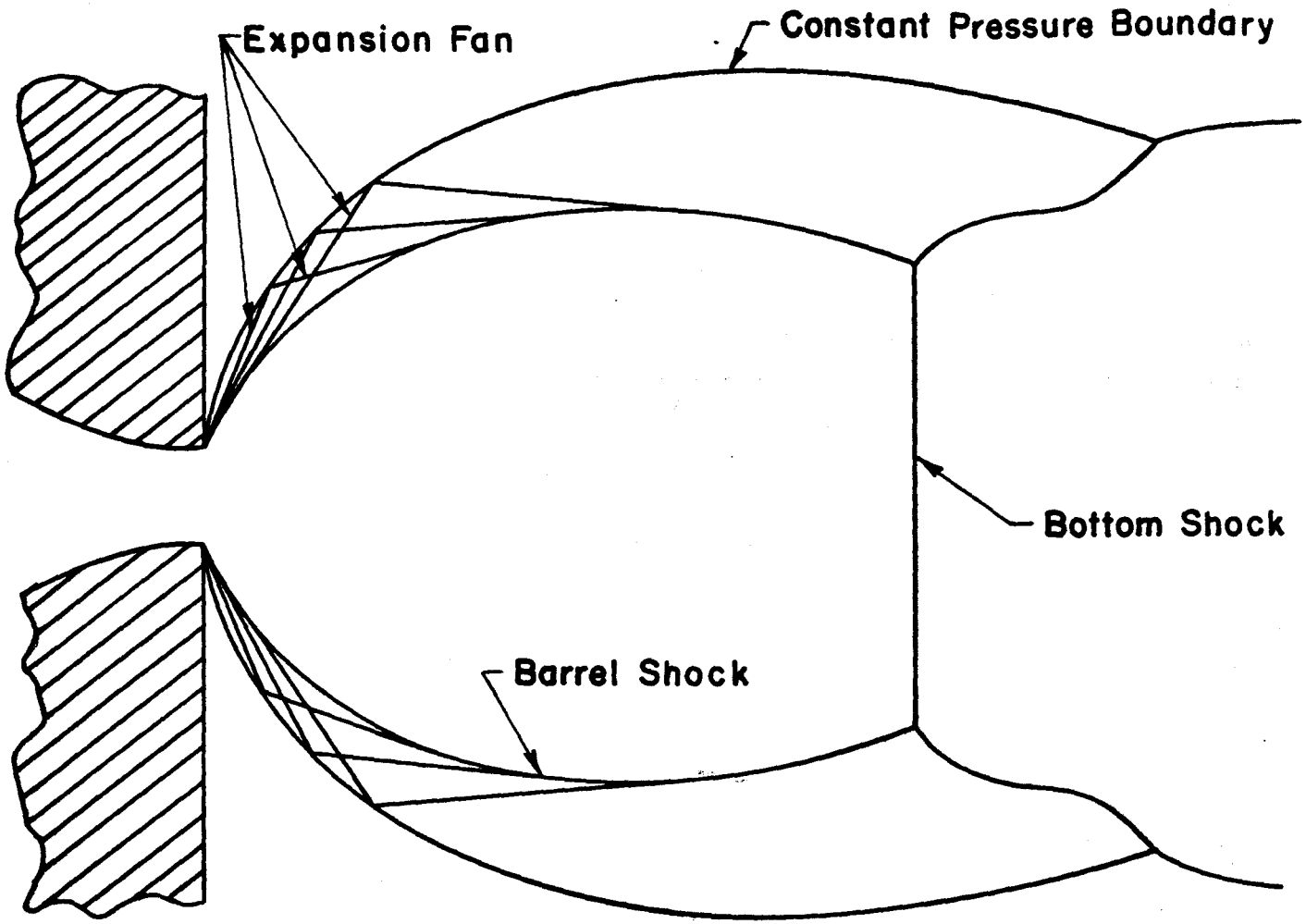

FIG.4 APPEARANCE OF FREE JET FLOW FIELD

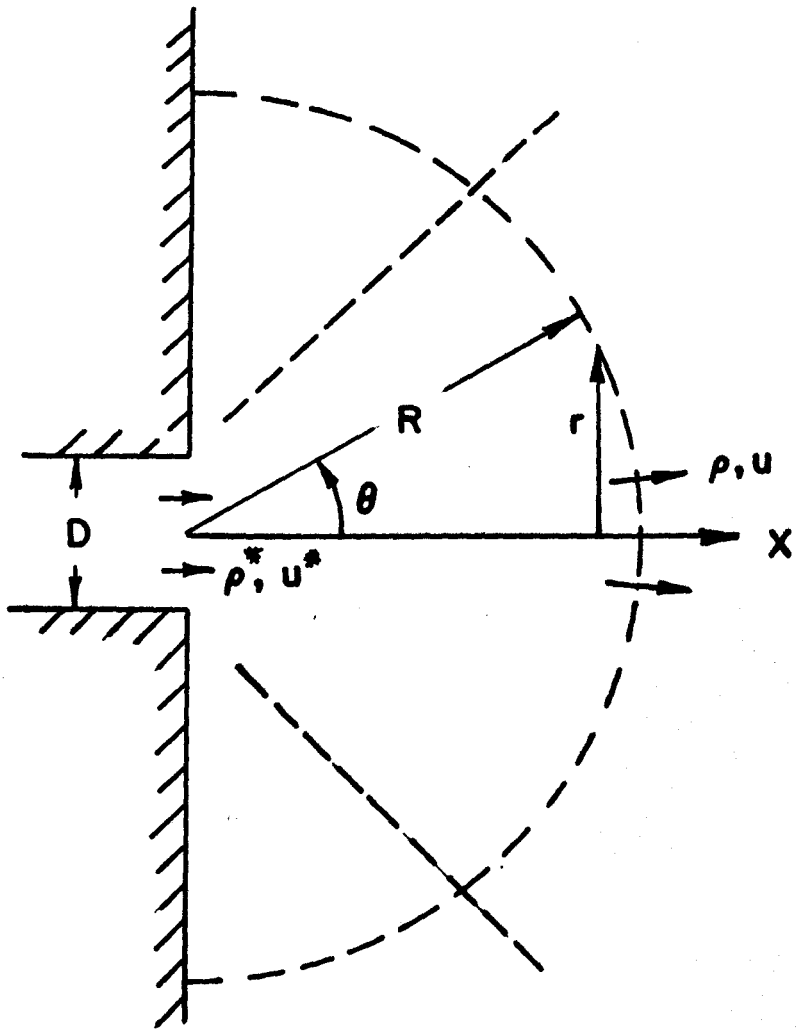

FIG. 5 FLOWFIELD COORDINATES

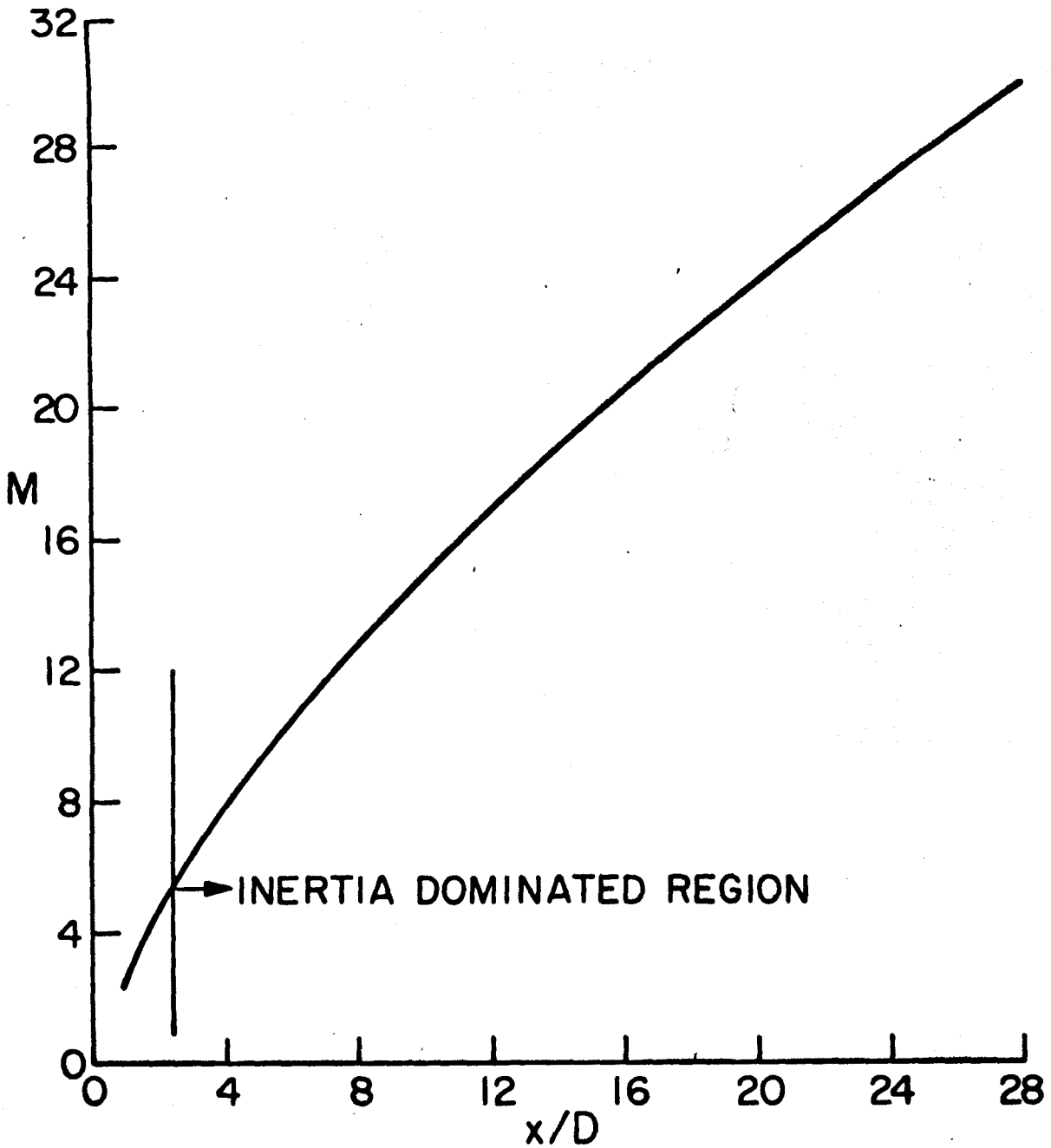

FIG. 6 MACH NUMBER DISTRIBUTION

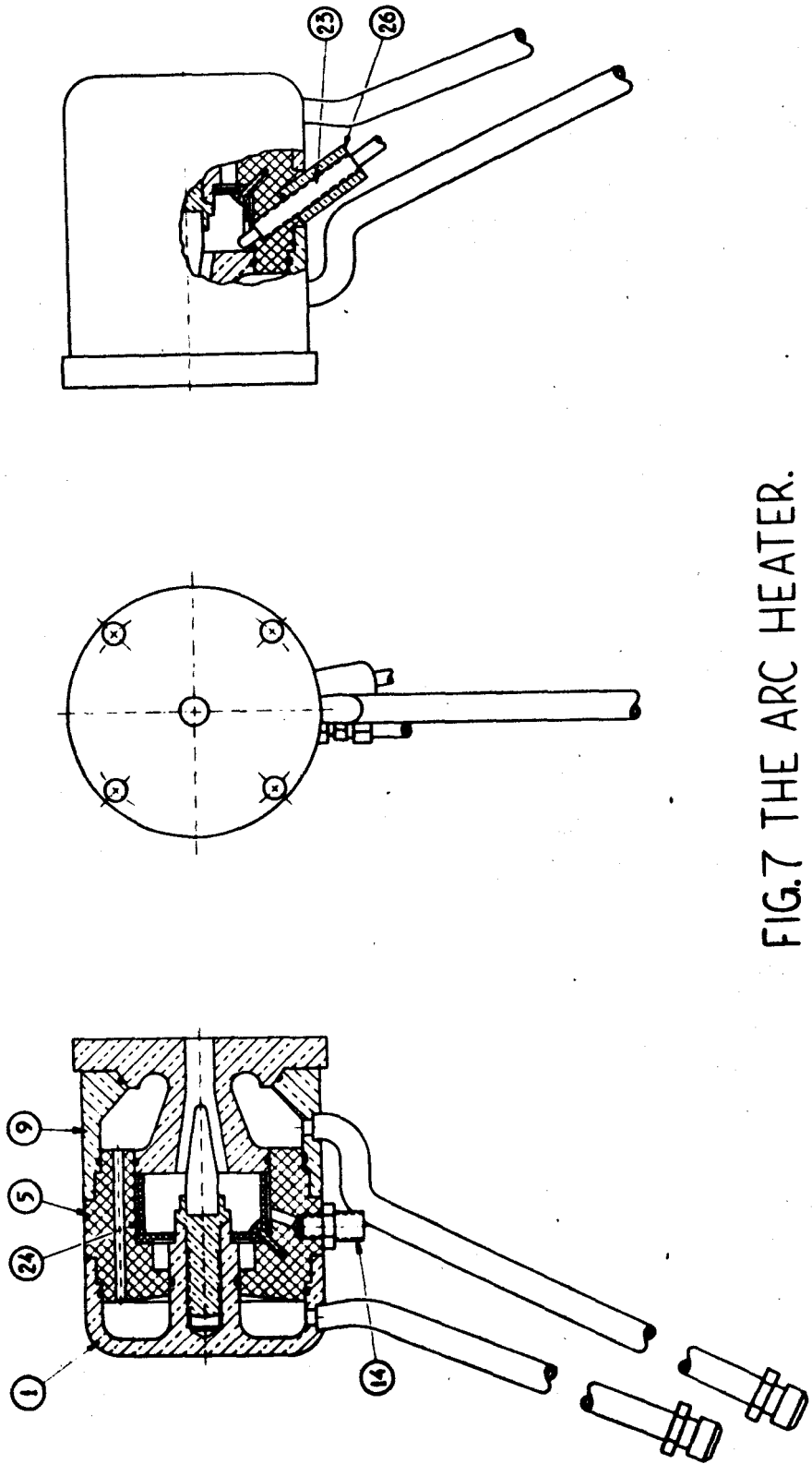

FIG.7 THE ARC HEATER.

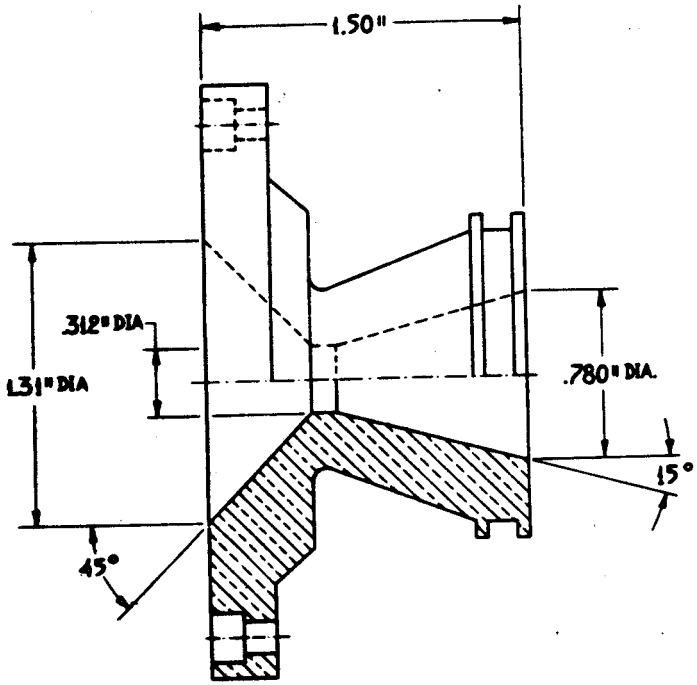

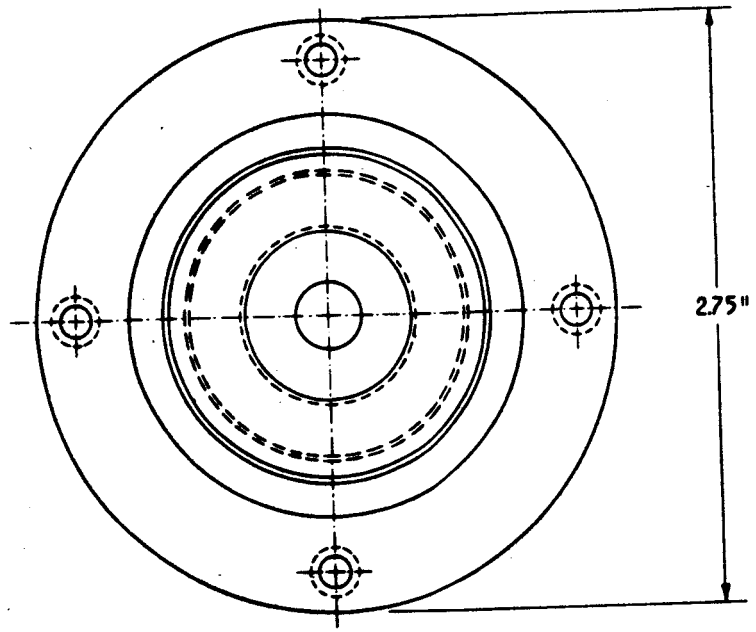

255

FIG. 8. THE SHORT ANODE.

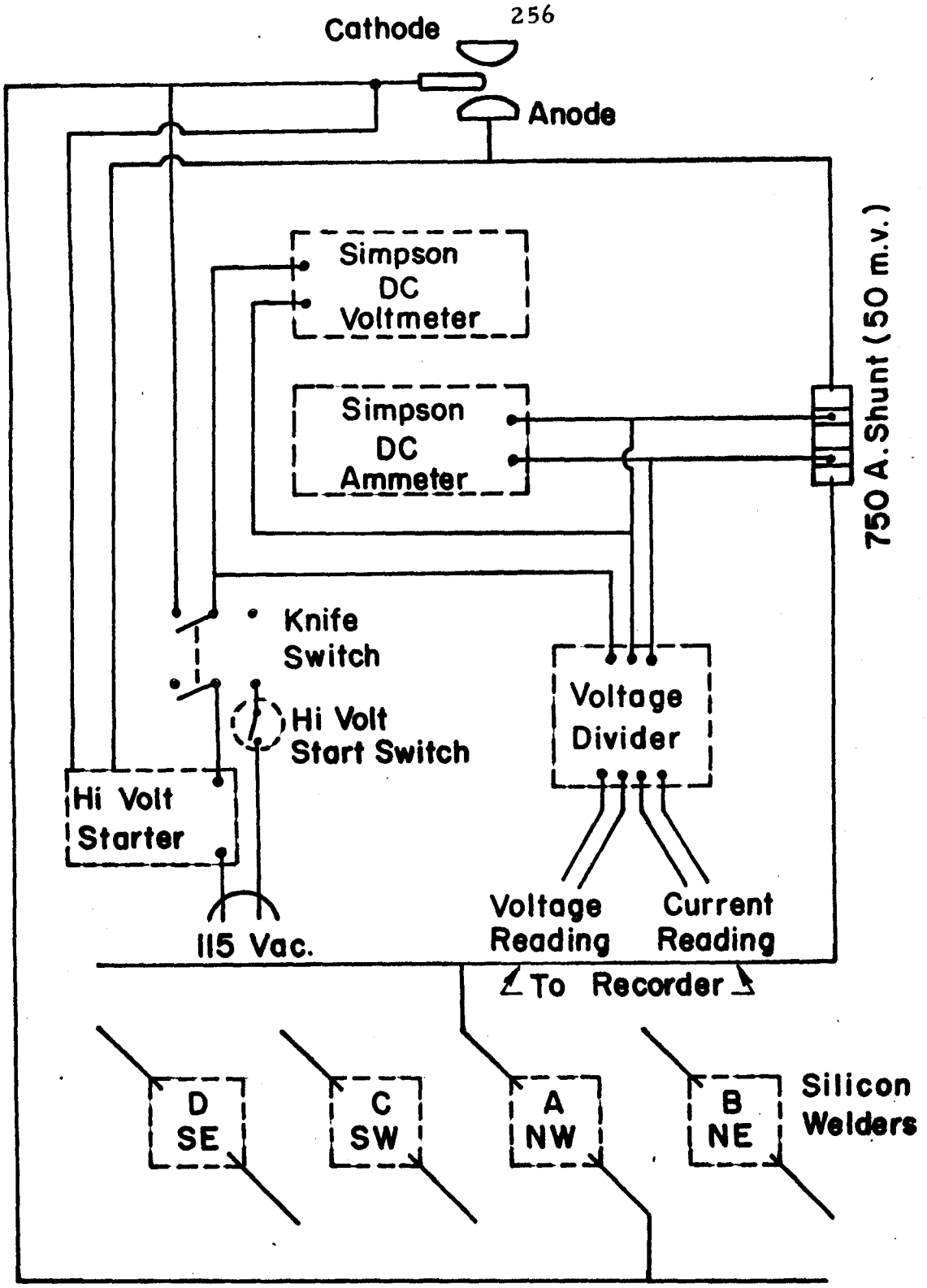

FIG. 9 D.C. POWER SUPPLY SYSTEM FOR ARC

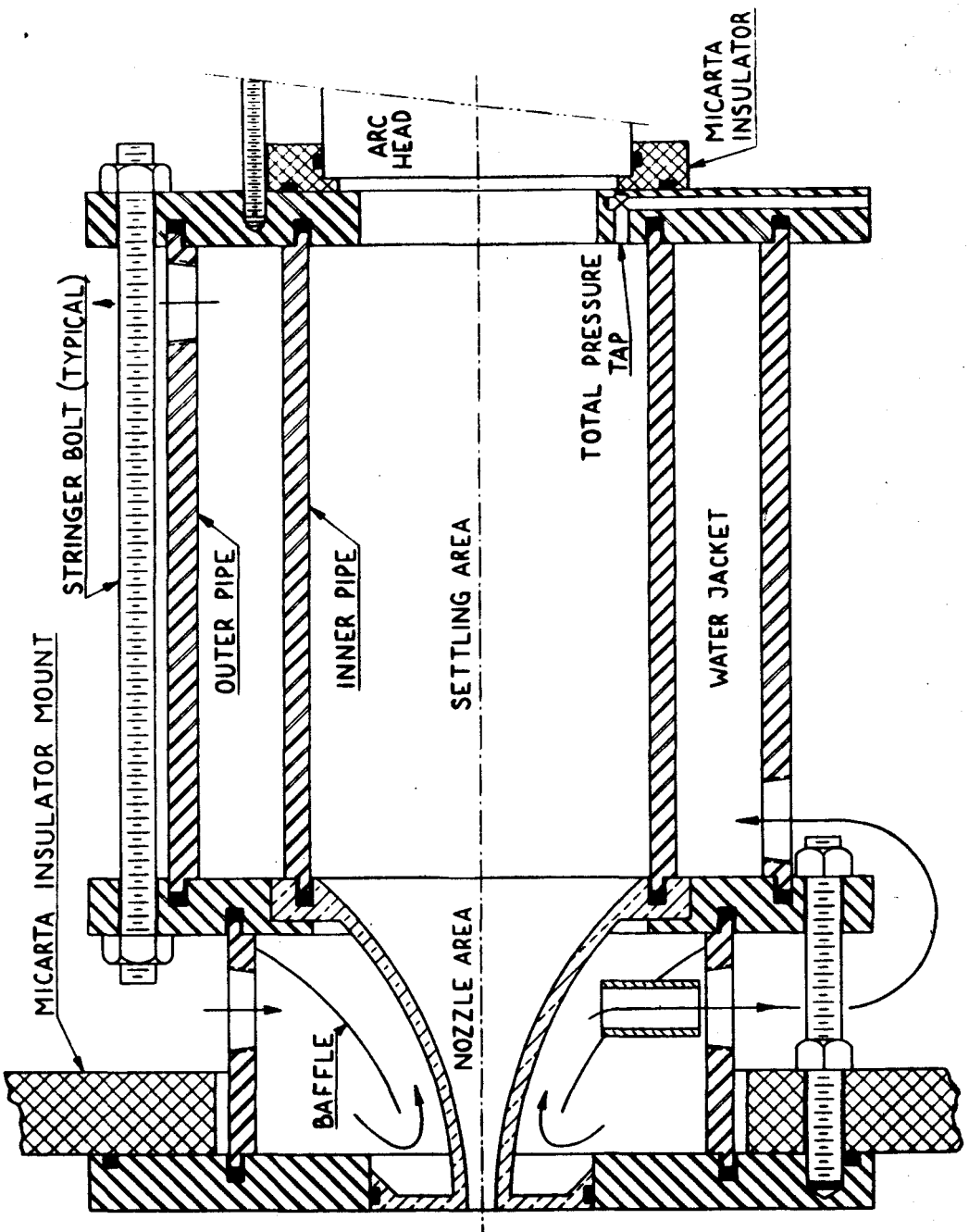

FIG.10 THE SETTLING CHAMBER.

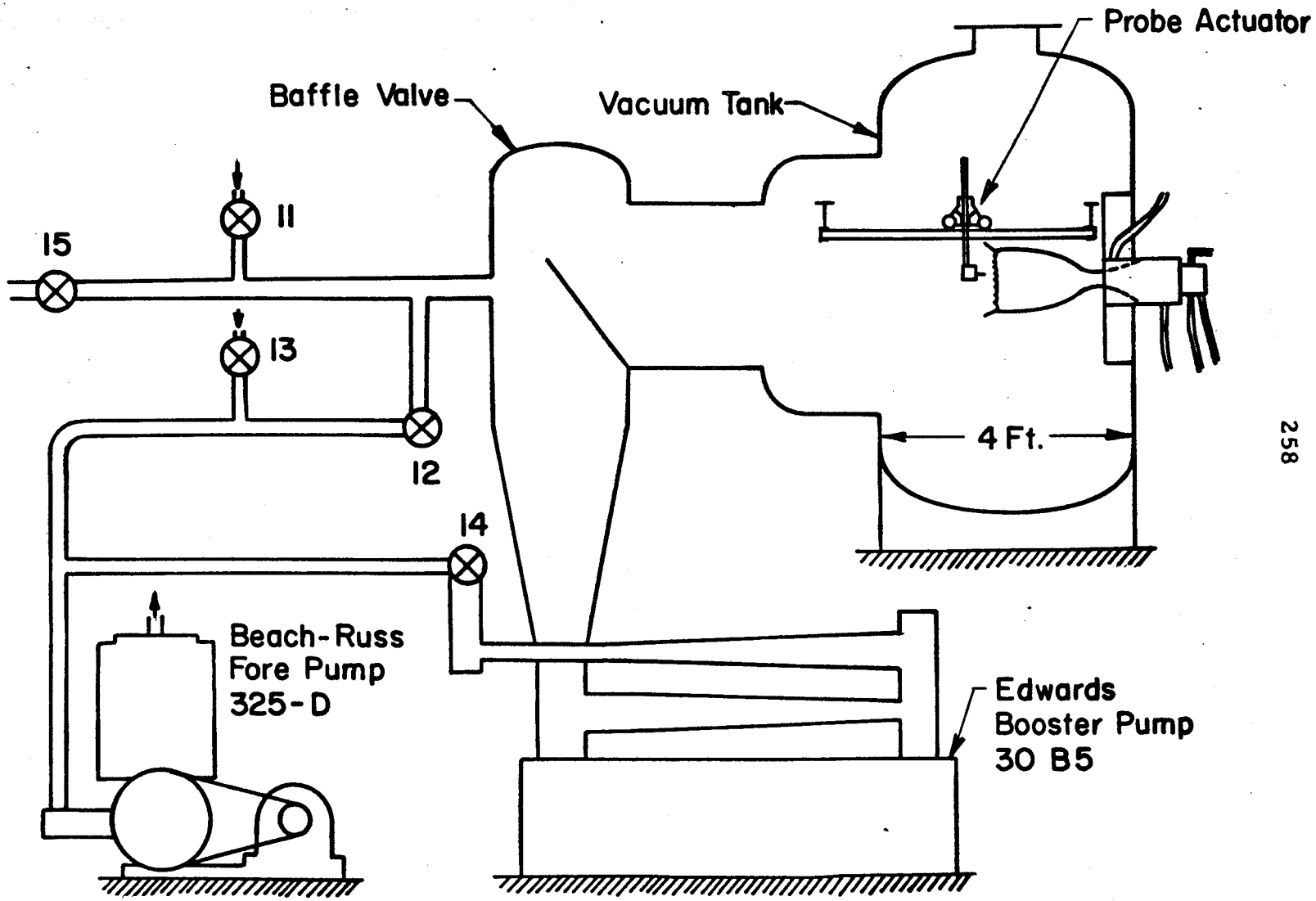

FIG. 11 LOW DENSITY FACILITY

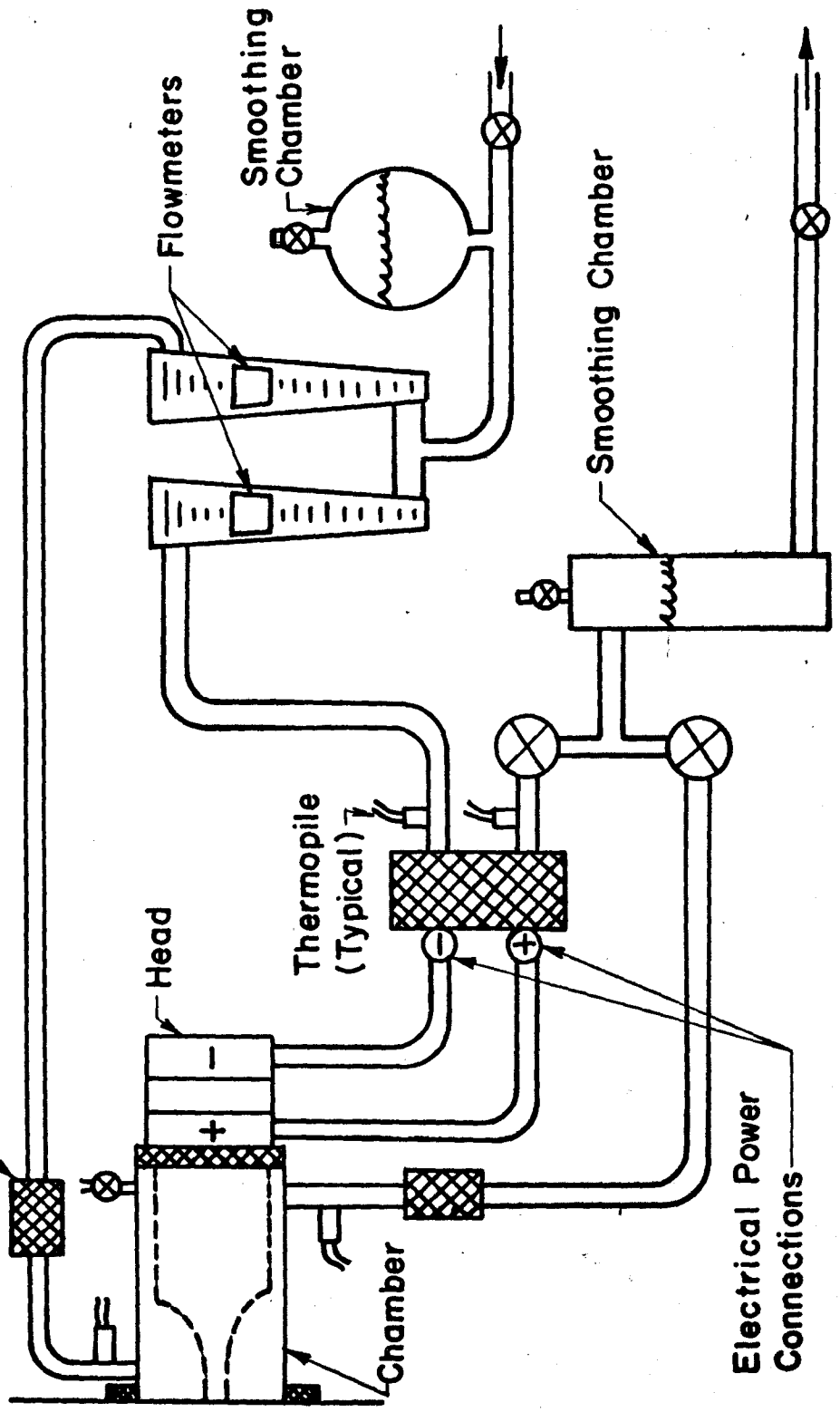

FIG.12 SKETCH OF HEAD AND CHAMBER COOLING WATER CIRCUIT

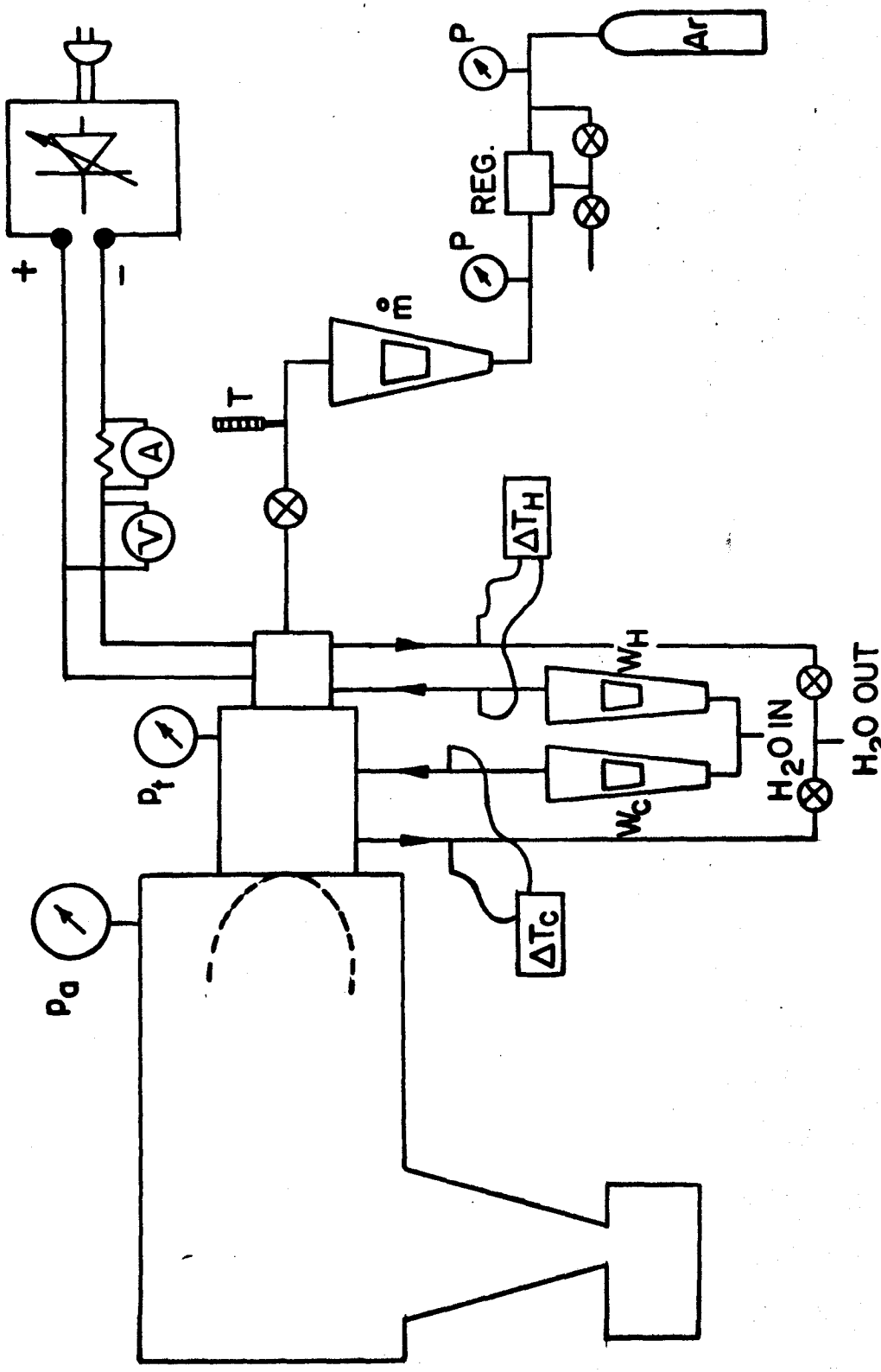

FIG.13 SKETCH OF FACILITY INSTRUMENTATION

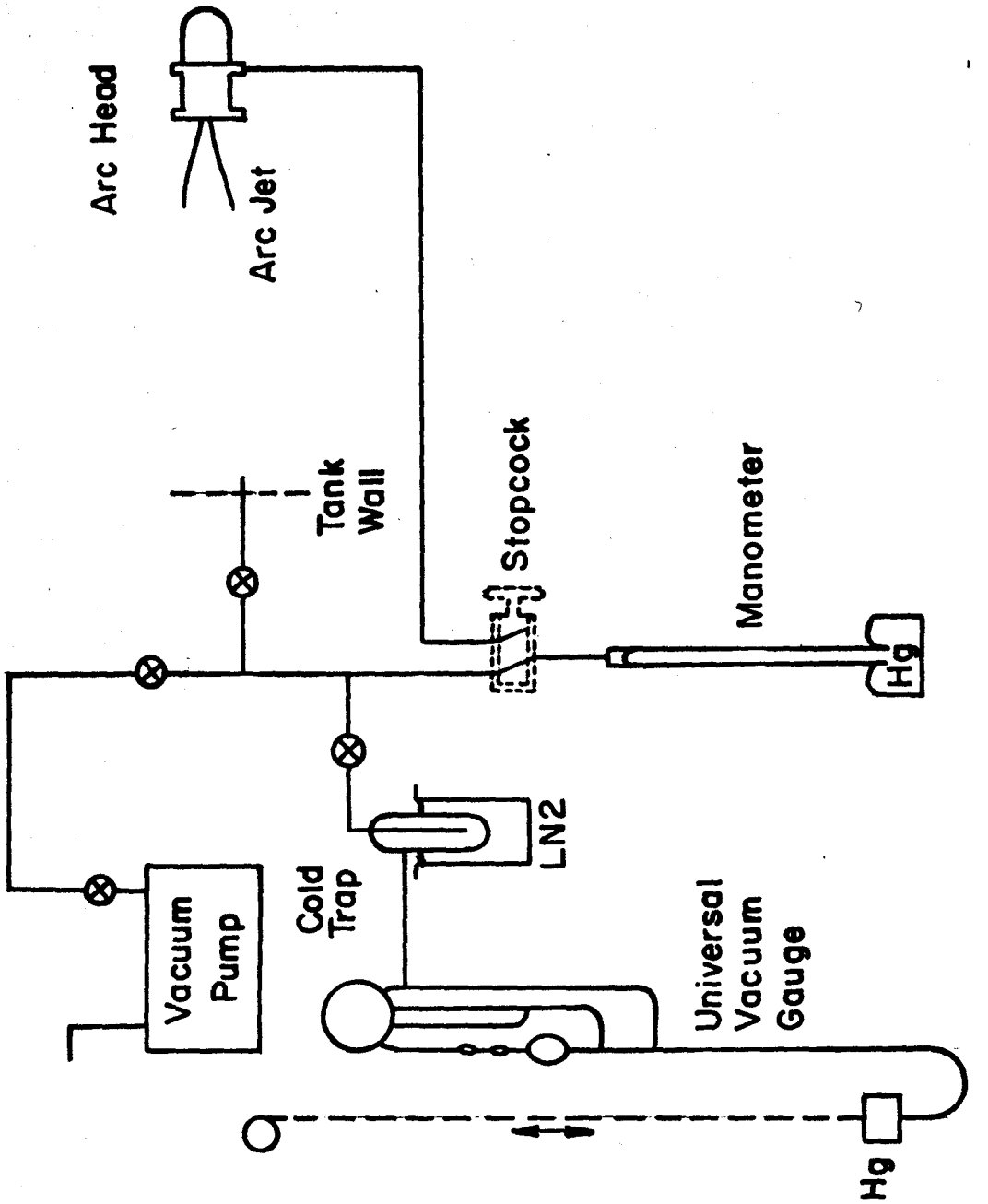

FIG. 14 AMBIENT AND TOTAL PRESSURE MEASUREMENT

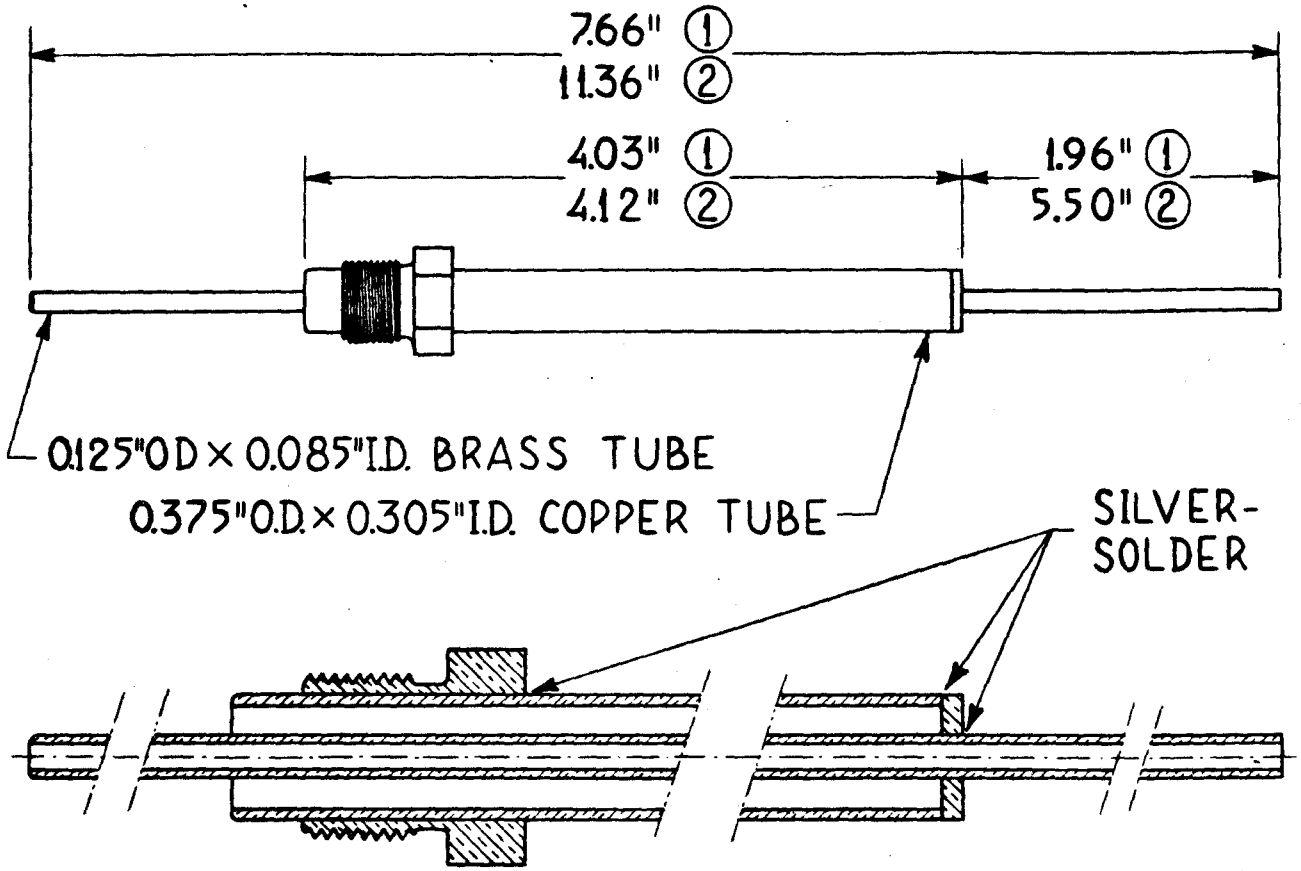

FIG.15 PITOT PROBES ① AND ②

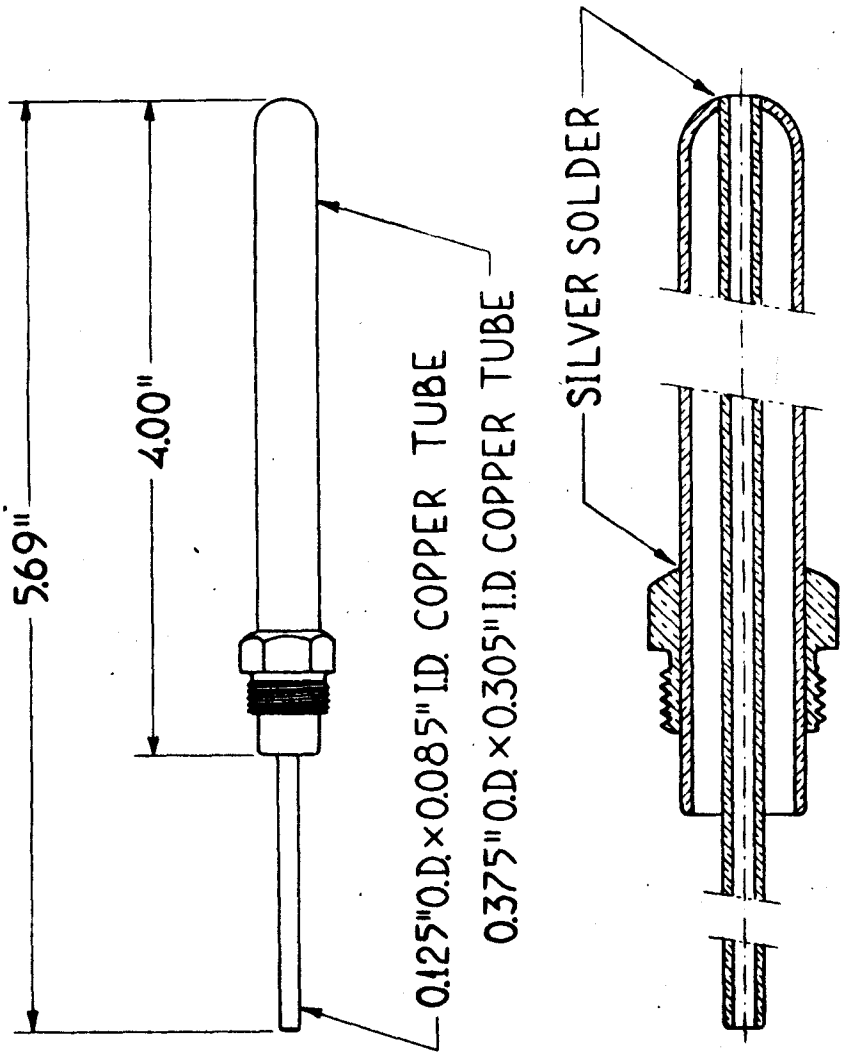

FIG.16. PITOT PROBE 3.

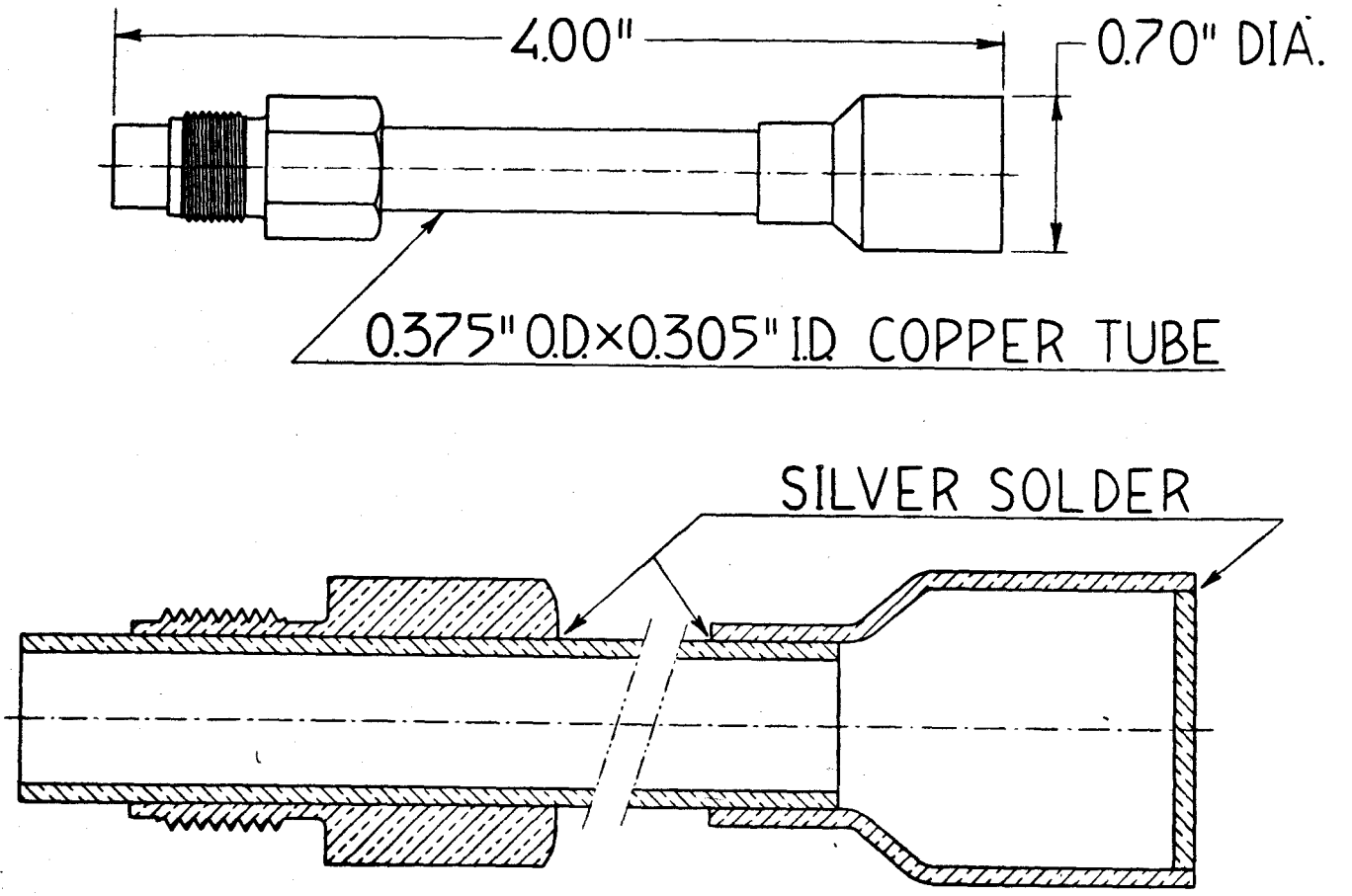

FIG.17 BLUNT BODY MODEL.

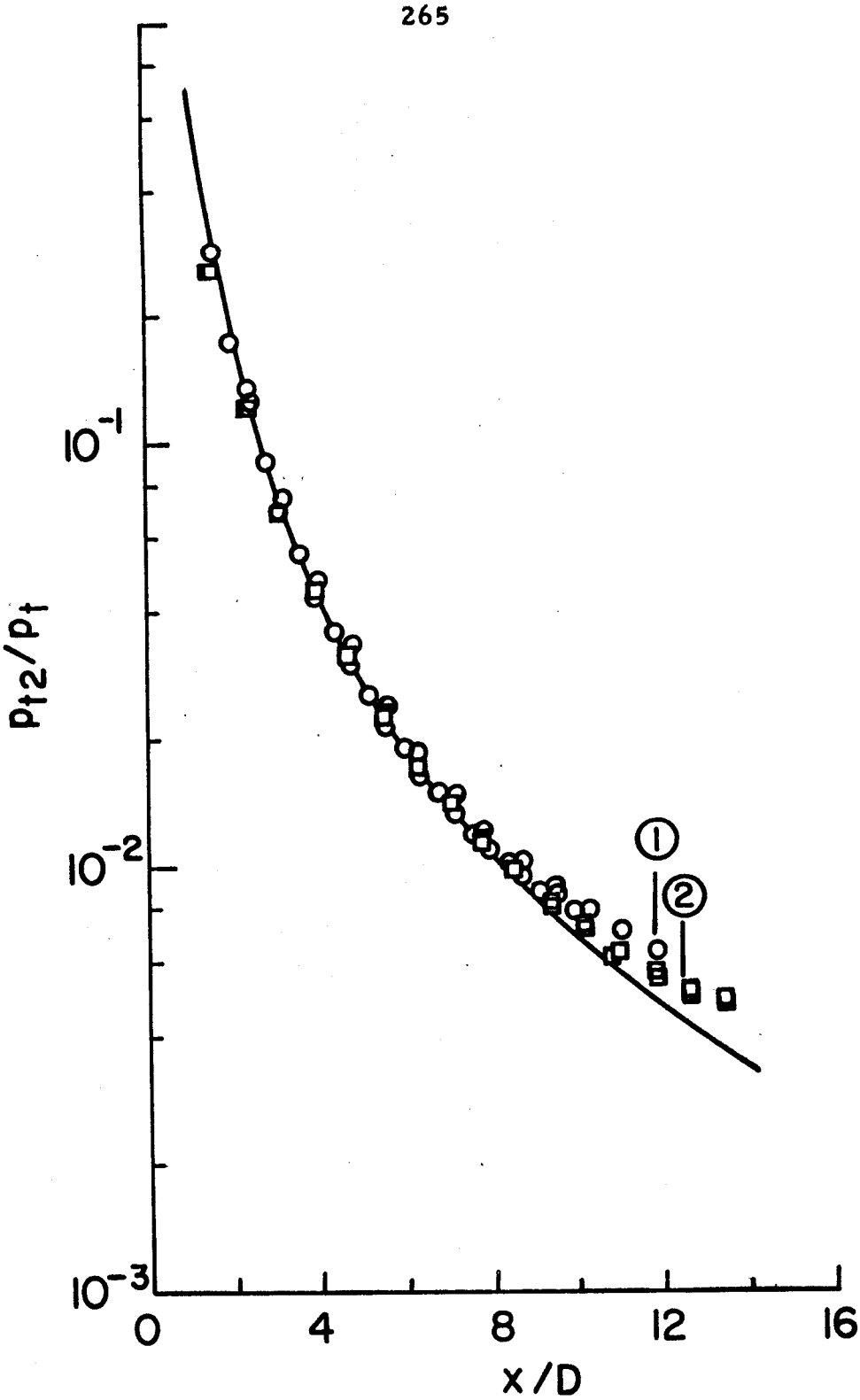

FIG. 18 PITOT PRESSURE IN COLD JET

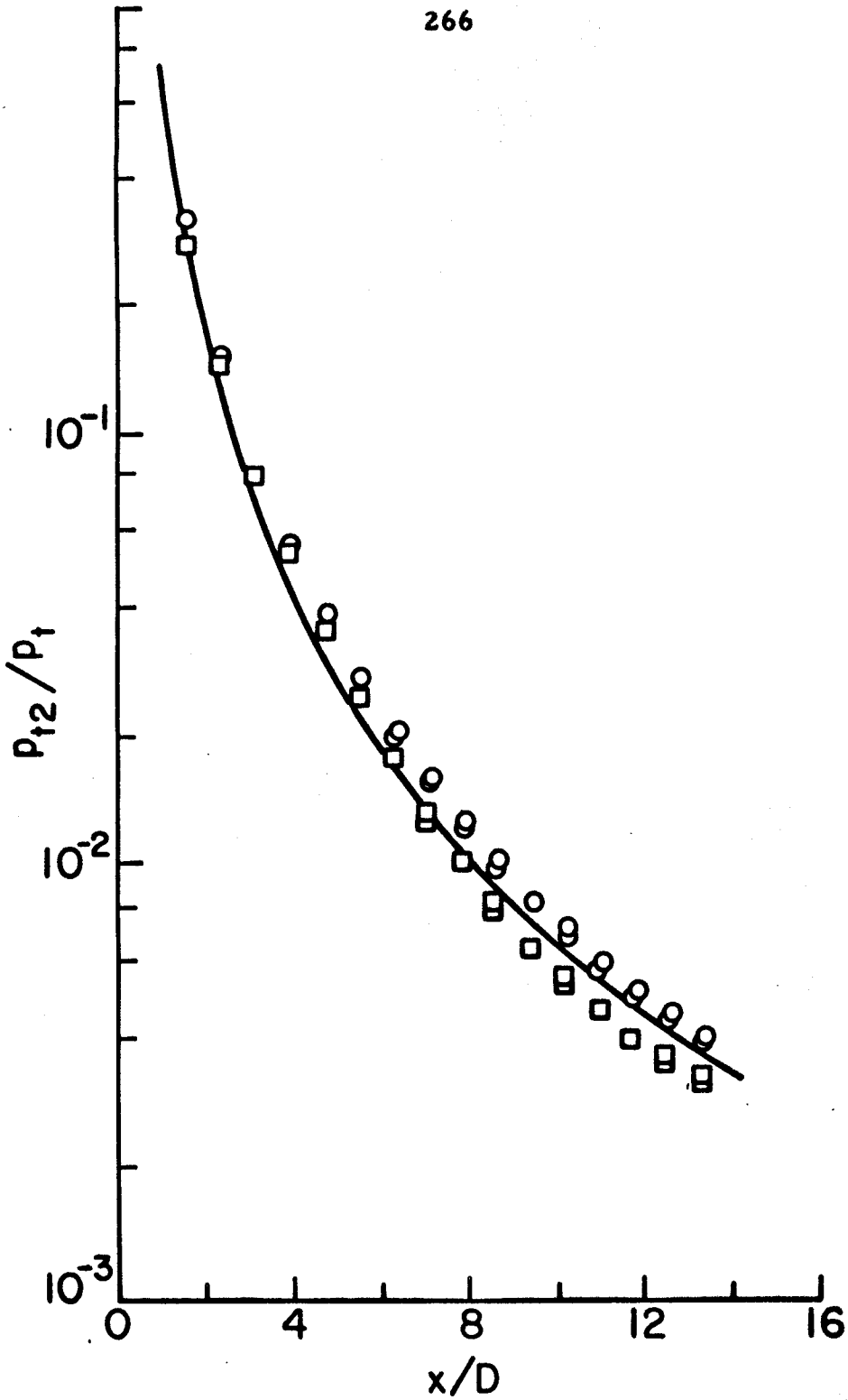

FIG. 19 PITOT PRESSURE IN HOT JET

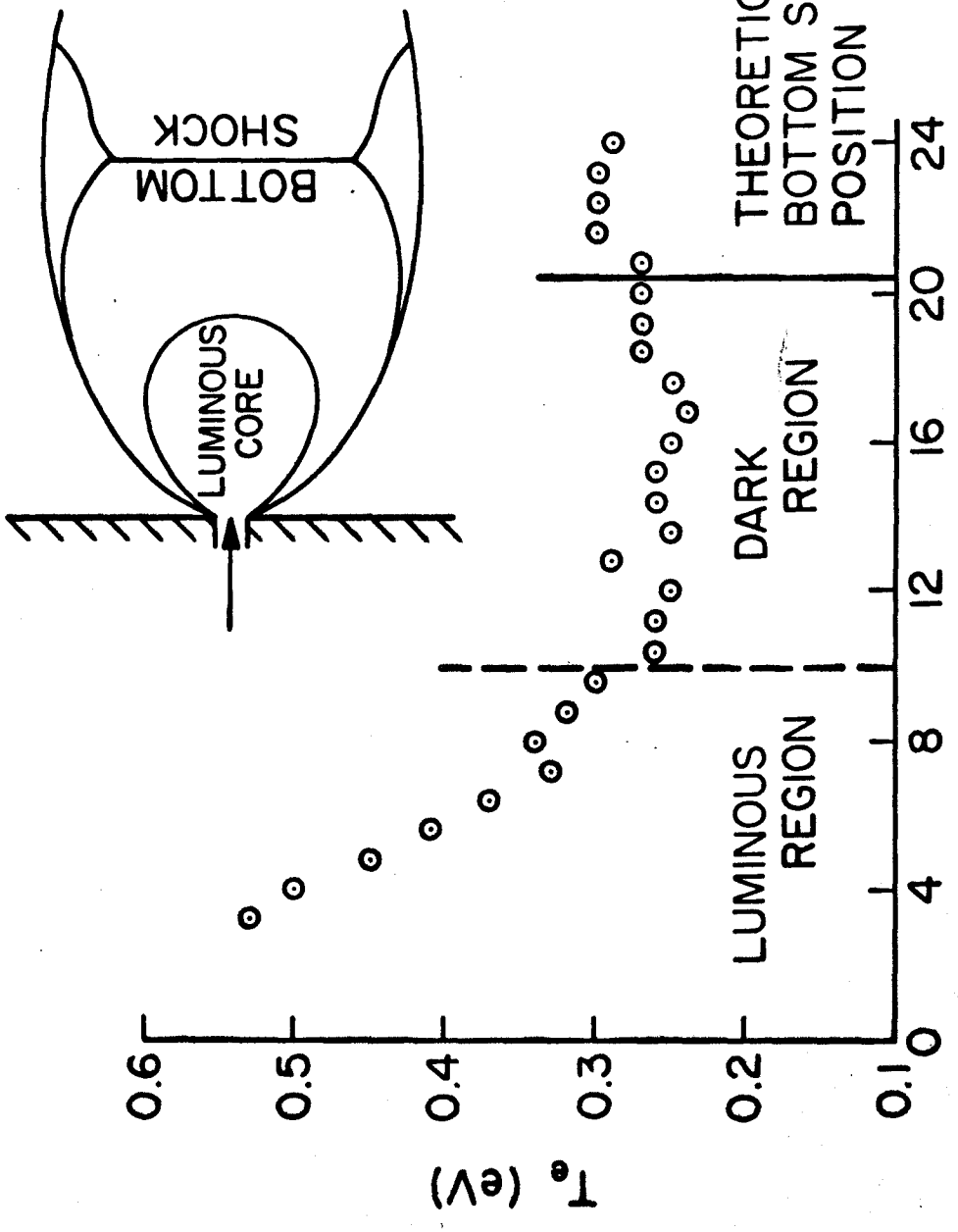

FIG. 20 T_e PROFILE WITH REGIONS MARKED - TEST I

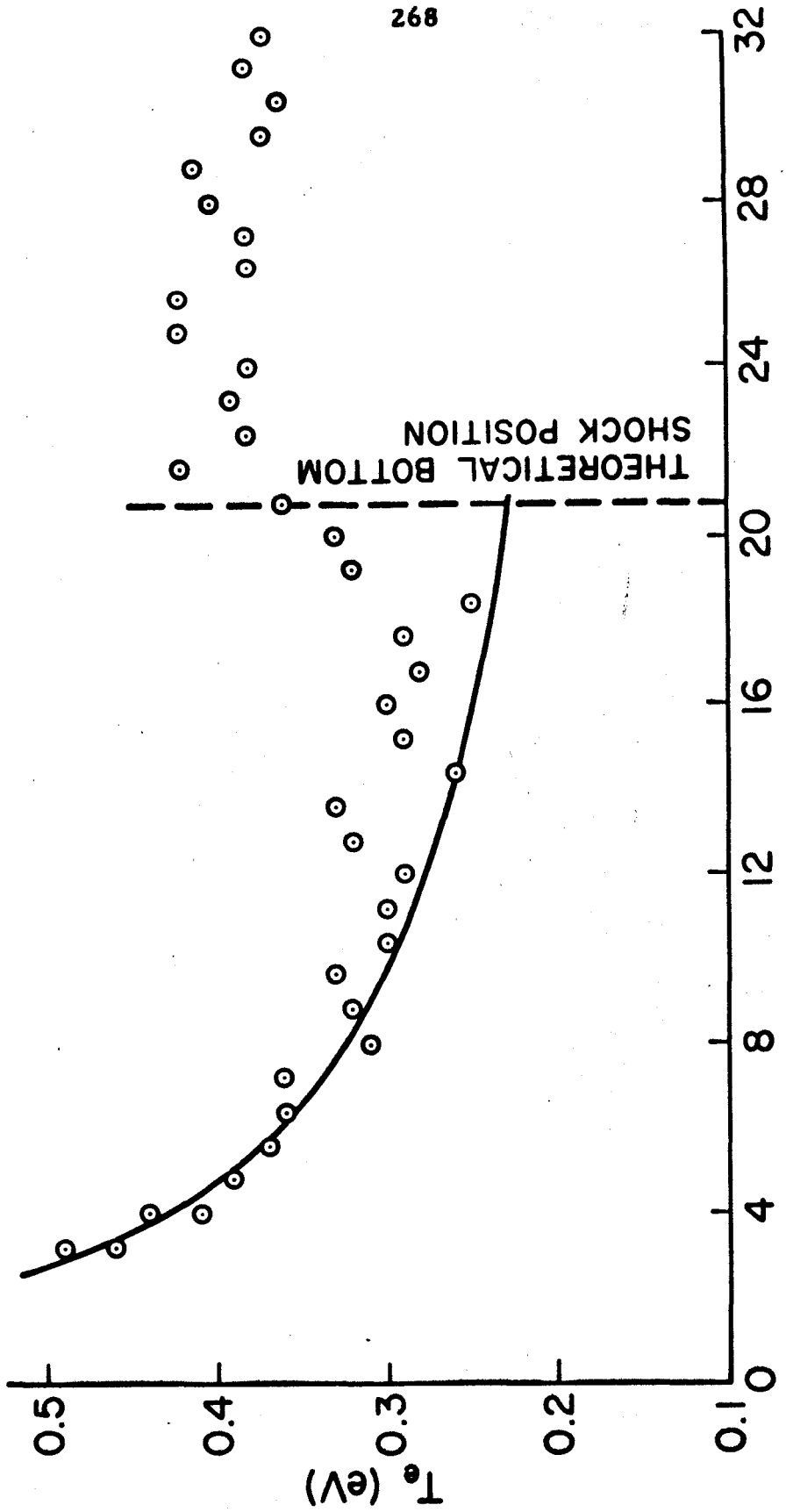

FIG. 21 T_e DISTRIBUTION IN EMPTY FREE JET – TEST 2

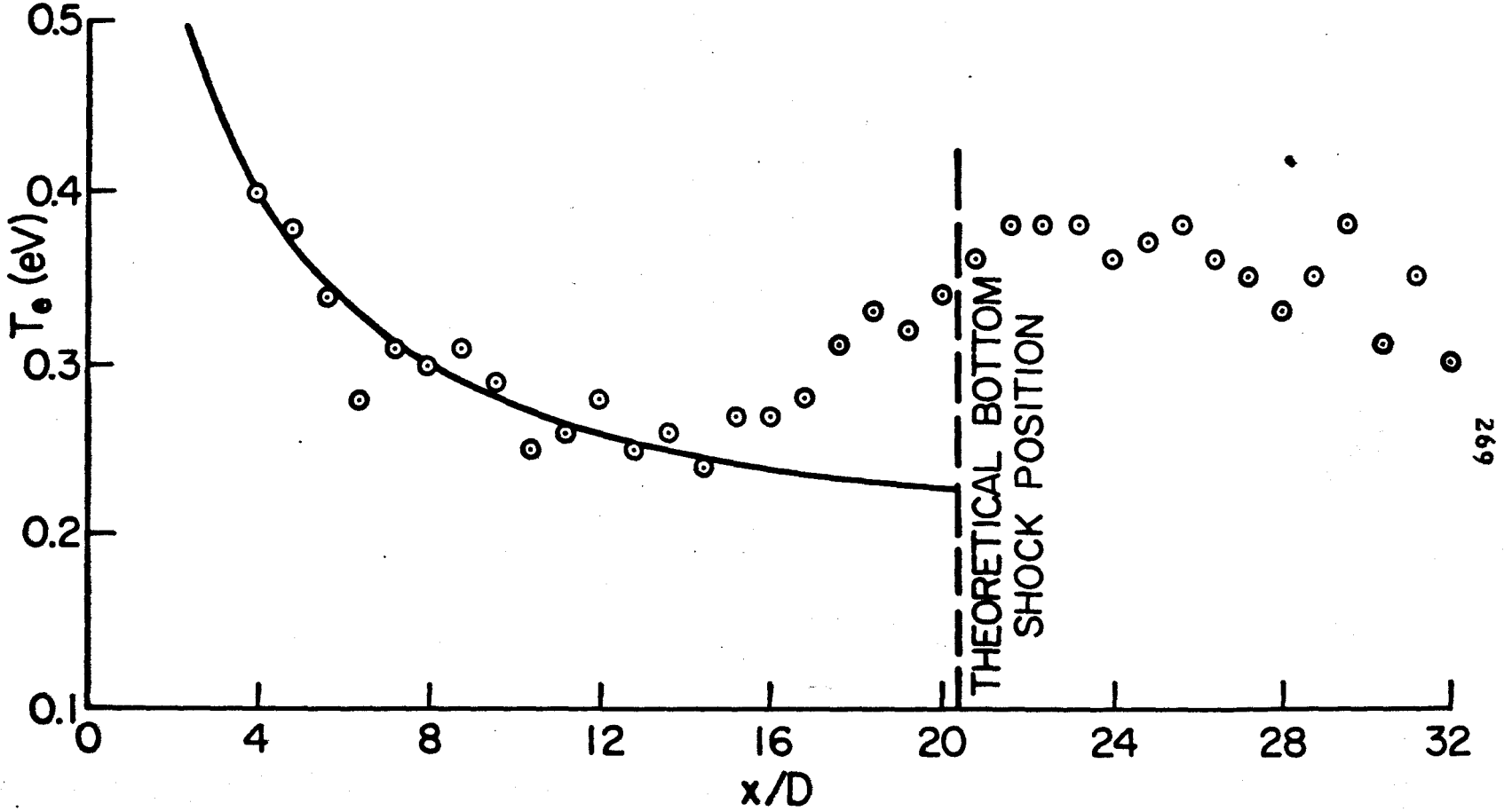

FIG. 22 T_e DISTRIBUTION IN EMPTY FREE JET—TEST 3

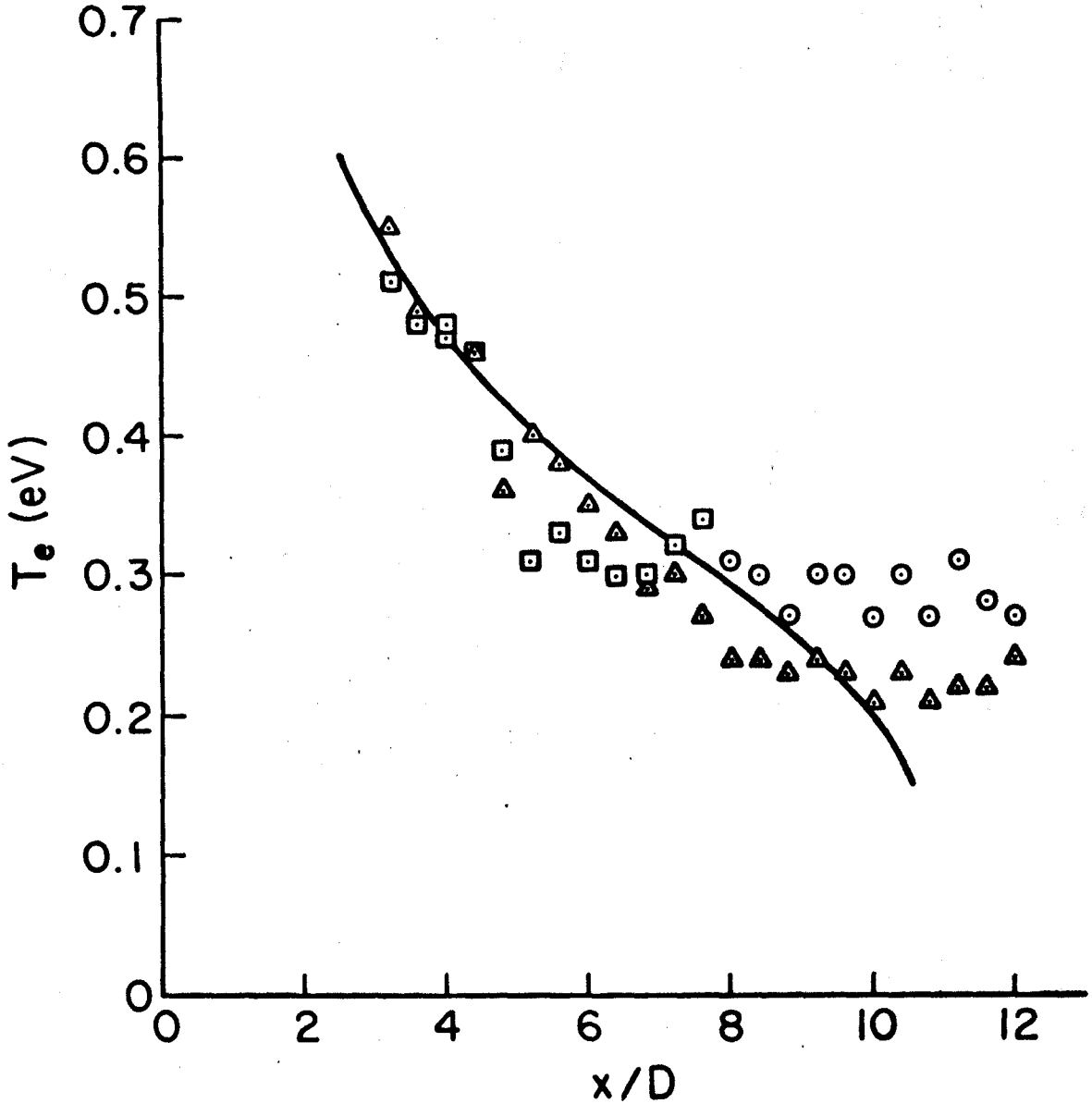

FIG. 23 T_e DISTRIBUTION NEAR ORFICE – TEST 4

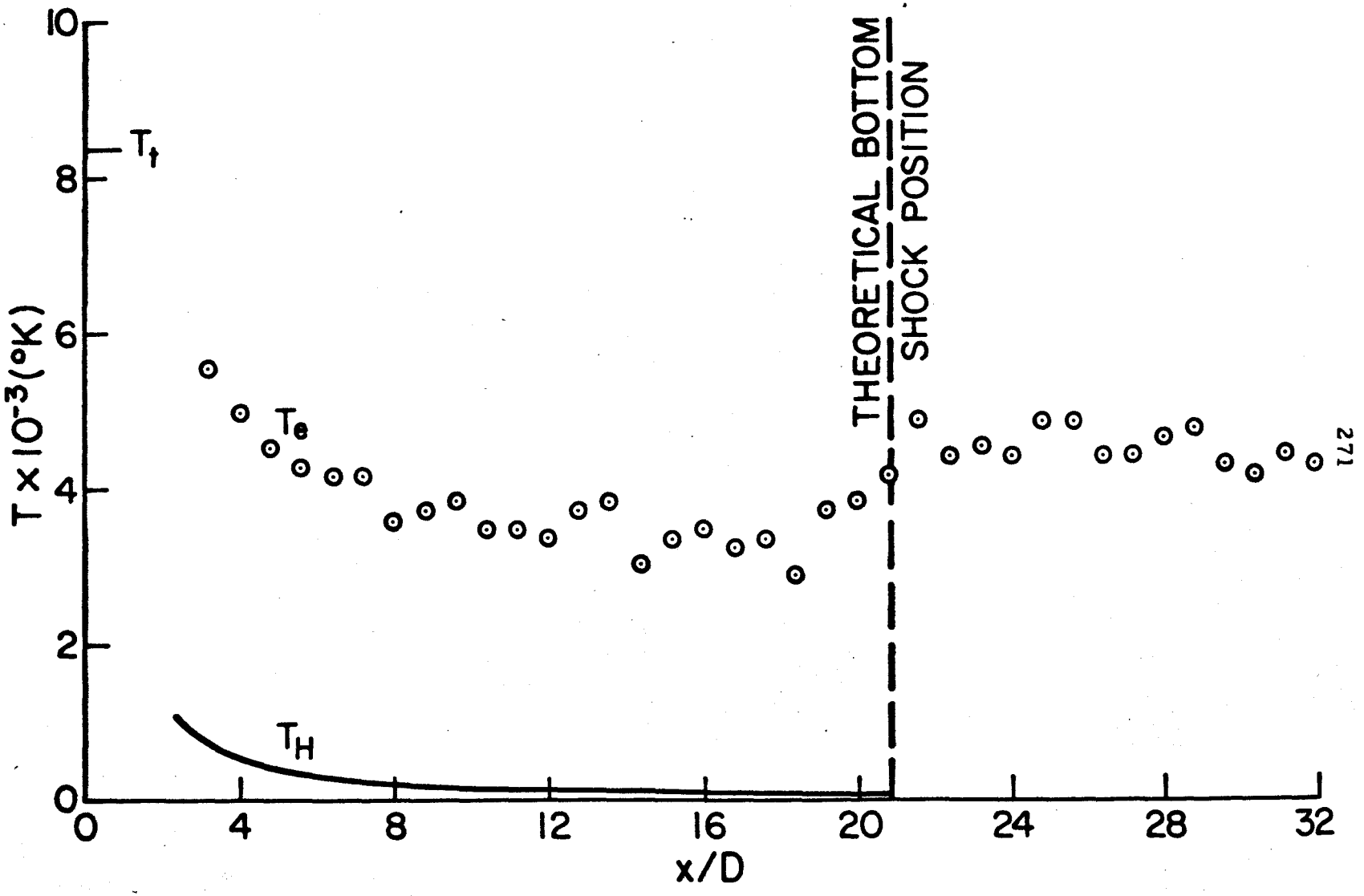

FIG. 24 SPECIE TEMPERATURE DISTRIBUTIONS – TEST 2

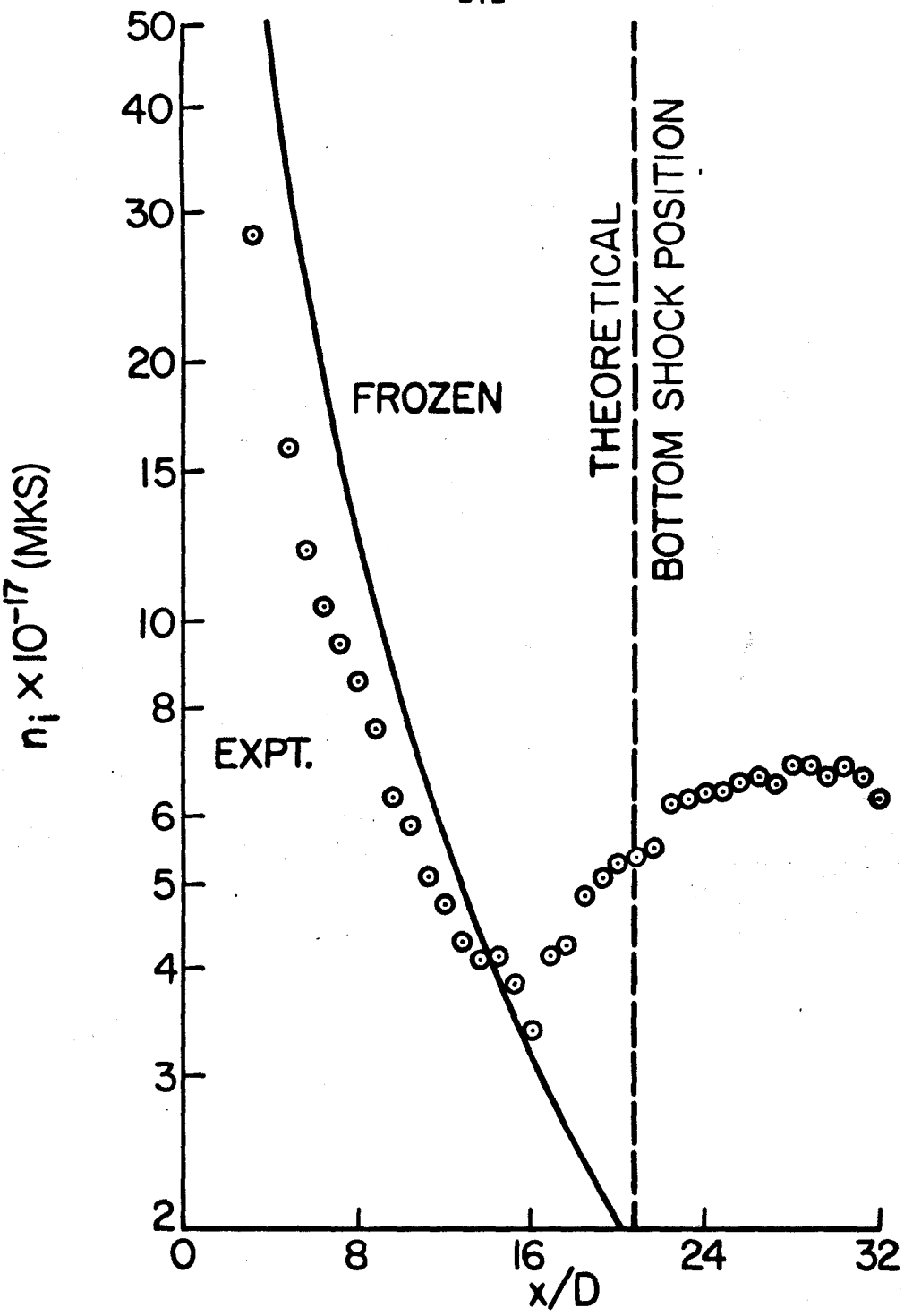

FIG. 25 n_i DISTRIBUTION IN EMPTY FREE JET-TEST 2

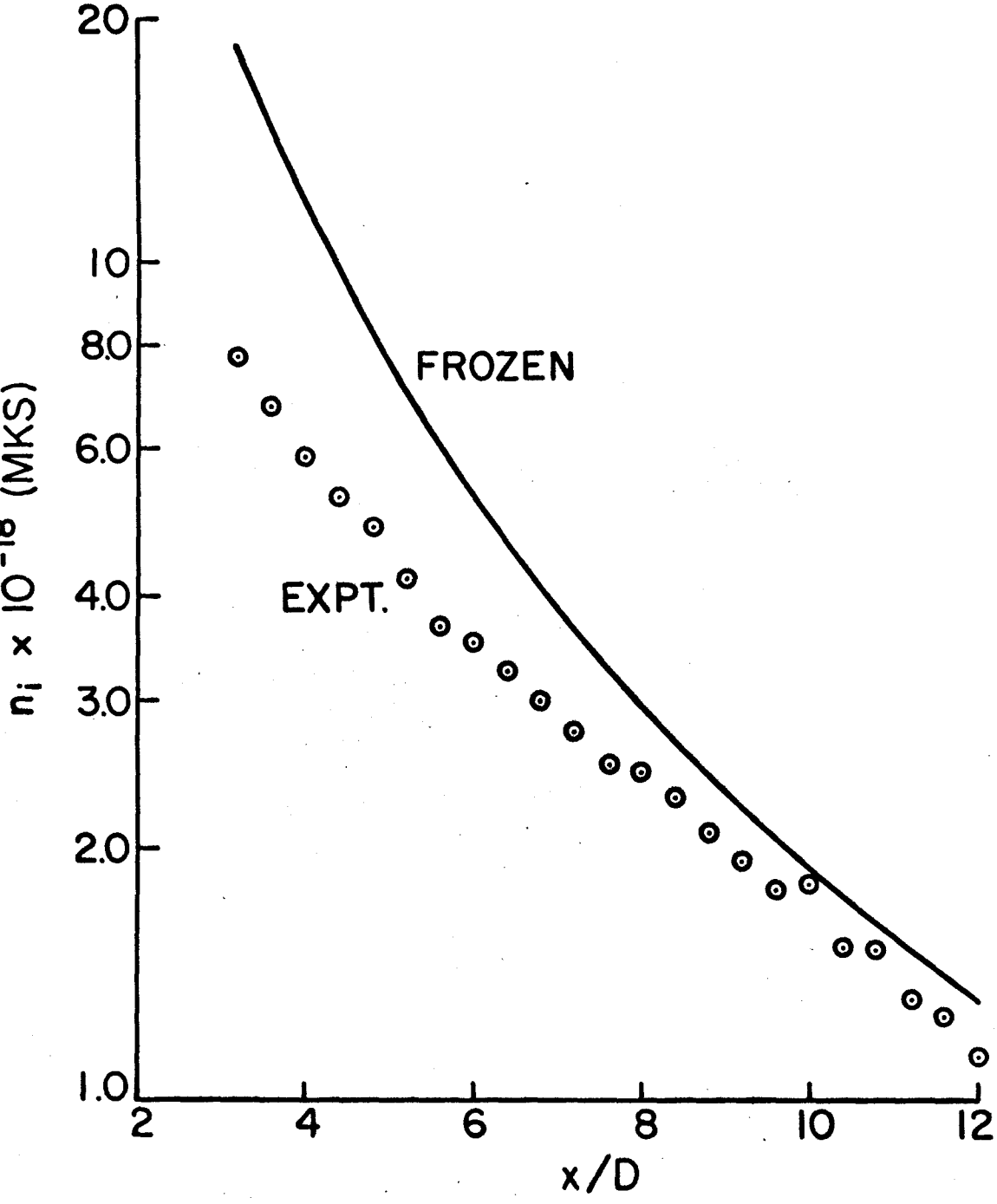

FIG. 26 n_i DISTRIBUTION IN EMPTY FREE JET. – TEST 4

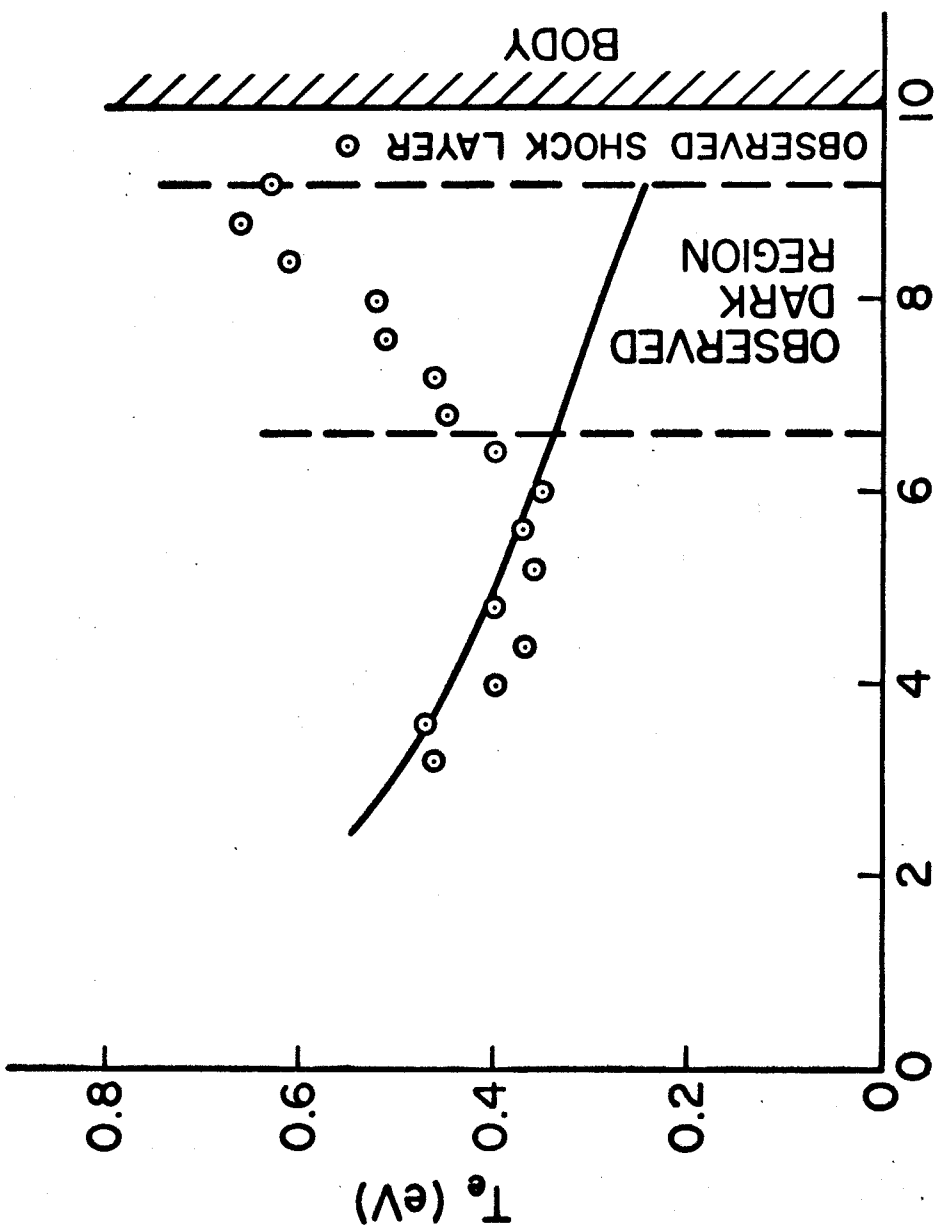

FIG. 27 T_e DISTRIBUTION IN FRONT OF BLUNT BODY – TEST 5

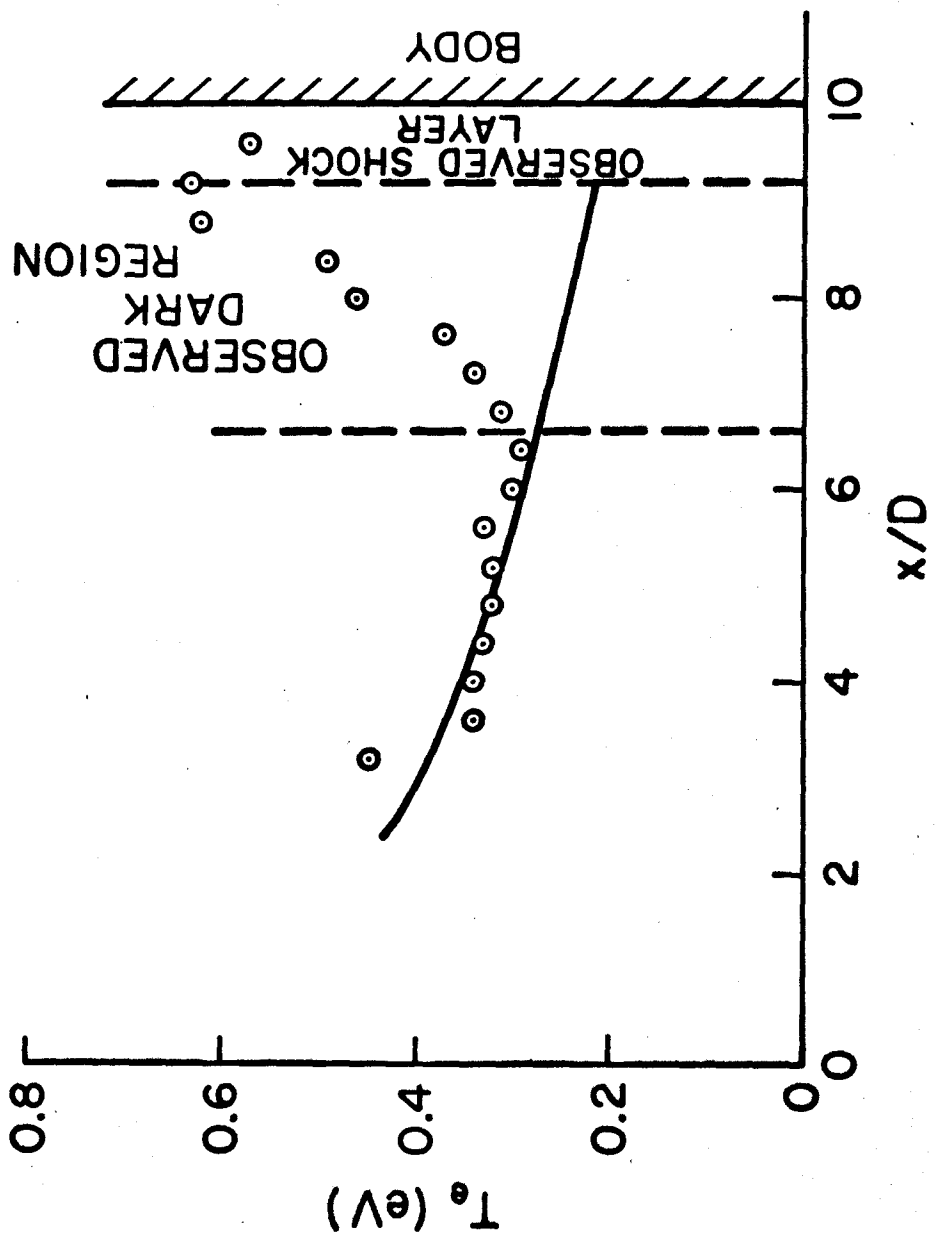

FIG. 28 T_e DISTRIBUTION IN FRONT OF BLUNT BODY-TEST 6

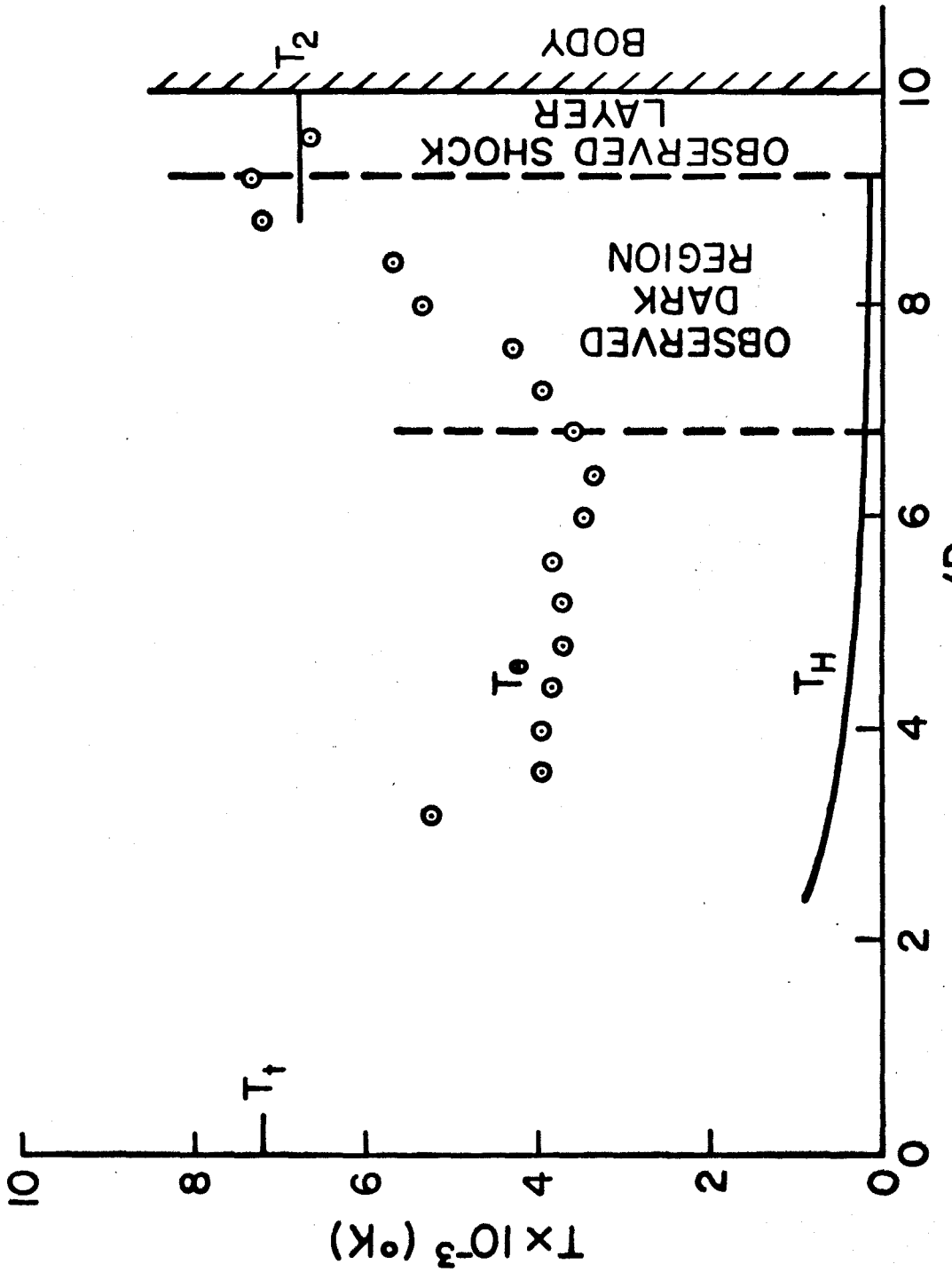

FIG. 29 SPECIE TEMPERATURE DISTRIBUTIONS – TEST 6

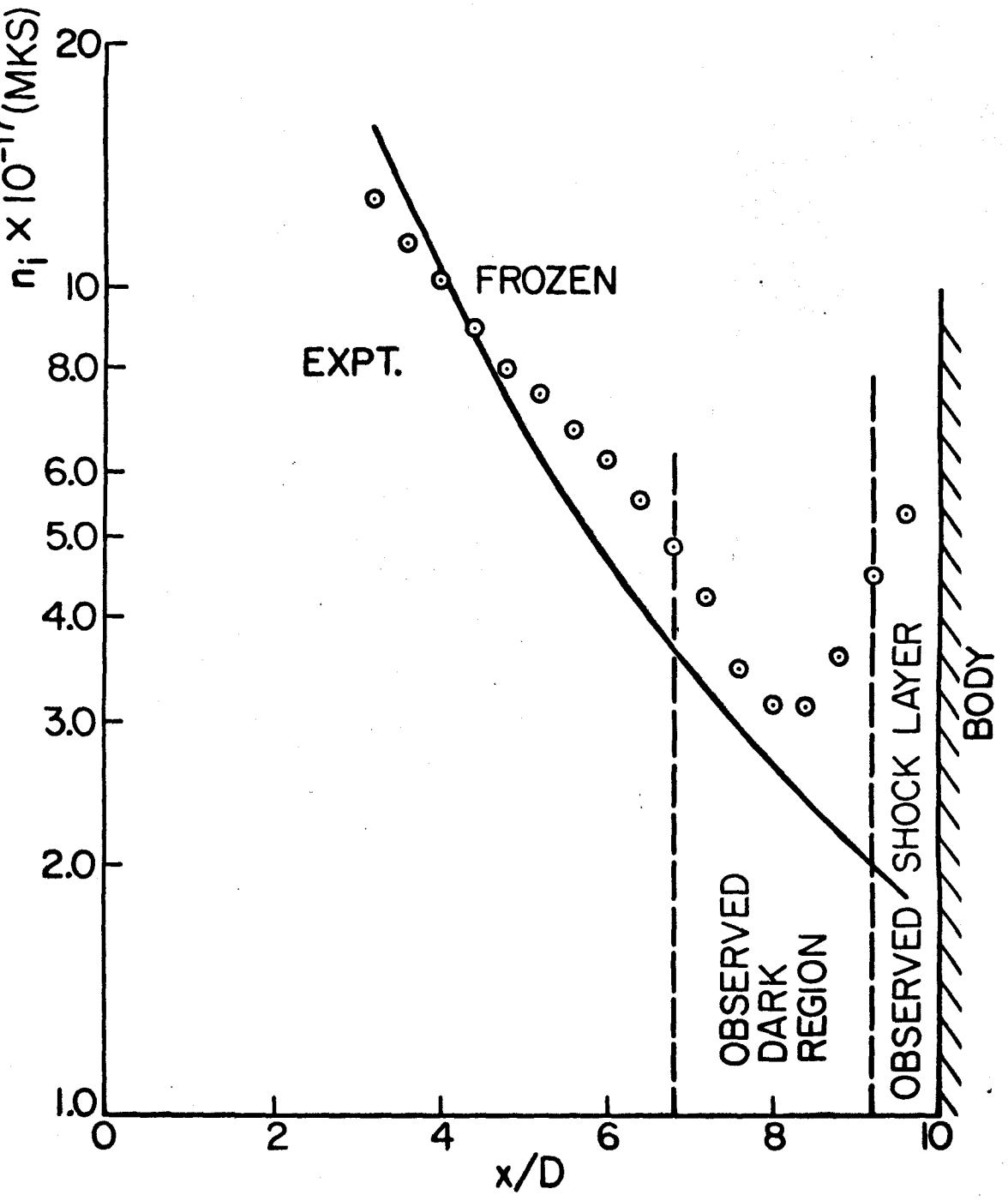

FIG. 30 n_i DISTRIBUTION IN FRONT OF BLUNT BODY-TEST 6

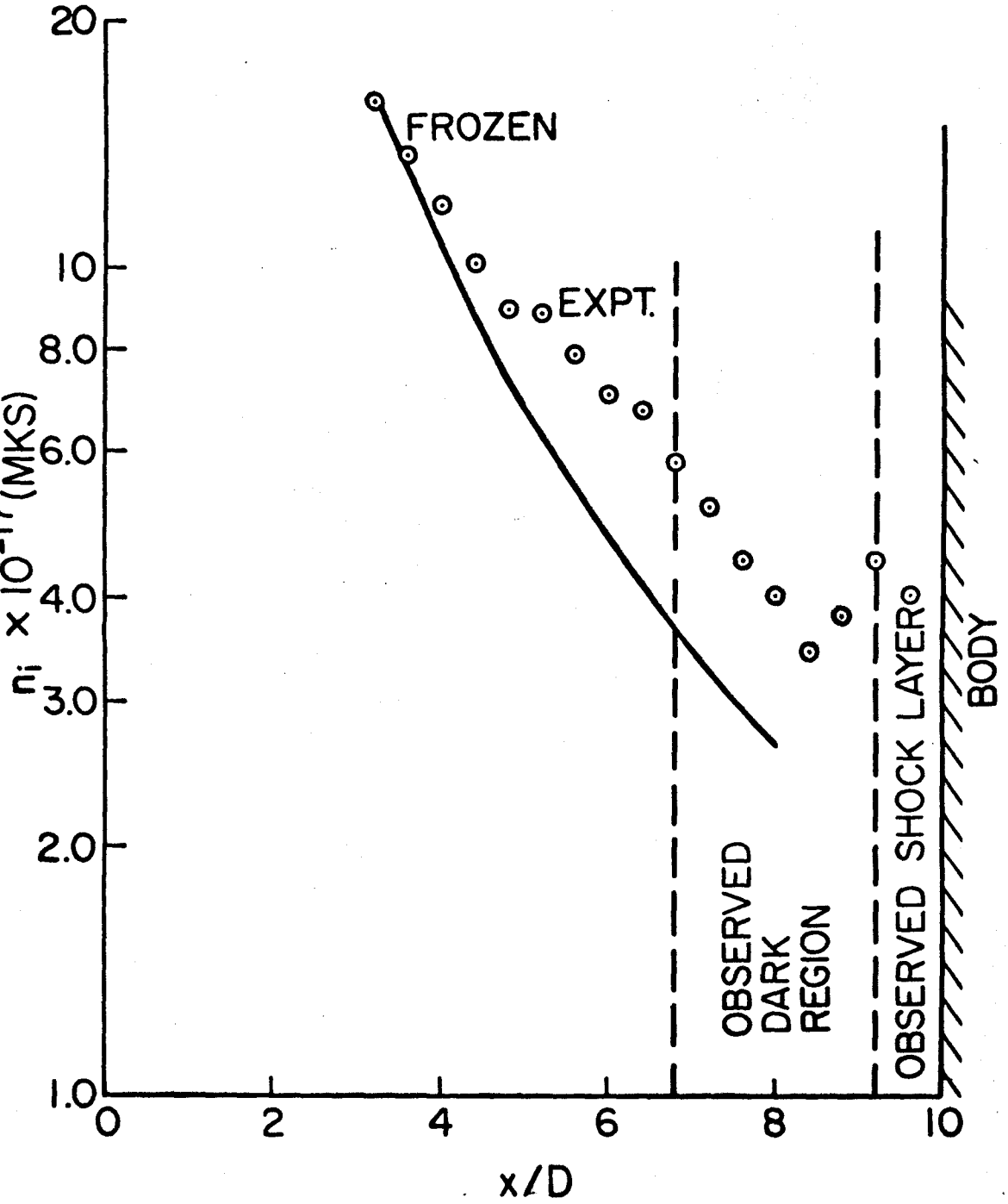

FIG. 31 n_i DISTRIBUTION IN FRONT OF BLUNT BODY- TEST 7

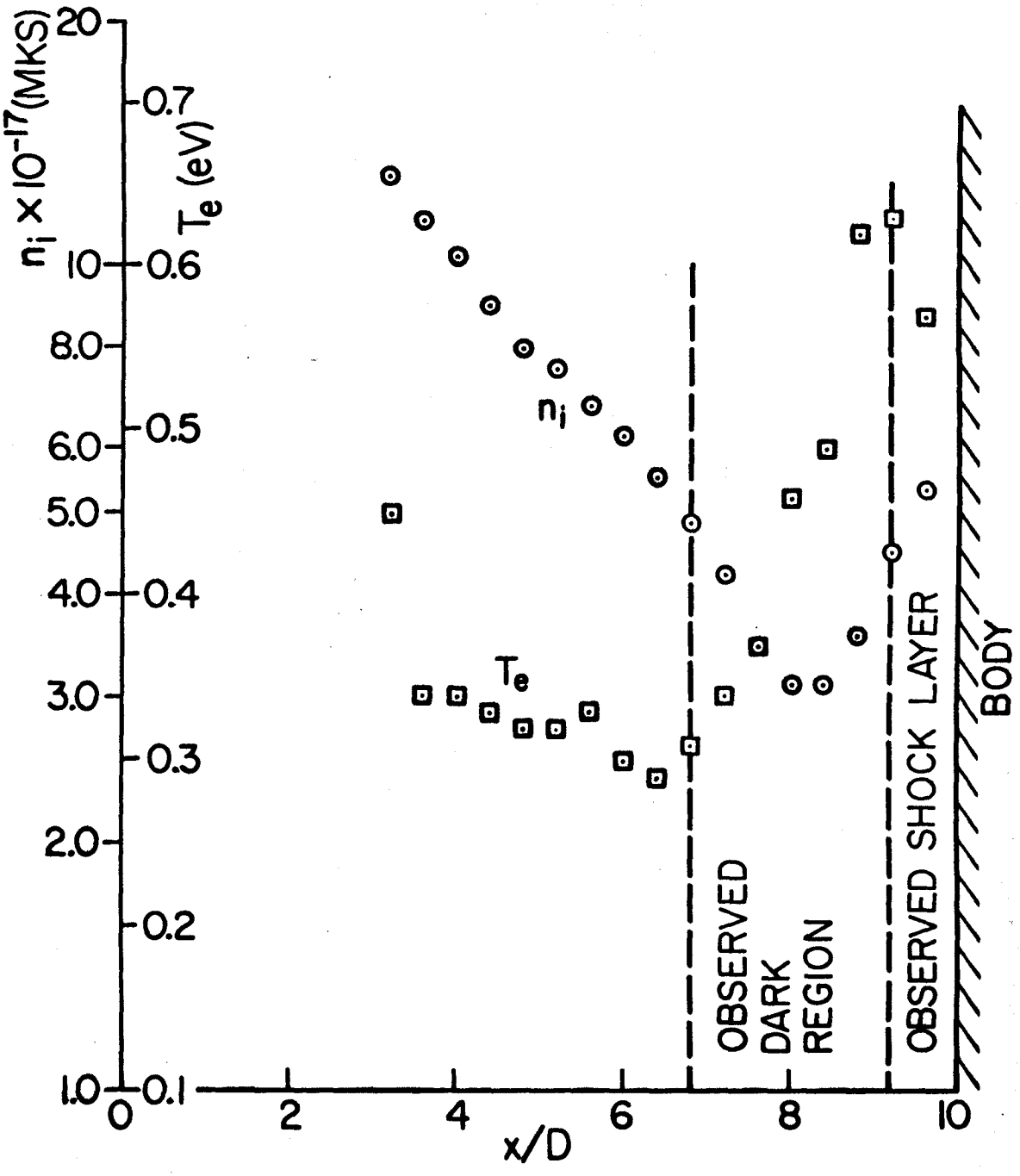

FIG. 32 T_e AND n_i IN FRONT OF BLUNT BODY–TEST 6

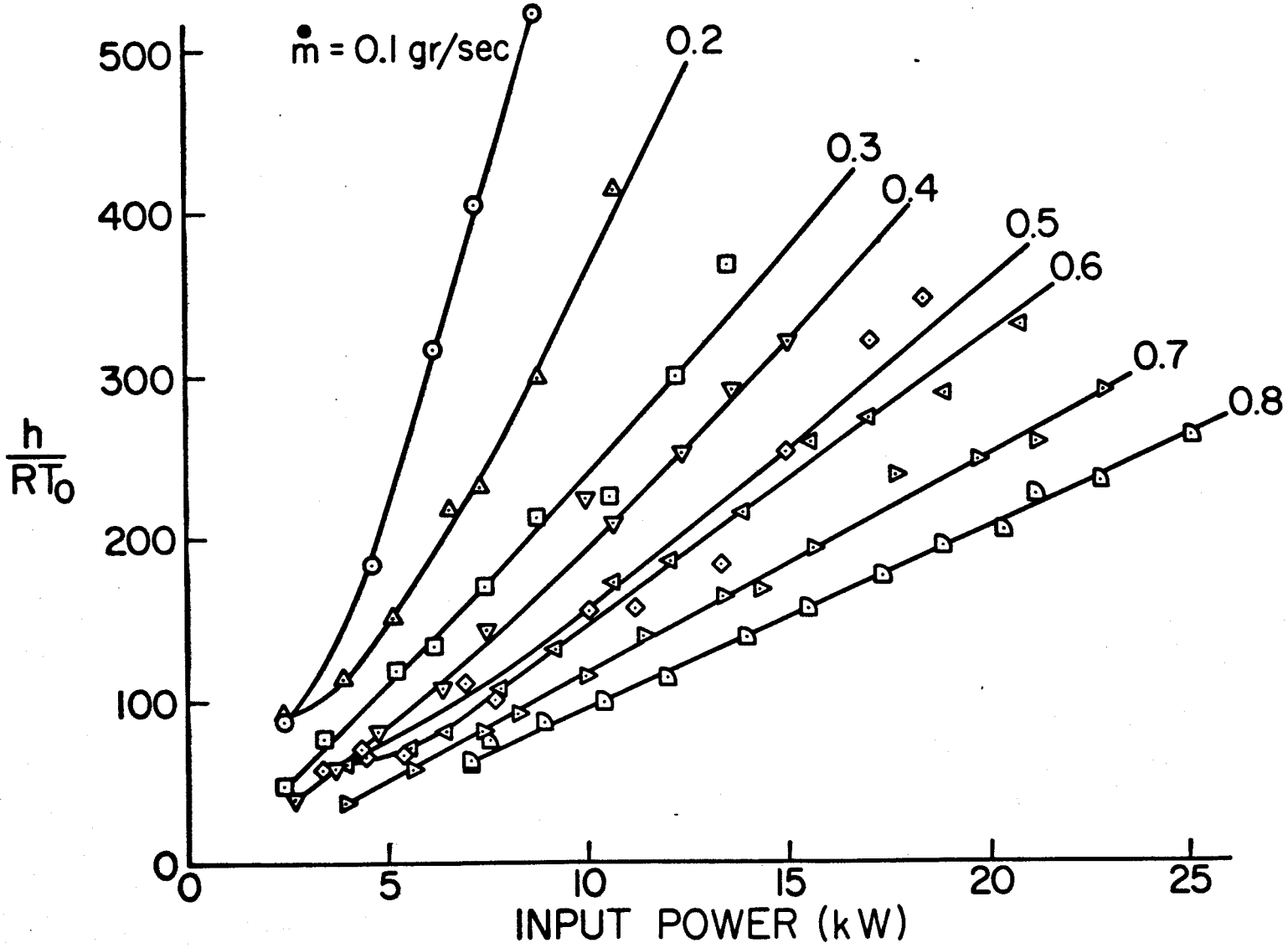

FIG. A1 ARC HEATER PERFORMANCE

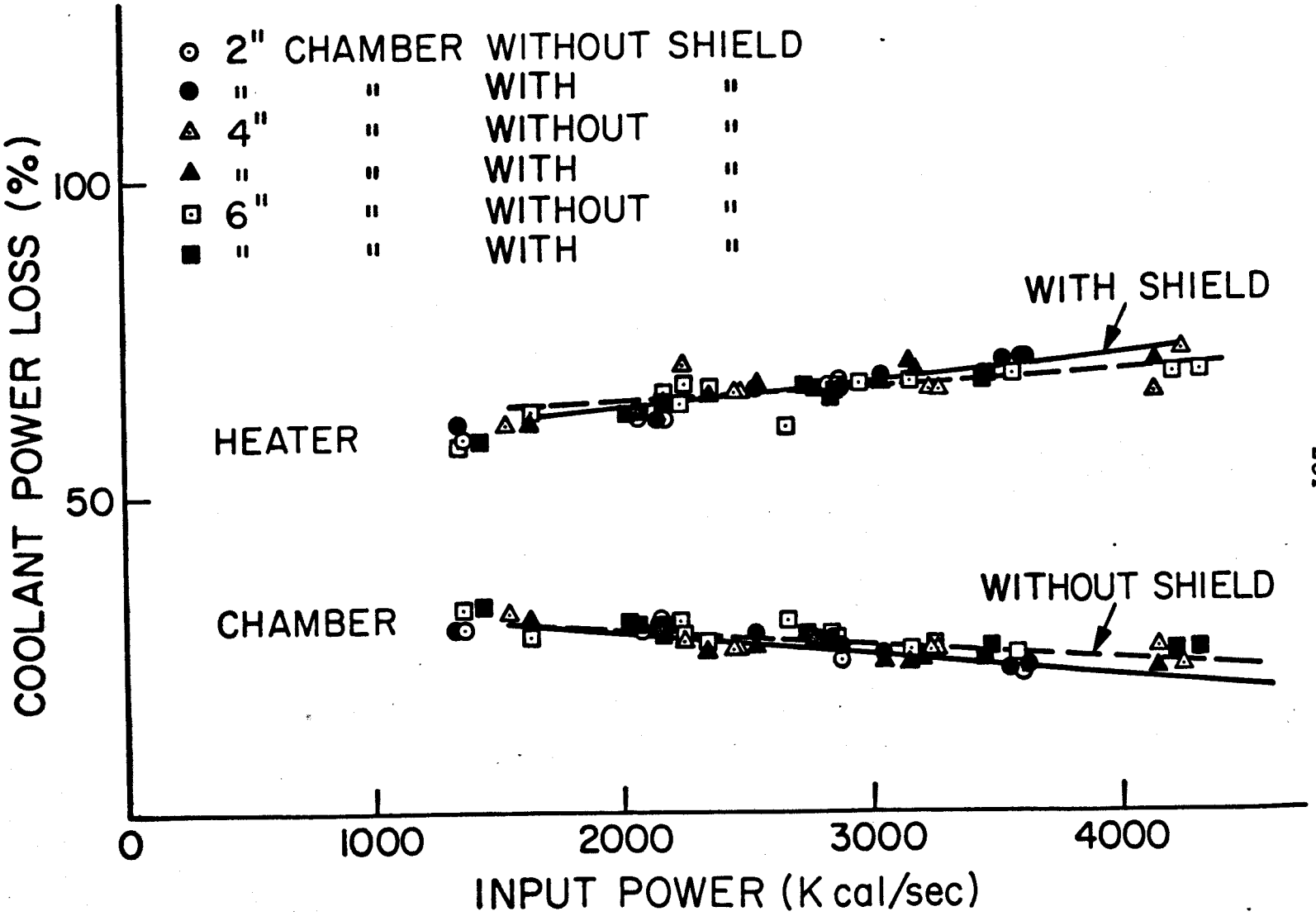

FIG.A2 COOLANT WATER POWER LOSS

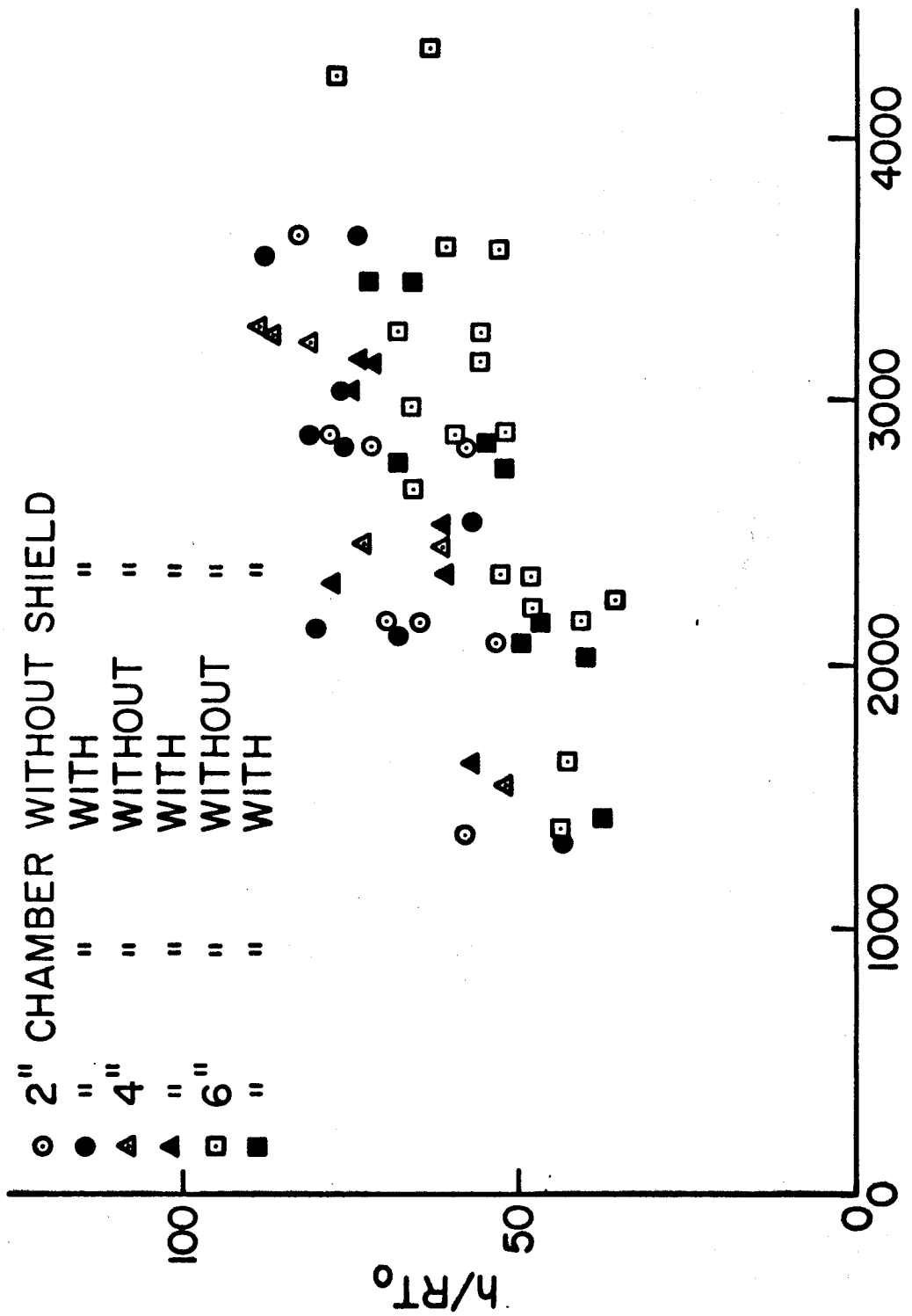

FIG. A3 ENTHALPY DELIVERED TO GAS

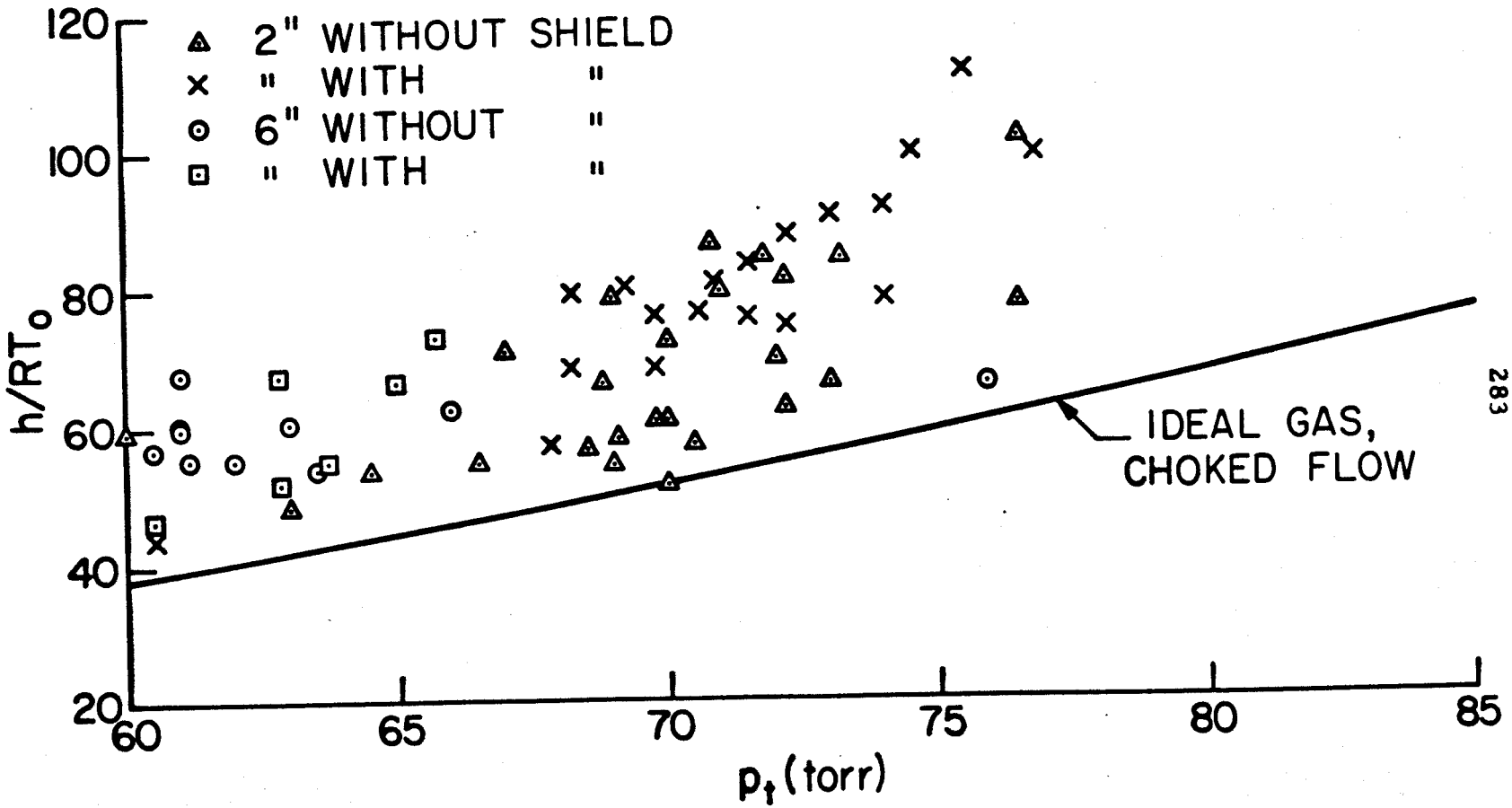

FIG. A4 COMPARISON OF METHODS OF CALCULATING h/RT_o

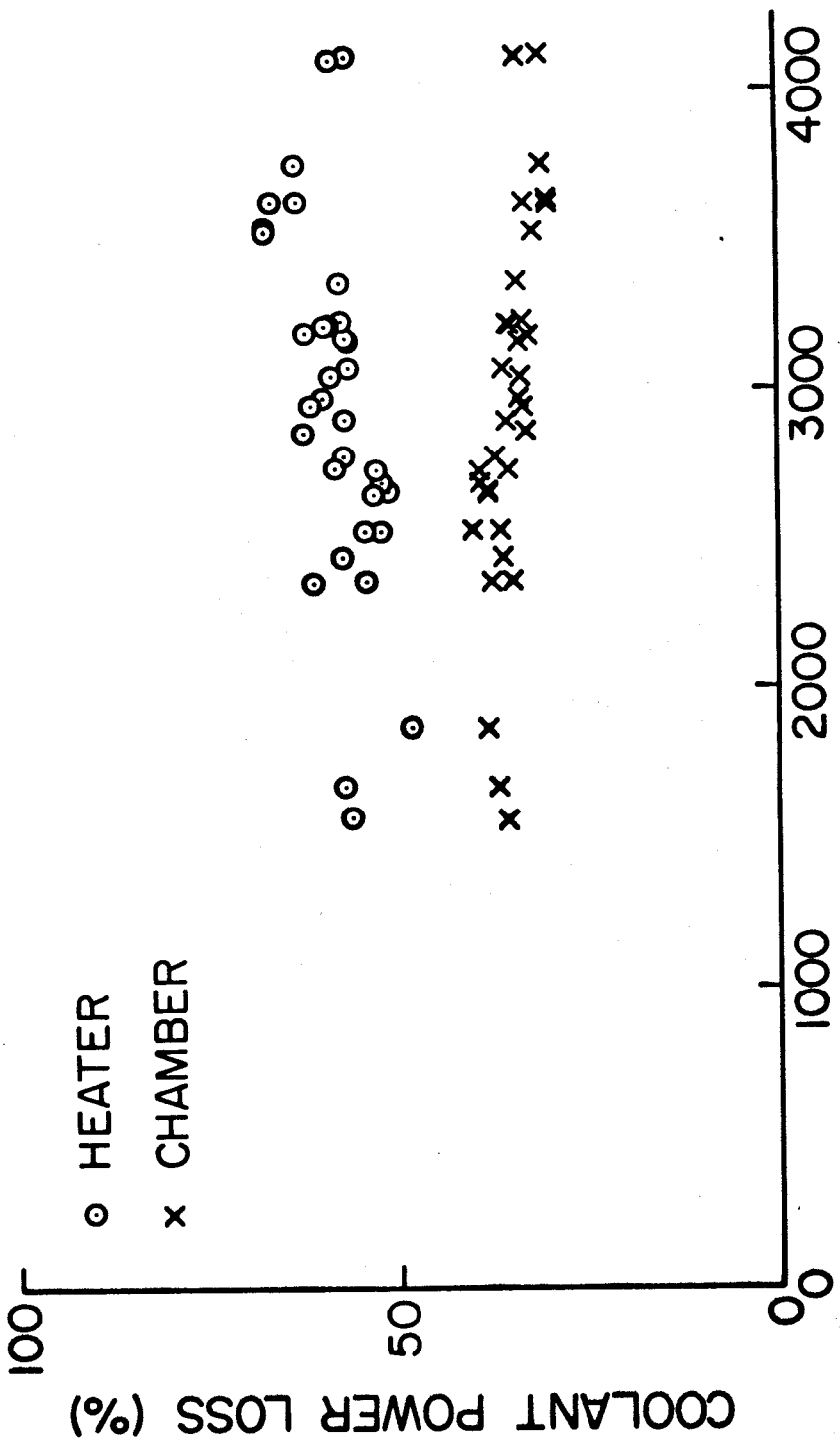

FIG. A5 COOLANT POWER LOSS - SHORT ANODE

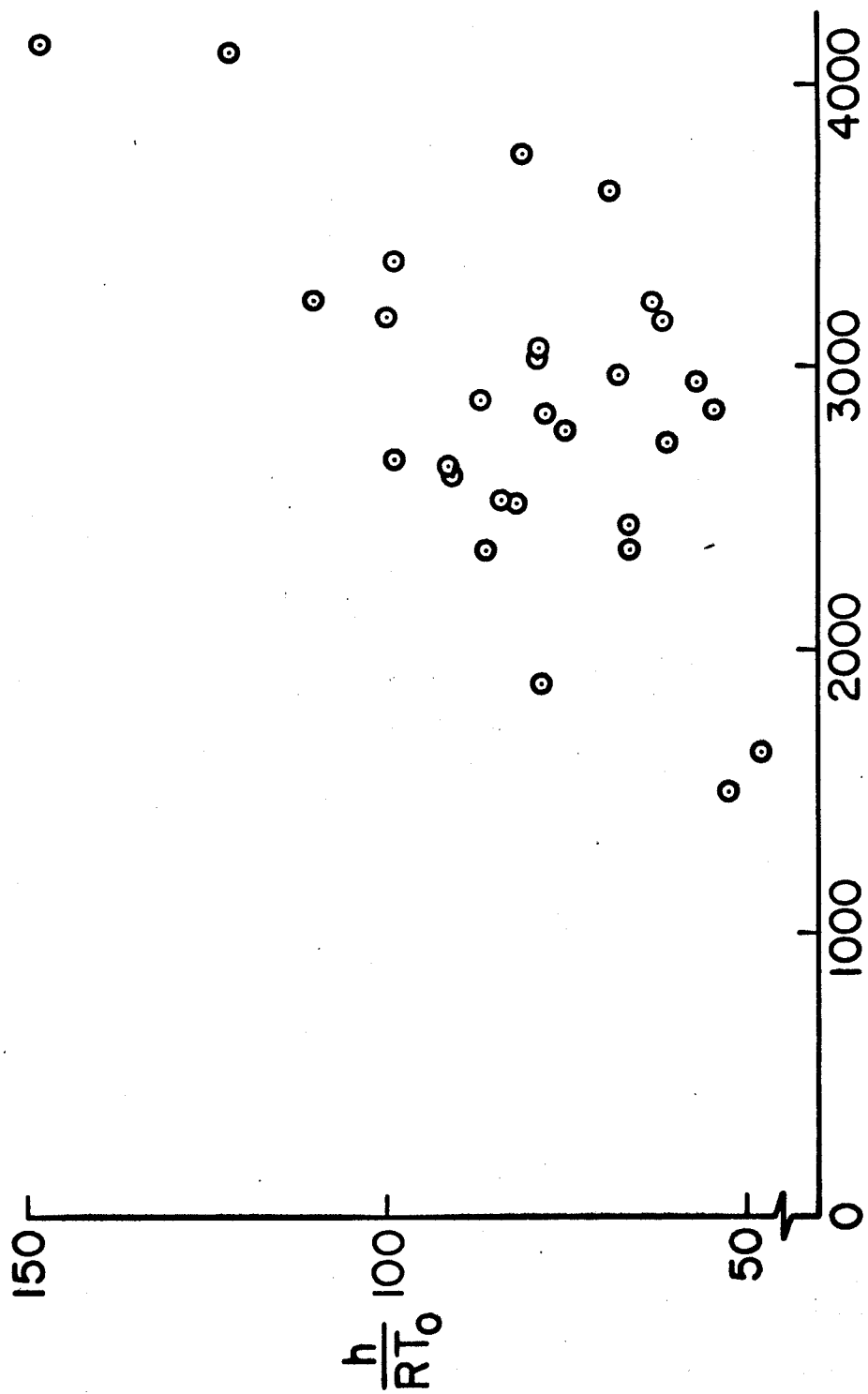

FIG. A6 ENTHALPY DELIVERED TO GAS – SHORT ANODE

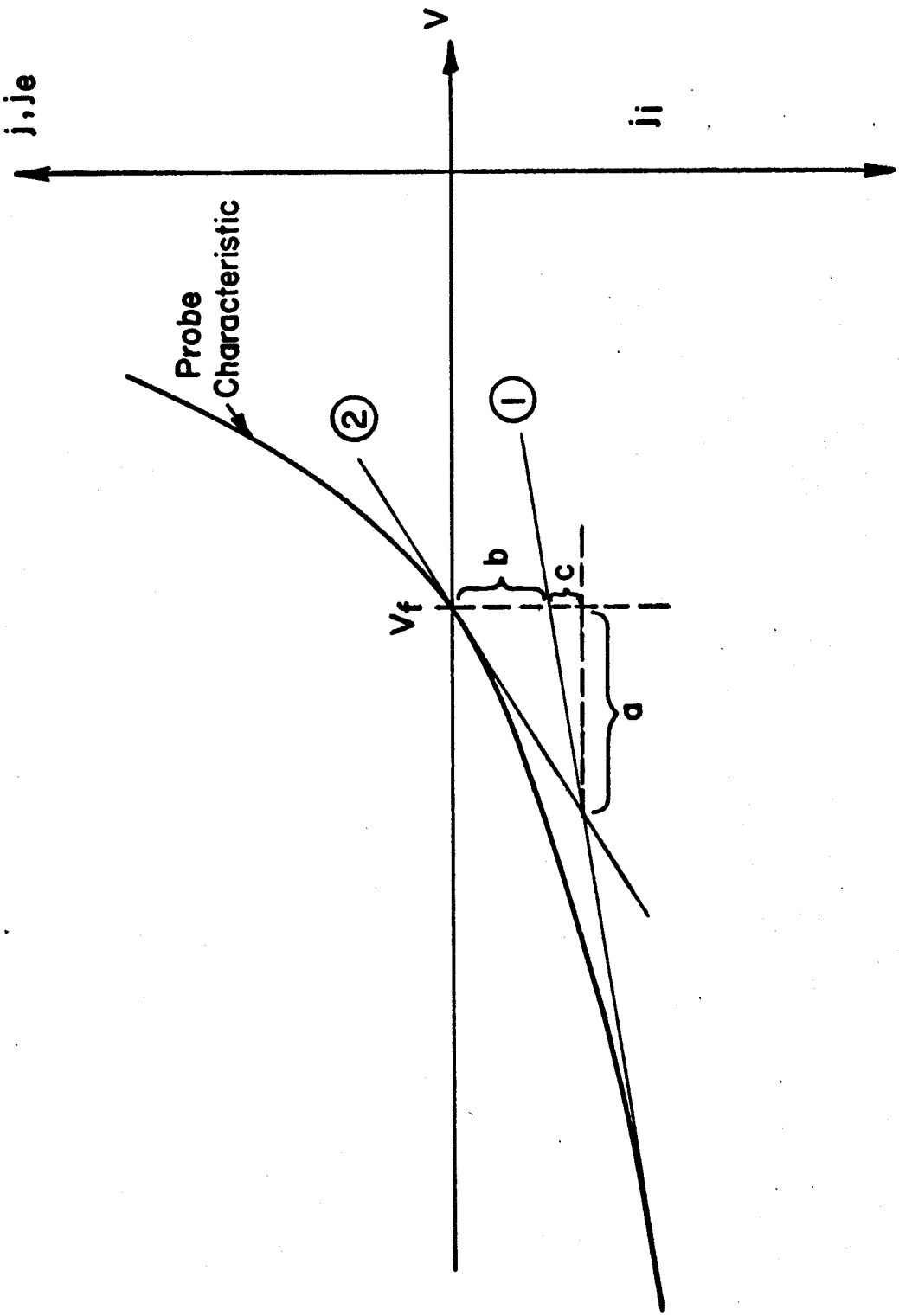

FIG.C1 ELECTRON TEMPERATURE DETERMINATION

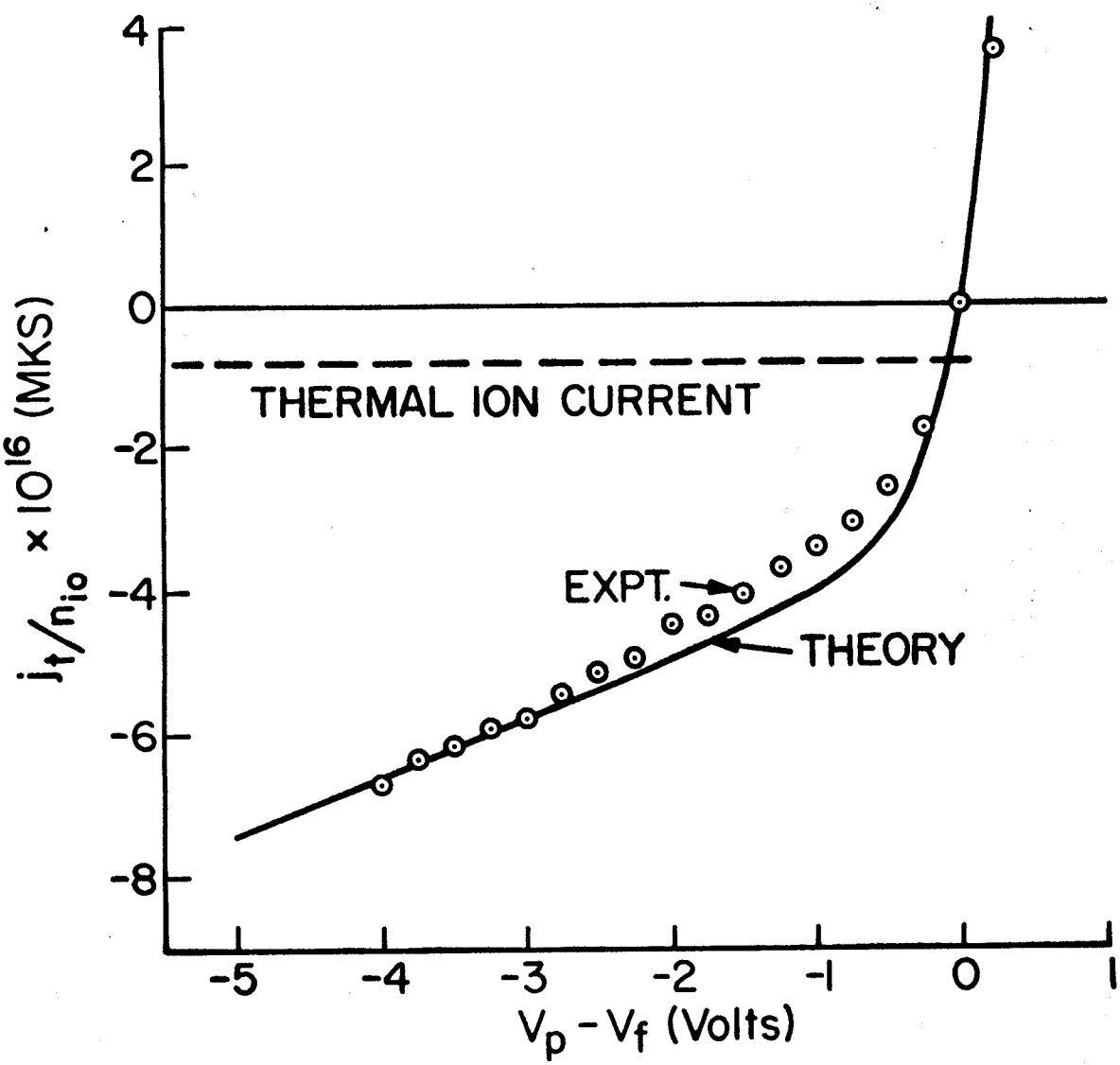

FIG. C2 THEORETICAL vs. EXPERIMENTAL PROBE CHARACTERISTIC

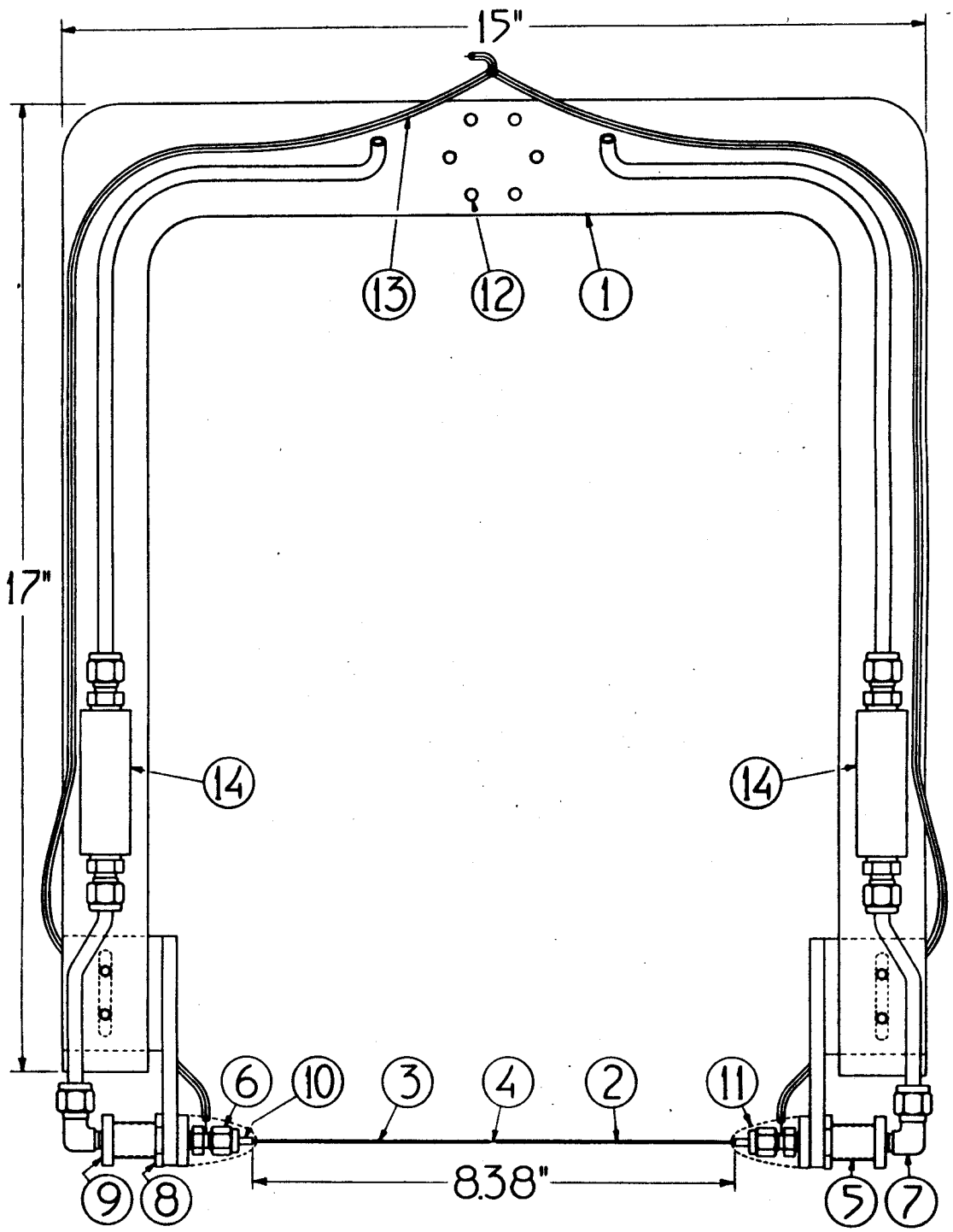

FIG.F1 THE LANGMUIR TUBE.

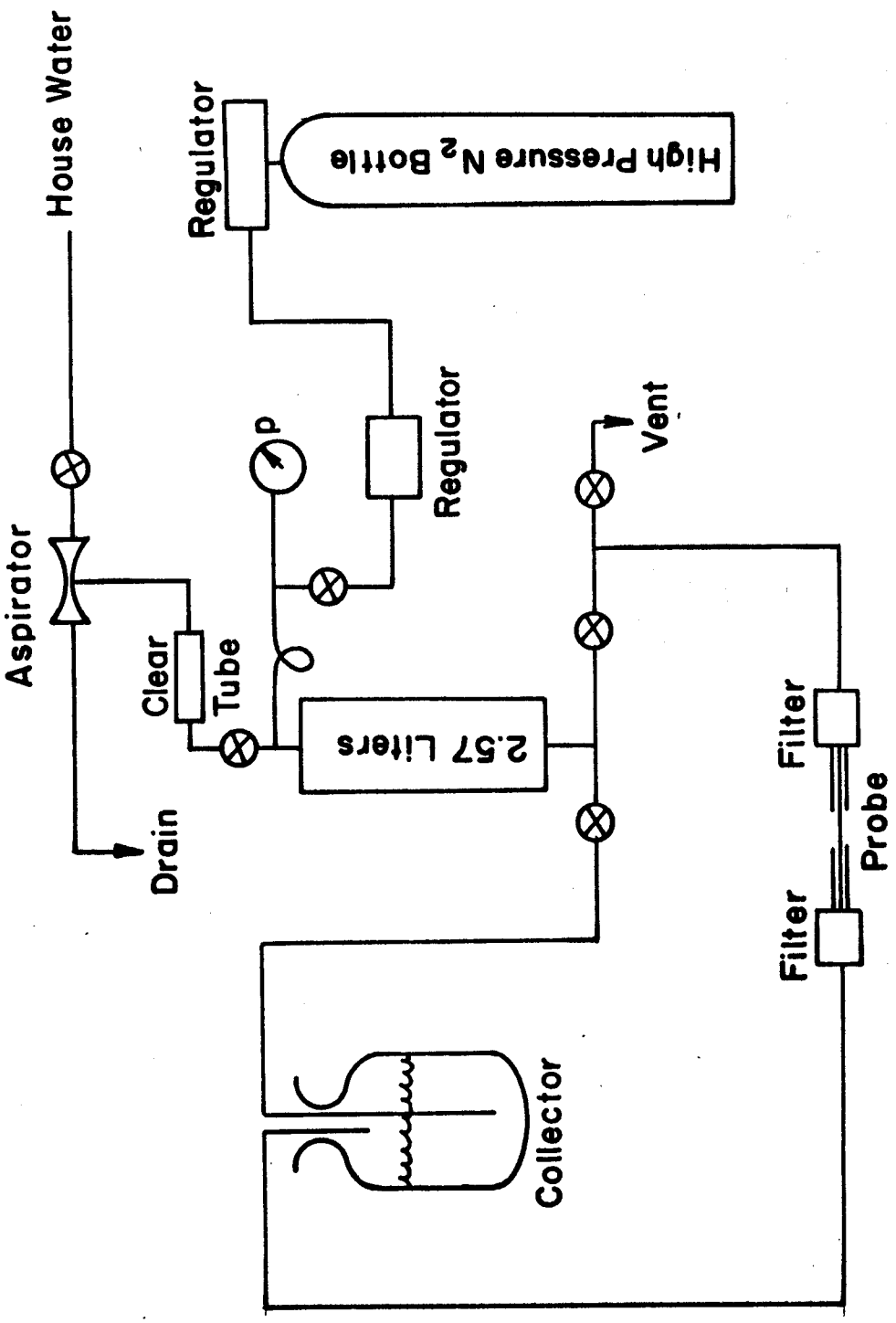

FIG. F2 SKETCH OF LANGMUIR TUBE COOLING CIRCUIT

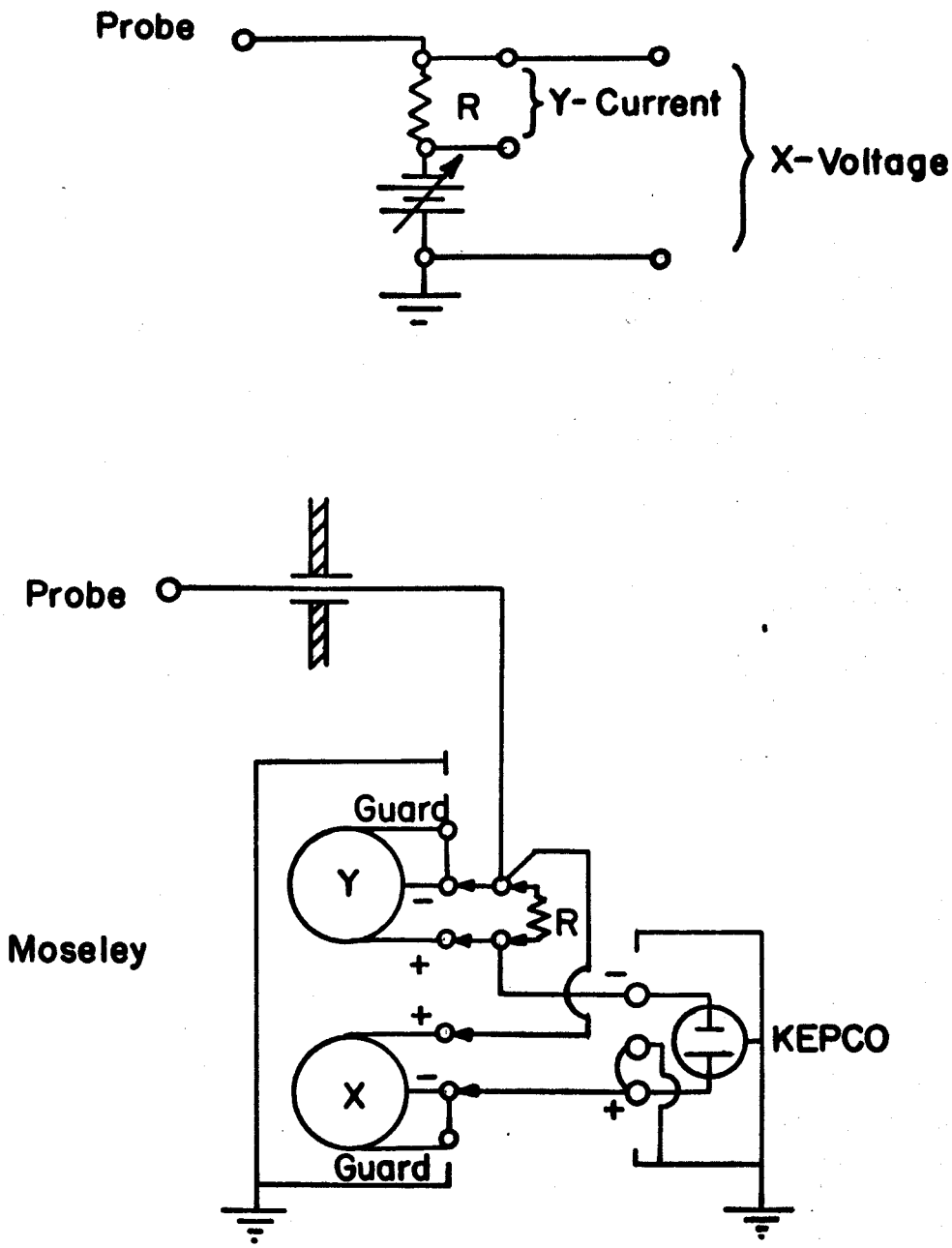

FIG. F3 LANGMUIR PROBE CIRCUIT

TABLE I

Units: p_t(torr), T_t(^oK), ρ_t(kg/m^3), n_{et}(m^{-3})

Test	h/RT_o	p_t	T_t	α	ρ_t	n_{et}
1.	34	52.3	9423	2.1-2	3.48-3	1.09+21
2.	30.1	52.5	8343	5.5-3	4.02-3	3.28+20
3.	30.3	52	8398	5.9-3	3.95-3	3.50+20
4.	32.6	53.5	9035	1.3-2	3.75-3	7.45+20
5.	25.5	49.9	7068	7.0-4	4.52-3	4.68+19
6.	25.9	48.5	7178	9.0-4	4.33-3	5.61+19
7.	26.3	48.1	7289	1.1-3	4.23-3	6.74+19

TABLE II

This table presents a sampling of the mean free paths existing in the experiments that are described in Section V. Five of the mean free paths are listed together with the Debye length at a selected number of stations in the flow field. The remaining mean free paths can be calculated from relations existing between the formulas presented in Appendix B.

$$L_{ne} \simeq L_{en}/\alpha$$

$$L_{ni} \simeq L_{in}/\alpha$$

$$L_{ei} = 0.716\, L_{ee}$$

$$L_{ie} \geq 1000\, L_{ii}$$

All mean free paths are given in meters with the power of ten following. The diameter of the Langmuir tube is 4.57×10^{-4} meters.

TABLE II

Test 1

x/D	L_{nn}	L_{in}	L_{ii}	L_{en}	L_{ee}	L_D
3.2	1.27-3	1.07-3	6.19-6	2.71-1	3.39-4	1.01-6
9.6	1.14-2	9.60-3	2.87-6	2.49	9.44-4	2.28-6
16.0	3.17-2	2.66-2	1.98-6	6.67	1.76-3	3.47-6
22.4	6.22-2	5.24-2	1.46-6	1.35+1	4.60-3	5.31-6

Test 2

x/D	L_{nn}	L_{in}	L_{ii}	L_{en}	L_{ee}	L_D
3.2	1.18-3	9.88-4	1.47-5	2.59-1	9.40-4	1.83-6
9.6	1.06-2	8.90-3	6.62-6	2.34	3.73-3	4.55-6
16	2.94-2	2.48-2	4.50-6	6.40	8.19-3	7.23-6
22.4	5.76-2	4.84-2	3.33-6	1.29+1	2.38-2	1.14-5
28.8	9.53-2	8.00-2	2.70-6	2.14+1	4.41-2	1.52-5

Test 3

x/D	L_{nn}	L_{in}	L_{ii}	L_{en}	L_{ee}	L_D
3.2	1.18-3	9.92-4	1.43-5	2.63-1	7.78-4	1.70-6
9.6	1.06-2	8.94-3	6.50-6	2.30	2.74-3	4.10-6
16	2.95-2	2.48-2	4.40-6	6.30	6.28-3	6.59-6
22.4	5.78-2	4.86-2	3.18-6	1.30+1	2.21-2	1.09-5
28.8	9.56-2	8.04-2	2.66-6	2.13+1	3.06-2	1.35-5

Test 4

x/D	L_{nn}	L_{in}	L_{ii}	L_{en}	L_{ee}	L_D
3.2	1.23-3	1.04-3	7.92-6	2.59-1	5.44-4	1.28-6
4.8	2.78-3	2.34-3	6.24-6	6.20-1	5.41-4	1.55-6
6.4	4.93-3	4.14-3	5.04-6	1.09	7.91-4	1.98-6
8.0	7.71-3	6.48-3	4.50-6	1.60	6.78-4	2.11-6
9.6	1.11-2	9.34-3	3.92-6	2.29	8.81-4	2.48-6

Test 5

x/D	L_{nn}	L_{in}	L_{ii}	L_{en}	L_{ee}	L_D
3.2	1.08-3	9.06-4	6.52-5	2.39-1	5.59-3	4.83-6
4.8	2.42-3	2.04-3	4.87-5	5.44-1	9.29-3	6.75-6
6.4	4.31-3	3.62-3	3.89-5	9.66-1	1.60-2	9.00-6
8.0	6.73-3	5.66-3	3.13-5	1.45	3.95-2	1.28-5
9.6	9.69-3	8.16-3	2.70-5	2.03	6.19-2	1.58-5

Test 6

x/D	L_{nn}	L_{in}	L_{ii}	L_{en}	L_{ee}	L_D
3.2	1.09-3	9.12-4	5.78-5	2.42-1	4.38-3	4.28-6
4.8	2.44-3	2.06-3	4.47-5	5.38-1	5.05-3	5.42-6
6.4	4.34-3	3.66-3	3.63-5	9.40-1	7.25-3	6.88-6
8.0	6.79-3	5.70-3	2.82-5	1.50	2.57-2	1.08-5
9.6	9.77-3	8.22-3	2.37-5	2.01	5.38-2	1.45-5

Test 7

x/D	L_{nn}	L_{in}	L_{ii}	L_{en}	L_{ee}	L_D
3.2	1.09-3	9.20-4	5.32-5	2.43-1	2.18-3	3.37-6
4.8	2.46-3	2.08-3	3.84-5	5.48-1	4.92-3	5.13-6
6.4	4.38-3	3.68-3	3.09-5	9.68-1	7.59-3	6.64-6
8.0	6.84-3	5.76-3	2.47-5	1.53	1.96-2	9.58-6
9.6	9.85-3	8.28-3	2.01-5	1.78	6.16-2	1.43-5

TABLE III

Hookup	Anode	Chamber	Probe Return	1. Anode / Cathode } sheath?	2. Wall Return Current?	3. Through Probe Circuit?
I.	Grounded	Grounded	Grounded	Partly	Yes or No	Partly
II.	Grounded	Floating	Grounded	Yes	Yes or No	Partly
III.	to Probe	Grounded	to Anode	Yes	Yes or No	None
IV.	to Probe	Floating	to Anode	Yes	No	None
V.	Floating	Grounded	Grounded	No	Yes or No	All
VI.	Grounded	to Probe	to Chamber	No	Yes or No	None
VII.	Floating	to Probe	to Chamber	No	No	None
VIII.	Floating	Floating	Grounded	No	Yes	All